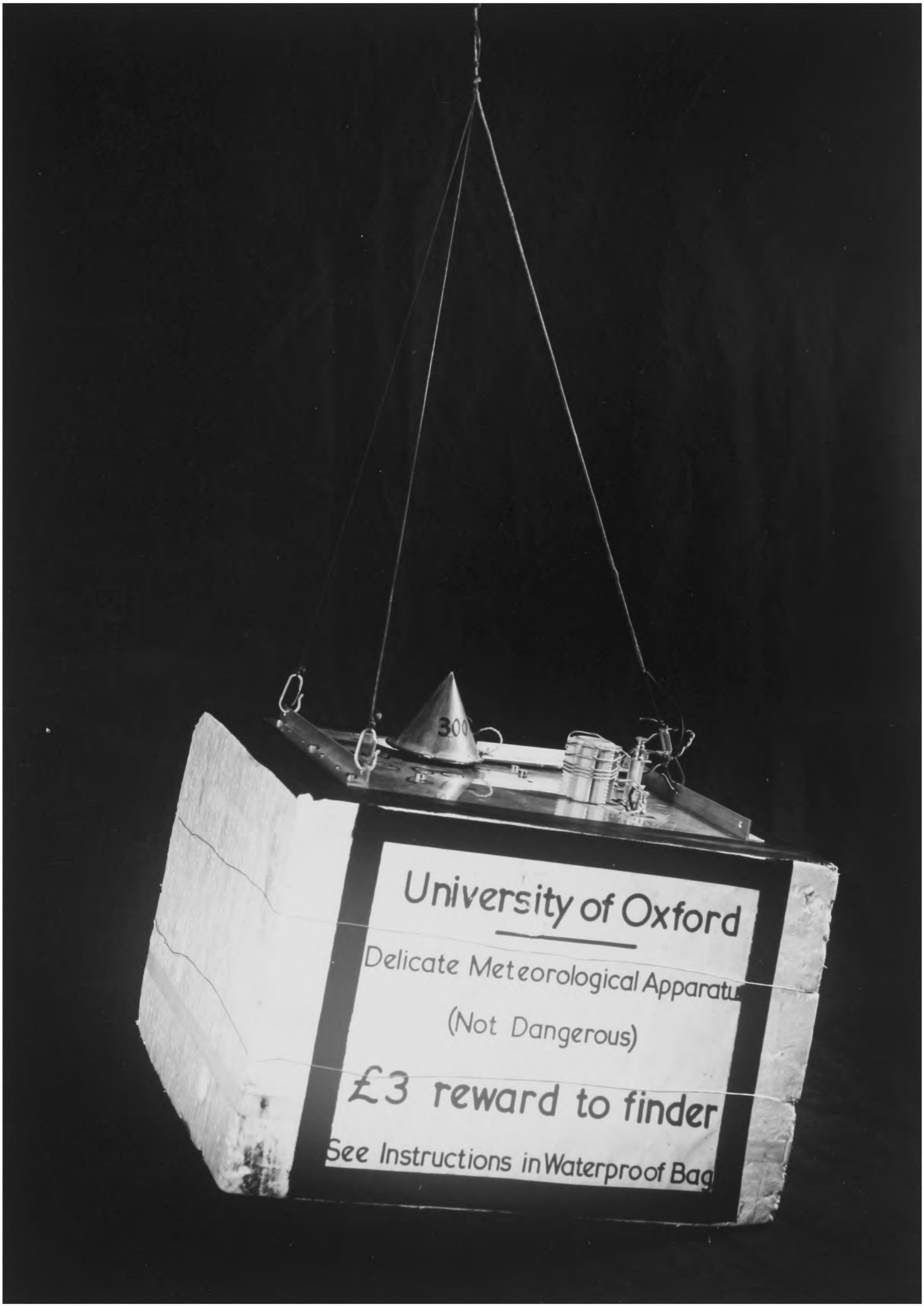


Plate 1 The radiometer-sonde frontispiece

THE SPECTRAL DISTRIBUTION OF THERMAL RADIATION IN THE EARTH'S ATMOSPHERE

A Radiometric Determination of Stratospheric Humidity

by

E. J. Williamson, B.A.

University College

A Thesis submitted for the Degree of Doctor of Philosophy

in the University of Oxford

Clarendon Laboratory

April 1964



To Margaret

who has been very patient

Contents

Abstract - - - - - - - - - - ix

Acknowledgements - - - - - - - - xii

Chapter 1. Introduction

1.1 The problem of atmospheric radiation transfer 1

1.2 Meteorological significance of radiative processes - - - - - - - - - 4

1.3 Infra-red absorbers in the atmosphere - - 6

1.4 Scope of the present study - - - - 7

Chapter 2. The humidity of the stratosphere

2.1 Frost point measurements in the stratosphere - 10

2.2 Some spectroscopic humidity measurements - 14

2.3 Miscellaneous measurements of stratospheric humidity - - - - - - - - - 21

2.4 Theoretical considerations of stratospheric humidity - - - - - - - - - 22

Chapter 3. The development of a practical gold-doped germanium detector and chopper assembly

3.1 Introduction - - - - - - - - 27

3.2 Photoconductive properties of gold-doped germanium - - - - - - - - - 27.

3.3 Preparation of samples for use as detectors - 29

3.4 Limitations of a simple D.C. measuring system 32

3.5 General considerations of an A.C. system - 35

3.6 The vibrating vane chopper - - - - 36

3.7 The complete detector - - - - - 43

Chapter 4. The radiometer-sonde

4.1 Introduction - - - - - - - - 48

4.2 Circuits associated with the detector

4.2.1 Electrical properties of the detector - 51

4.2.2 The cathode follower - - - - 53

4.2.3 The emitter follower - - - - 55

4.2.4 Reduction of input capacitance by the use of a guard - - - - - 55

4.2.5 Automatic gain change - - - - 59

4.2.6 Zero signal measurement - - - 60

4.3 Signal amplifier and phase sensitive rectifier

4.3.1 Basic amplifier circuit - - - 64

4.3.2 The phase inverter - - - - 68

4.3.3 The phase sensitive rectifier - - 69

4.4 The reference signal generator

4.4.1 The circuit in its original form - - 73

4.4.2 Reasons for abandoning the original circuit - - - - - - - 76

4.4.3 The second phase shifting circuit - 77

4.5 Black body and temperature element - - - 82

4.6 Multiplexing and telemetry

4.6.1 The multiplexor - - - - - 89

4.6.2 Telemetry - - - - - - 91

4.6.3 Aerial tuning - - - - - 96

4.7 General construction and layout of sonde - 100

4.8 The ground installation - - - - - 102

Chapter 5. Mathematics and radiation transfer

5.1 The extent of the problem - - - - 106

5.2 Line shapes and transmission models - - 107

5.3 Slant path approximations - - - - 113

5.4 The calculation of radiation flux - - - 115

Chapter 6. The ascents - - - - - - - 118

Chapter 7. Analysis of ascent data

7.1 Optical considerations - - - - - 134

7.2 Evaluation of water vapour mixing ratios - 135

7.3 Determination of the parameters G_ν and H_ν - 139

7.4 Spurious signals - - - - - - 144

Chapter 8. Interpretation of results based on data from ascent 9

8.1 Introduction - - - - - - - 149

8.2 Data smoothing - - - - - - - 151

8.3 Residual mixing ratio - - - - - 154

8.4 Excessive mixing ratios - - - - - 155

8.4.1 A check on the computer programme - 157

8.4.2 The accuracy of the statistical model - 157

8.4.3 Detector spectral sensitivity data - 158

8.4.4 The emissivity of the black body - - 161

8.4.5 Atmospheric emissions other than from water vapour - - - - - - 163

Chapter 9. The remaining ascents - - - - 172

Chapter 10. Summary and further work - - - - 178

Appendix I - - - - - - - - - 181

Appendix II - - - - - - - - - 182

Appendix III - - - - - - - - - 184

References - - - - - - - - - 187

Abstract

The humidity of the stratosphere is, from the point of view of radiation transfer studies, a subject of some importance to the meteorologist. It has, nevertheless, presented many problems to the experimentalist. Owing to the extreme dryness of air above the tropopause, compared with that at ground level, great care has to be taken to avoid the contamination of any measuring instrument by water carried up during an ascent into the stratosphere. An indirect method of approach, which to a large extent overcomes these difficulties, is the subject of the work described in this thesis.

Measurements of stratospheric humidity which have been made to date by other workers, are reviewed together with some of the theoretical arguments which have been put forward to account for various water vapour distributions. Good evidence, both theoretical and experimental, exists in favour of a water vapour mixing ratio in the region of 3×10^{-6} gm/gm in the lower stratosphere. Above about 50,000 ft experimental results have shown considerable diversity, and somewhat larger mixing ratios have been found in many cases. Recent measurements which suggest that the dry region of the stratosphere extends to much greater heights, have thrown doubt on a lot of the early work.

The instrument which is the subject of the present

study measures the night emission from the 6.3 μ water vapour band in the atmosphere, using a liquid air cooled gold-doped germanium detector. By utilising the variation with height of the boiling point of liquid air, and with it the change in sensitivity of the detector, measurements of emission over about four orders of magnitude have been possible during an ascent. Calibration is performed by means of a black body at a measured temperature. The detector responds to the total incident radiation within a pass band from about 5.5 μ to 7 μ. Since no information is obtained regarding the spectral distribution of radiation within the pass band, but only the combined effect of the whole, a somewhat lengthy analysis has been necessary in order to interpret ascent data in terms of water vapour mixing ratios.

Results from one ascent, which was by far the most successful, are discussed in detail. Mixing ratios obtained from the analysis show good agreement with values deduced from radiosonde humidity data below 300 mb and with the well established value a few kilometers above the tropopause. Above this the mixing ratio is found to vary between 2×10^{-6} and 4×10^{-6} up to 25 km. Interpretation of data at greater heights than this presented difficulties due to the presence of a large background component in the measured downward emission. Whilst the exact nature of

this emission is not known, it has with some justification been assumed in the analysis that it is not due to water vapour.

Acknowledgements

It is a pleasure to thank Dr. J. T. Houghton for suggesting the problem for study and for his continued advice and encouragement. My thanks are also due to Professor B. Bleaney for the facilities of the Clarendon Laboratory. Mr. G. B. Marshall has provided skilful assistance in the construction of apparatus and I am indebted to him and to other members of the laboratory staff who have helped in one way or another.

I wish to thank Professor L. Fox for the facilities of the Computing Laboratory and other members of the staff for their help and co-operation. Dr. J. S. Rollett gave much useful advice in connection with numerical methods.

The work would not have been possible but for the generous assistance of the staff of the Meteorological Office Radio-sonde Station at Aughton near Liverpool. I am also indebted to the Meteorological Office for the provision of a maintenance grant during the period of this work.

Mr. T. Williamson read the manuscript with care and I am grateful to him for many helpful suggestions.

Chapter 1

INTRODUCTION

1.1 The problem of atmospheric radiation transfer

The earth's atmosphere is a vast thermodynamic machine and one of such complexity that man is still a long way from understanding fully some of the processes which are known to take place in it. The ultimate source of energy for the atmosphere is the sun, which radiates approximately as a black body at 6000°K in the visible spectrum - the effective temperature being rather less in the ultra-violet and considerably more in the far infra-red. At mean solar distance the flux of solar energy amounts to about 350 watts for every square metre of the atmosphere. Of this about 35% is reflected back into space by cloud and about 10% is absorbed by constituents of the atmosphere - largely ozone and oxygen in the ultra-violet and water vapour in the near infra-red. The remainder reaches the earth's surface where the greater part of it is absorbed heating the ground and the lower layers of the air.

To maintain an overall heat balance, the earth re-radiates an equal amount of energy, but, being at a much lower temperature than the sun, this energy is concentrated into the infra-red rather than the visible part of the spectrum. It is in the infra-red that minor atmospheric

constituents possess many intense absorption bands, those of major importance being due to water vapour, carbon dioxide and ozone. These bands strongly absorb the outgoing radiation the result of which is seen as the 'greenhouse effect'. If the mean temperature of the earth's surface is calculated simply on the basis of radiative equilibrium with the incident solar energy, the result is a figure of about 245°K. The actual temperature of the earth's surface is considerably higher than this and it follows that it must radiate at a correspondingly higher rate. However, most of the energy emitted by the surface of the earth is absorbed in the lower atmosphere and subsequently re-emitted at the lower temperature of the absorber. The result is that the ground receives energy from the atmosphere in addition to solar energy. This accounts for the higher temperature observed.

Looking at the problem another way, it is mainly the atmosphere rather than the surface which radiates to space to maintain a balance with the sun. The calculated figure of 245°K corresponds to the effective temperature of atmospheric emission.

The transfer of radiation through an absorbing atmosphere depends on many factors. Each absorption band may consist of many thousands of individual spectral lines over which the absorption coefficient is highly frequency

dependent. At any one frequency, absorption is a function of the pressure, temperature and concentration of the absorber, all of which vary along an atmospheric path. In addition, in accordance with Kirchhoff's law, the absorbing material is itself radiating at every point along the path at a rate dependent upon its absorption coefficient, its concentration and the Planck function corresponding to the temperature at that point.

The problem is thus a formidable one and it has been necessary to adopt graphical and numerical methods of approach in most cases. Charts were constructed by a number of workers (Elsasser (1942); Yamamoto (1952); Robinson (1947, 1950)) to facilitate the calculation of radiation flux. These charts were based on theoretical models of radiation transfer but, until recently, no measurements above ground level were available to test their predictions.

Today, high speed electronic computers have made possible calculations the size and complexity of which would have been prohibitive a few years ago. Also there are many approximations which can usually be made to simplify calculations by reducing the number of independent variables. Some of these will be described in Chapter 5.

1.2 Meteorological significance of radiative processes

It is now known that radiation transfer is the mechanism largely responsible for large scale atmospheric motions in the troposphere. That the earth's atmosphere is not in radiative equilibrium can be shown simply by calculating the temperature structure of an atmosphere under such equilibrium conditions. Goody (1958) gives an example of one such calculation based on the assumption that water vapour is the only important absorber and that it is distributed exponentially with a scale height of 2 km. It is further assumed that the absorption coefficient is uniform for all wavelengths from 4 μ to ∞, being zero elsewhere, and that the atmosphere absorbs 90% of the radiation originating at the earth's surface. The resulting temperature structure is shown in fig. 1.1. Other assumptions yield slightly different profiles, but three features generally stand out.

1. The lapse rate near the surface is much greater than the dry adiabatic, which would immediately lead to instability.

2. The temperature of the stratosphere, although uniform, is considerably lower than that observed.

3. The temperature at any point in the troposphere is lower than the frost point corresponding to the initial assumptions of water vapour concentration - which is

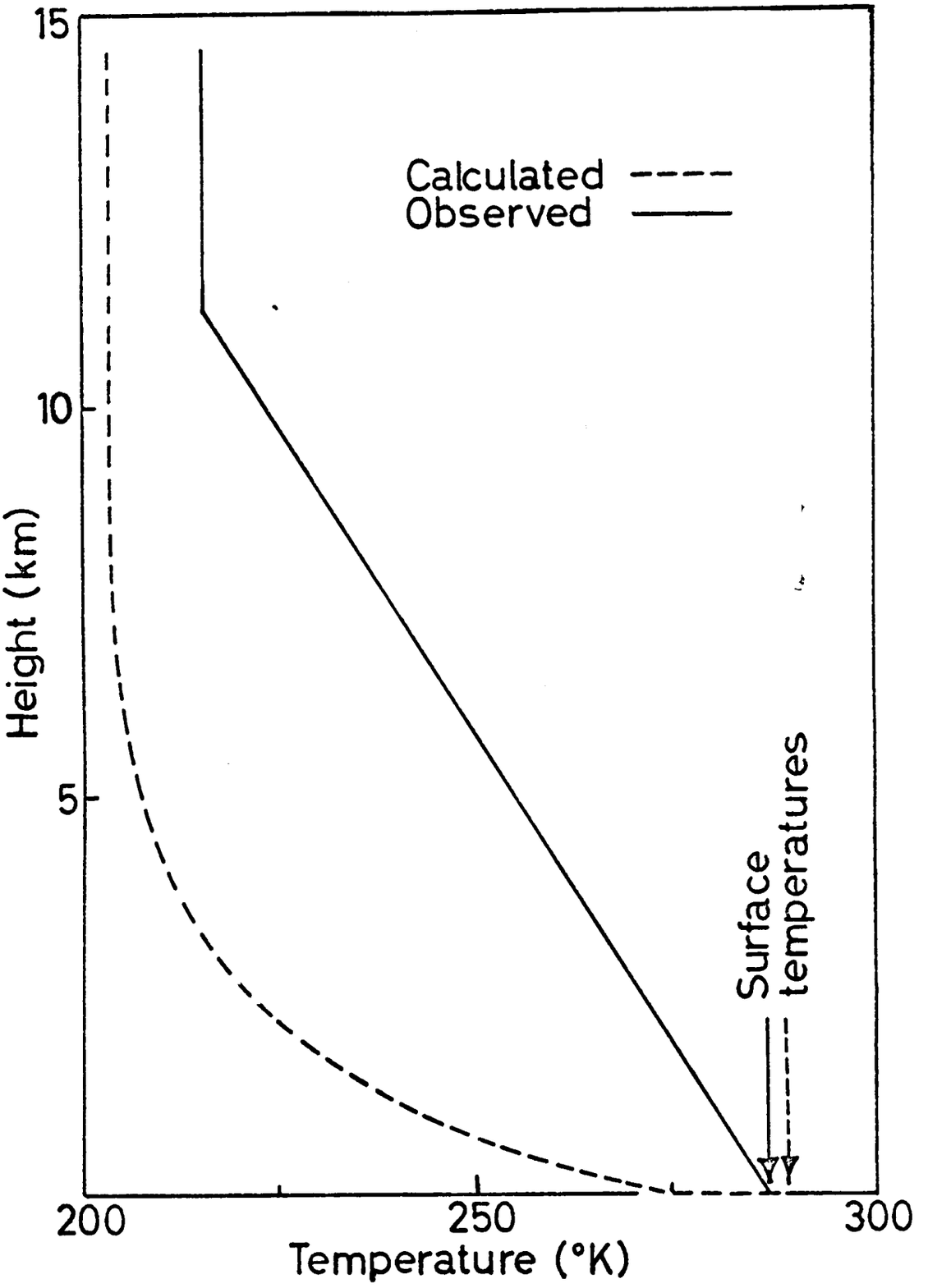


Fig. 1.1. The temperature structure of an atmosphere in radiative equilibrium, compared with that actually observed. After Goody (1958)

clearly impossible.

Thus the atmosphere cannot be in both radiative equilibrium and thermodynamic equilibrium at the same time. Overall heating and cooling will occur and provide sources and sinks for other thermodynamic processes which, together with certain geophysical factors, are responsible for the ever changing pattern of weather that is observed.

1.3 Infra-red absorbers in the atmosphere

Important to any study of radiative processes in the atmosphere is a knowledge of the quantitative distribution of the minor constituents responsible for radiation transfer, chiefly carbon dioxide, ozone and water vapour.

The first of these, carbon dioxide, is produced at ground level and measurements have shown that it is uniformly mixed in the lower atmosphere, representing a fairly constant 0.03% of the air by volume, at least up to 30 km. Ozone is produced by photochemical reaction of the sun's ultra-violet on oxygen in the upper layers of the stratosphere, but is destroyed lower down in the atmosphere forming a layer of maximum concentration at about 25 km. Sensitive methods have been devised by a number of workers for the measurement of ozone distribution and a substantial amount of data is now available.

Humidity is a very variable quantity. Measurements at

ground level and in the troposphere are easy to make, but above the tropopause highly conflicting results have been obtained. These are discussed in the next chapter. The chief difficulty attached to any direct measurement of humidity is one of contamination. It is very difficult to avoid water being carried up by the apparatus as it ascends through the relatively wet layers of the troposphere to regions higher up where the air is very much drier. There can be little doubt that the very high relative humidities measured in the stratosphere by some early workers have been the result of local contamination.

An attempt has been made in fig. 1.2 to summarise the magnitudes of the contributions of various atmospheric constituents to absorption in the troposphere (after Goody (1961a)). The curves are drawn for mid latitudes and for a solar zenith angle of 50°.

1.4 Scope of the present study

It is the object of the work described in this thesis to determine the humidity distribution of the atmosphere by observing infra-red emission from water vapour using a balloon-borne radiometer. This is an indirect method and does not measure local concentration but, rather, the combined effect of a large part of the atmosphere. A somewhat lengthy analysis has been necessary in order to

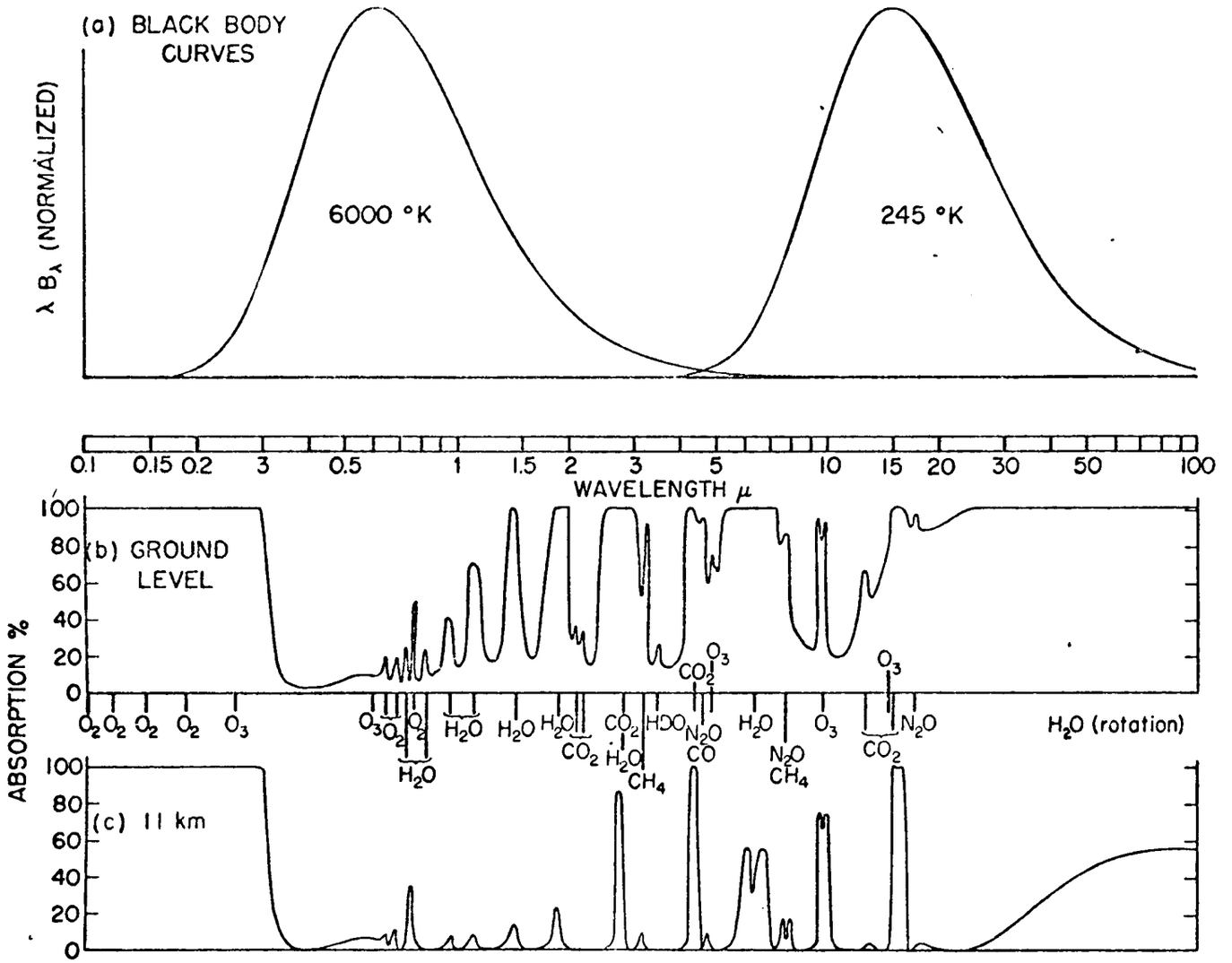


Fig. 1.2. Atmospheric absorptions

(a) Black-body curves for 6000°K and 245°K.
(b) Atmospheric gaseous absorption spectrum for a solar beam reaching ground level.
(c) The same for a beam reaching the temperate tropopause.

The axes are chosen so that areas in (a) are proportional to radiant energy. Integrated over the earth's surface and over all solid angles the solar and terrestrial fluxes are equal; consequently, the two black-body curves are drawn with equal areas beneath them. An absorption continuum has been drawn beneath bands in (b). This is partly hypothetical because it is difficult to distinguish from the scattering continuum, particularly in the visible and near infra-red spectrum.

obtain the final results but the method has the great advantage that it does not suffer, to any great extent, from the problem of contamination.

Measurements of thermal radiation in the atmosphere have been made by several workers using instruments sensitive to the whole spectrum of atmospheric emission, which extends from about 4 μ to 100 μ . Such measurements are important in connection with studies of the radiation budget of the atmosphere. If, however, the infra-red detector is restricted to radiation which is known to come only from water vapour, the results can be used to deduce the amount of water vapour present. The construction of an apparatus employing such a detector is described in Chapter 3 et seq. An account of the twelve ascents which have been made to date are presented together with the method adopted for the analysis of data and a discussion of the results obtained.

Chapter 2

The humidity of the Stratosphere

2.1 Frost Point Measurements in the Stratosphere

It has been known for twenty years that, in temperate latitudes, the relative humidity of the atmosphere decreases abruptly in the first two kilometers above the tropopause. This remarkable effect was discovered by Brewer in 1943 as a result of some of the first aircraft ascents with a frost-point hygrometer (Dobson, Brewer and Cwilong (1946)). Since then several hundred measurements of frost-point and air temperature have been made by the British Meteorological Research Flight (M.R.F.) on a routine basis over Southern England. Some of these are described by Murgatroyd, Goldsmith and Hollins (1955) and by Helliwell, Mackenzie and Kerley (1957).

A detailed analysis of the data from M.R.F. ascents and from those made prior to August 1946 by the High Altitude Research Flight at Boscombe Down, Wiltshire, has been made by Bannon, Frith and Shellard (1952) and extended to include all later ascents by Tucker (1957). A total of 399 ascents is considered in Tucker's paper and the results are remarkably consistent. There are three salient features.

1. The lapse rate of frost-point is usually continuous through the tropopause, but begins to decrease above it for a further 15,000 ft, tending to a constant value within a few degrees of 190°K.

2. There is no significant seasonal variation in the frost-point at 50,000 ft.

3. If the tropopause is high, the frost-point near the tropopause tends to be lower as does the air temperature.

In all the M.R.F. ascents, frost-points have been measured with the Dobson-Brewer frost-point Hygrometer, described by Brewer, Cwilong and Dobson (1948). This instrument, which is manually operated, consists of a blackened thimble, brightly illuminated, over which a fine jet of air is passed. It is cooled by a spray of liquid oxygen until frost is observed by the operator to form on the thimble. The frost-point is taken to be the temperature at which this deposit tends neither to increase nor decrease and is measured by a resistance thermometer attached to the thimble.

Shellard (1950) describes measurements made simultaneously from two aircraft flying close together, in an effort to test the reproducibility of frost-points measured with the aircraft instrument. At no time did the difference between readings taken by the two observers

exceed 2°F. Extensive tests have also been carried out on the ground to test the consistency of measurements made by independent operators using the same instrument. In the case of frost-points in the region of 190°K or lower, the deposit on the thimble is very thin and tends to be formed as a transparent film of ice. Accurate readings are then very much dependent on the skill of the operator. A method was suggested by Goldsmith (1954a) for overcoming this difficulty when the instrument is used in a jet aircraft. Air is taken from the engine compressor instead of directly from the atmosphere; its pressure has thus been increased and its frost-point thereby raised, so that the latter is more readily measurable. By observing the compression ratio the frost-point of the outside air can be determined. Goldsmith was able to show good agreement between simultaneous measurements made with and without this technique.

The weight of evidence in favour of the M.R.F. data is thus large. The humidity in the region of the tropopause, at least over southern England, must be one of the best authenticated quantities in meteorology.

Observations made at Tromso, N. Norway (69°35' N; 19°0' E) by Brewer (1955) and at Idris, Libya (32°40' N; 13°10' E) by Helliwell and Mackenzie (1957) are very similar

to those obtained over the south of England. The only measurements made near the equator by the M.R.F. were those of Goldsmith (1954b) at Khartoum ($15^{o}35'$ N; $32^{o}35'$ E). Ascents were made up to 38,000 ft., but none reached the tropopause.

The first direct measurements of frost-points to 30 km were made by Barrett, Herndon and Carter (1949, 1950) using an automatic hygrometer on a balloon. They found a seasonal difference between their ascents (two summer and one winter), but all their frost-points were warmer than the M.R.F. observations by 10 or 20 degrees and corresponding mixing ratios in the stratosphere differed by up to two orders of magnitude. Saturated layers were found both above and below the tropopause and the summer frost-point was found to remain constant in the stratosphere, indicating a mixing ratio which increased with height. Their results were quite inconsistent with the British measurements near the tropopause as is shown in a comparison given in Tucker's paper (1957).

Measurements by Mastenbrook and Dinger (1961) and by Mastenbrook (1962), using a similar type of instrument, again showed increasing mixing ratios above the tropopause. Minimum values of about 2×10^{-6} gm/gm at 2 km above the tropopause were in good agreement with the M.R.F. figures, but values at 30 km were nearly two orders of magnitude

higher than this.

Some doubt as to the accuracy of the earlier frost-point ascents has now been raised, following more recent measurements made by Mastenbrook (1963) in the late summer of 1962. On this occasion, near constant values of mixing ratio, of between 2×10^{-6} and 4×10^{-6} gm/gm, were found at levels above 16 km.

Ascents have also been made in Japan by Kobayashi and Toyama (1962) using an automatic frost-point instrument of compact design for use with conventional radiosonde balloons. With the relatively high tropopause in Japan, in the region of 100 mb, not very much information was gathered in the stratosphere. However, two ascents are described which reached 30 mb and frost-points of 190°K were recorded at this level.

2.2 Some spectroscopic humidity measurements

The intense absorption by water vapour in the infra-red offers a convenient method for the determination of its abundance in an atmospheric path. Most work in this field has centred on the measurement of absorption of solar radiation in one or other of the vibration-rotation bands in the near infra-red.

Gates (1956), making observations from the ground, measured the total absorption of sunlight by several of the

near infra-red bands of water vapour. Using the laboratory data of Fowle (1913), at that time the only data available, he was able to estimate the total water vapour content of the atmosphere. Values obtained ranged between 0.2 and 1 precipitable cm of water and were in reasonable agreement with quantities calculated from the humidity data of radiosonde ascents.

Perhaps the first measurements of solar absorption in the stratosphere were those made by a group at Johns Hopkins University (1949). Using a prism spectrometer in a B29 aircraft they were able to record the solar absorption spectrum from 2 to 25.6 μ at heights up to 36,000 ft.

Yarnell and Goody (1952) describe a spectrometer using a calcium fluoride prism and a thermistor bolometer which was installed in a Mosquito aircraft and used to record the solar spectrum from 4 μ to 8.5 μ with a resolution of 0.1 μ. At 35,000 ft, with a solar zenith angle of 79°, the absorption in the 6.3 μ band was observed to be about the same as that produced by 2 metres of laboratory air. This gives a value for the mean water vapour mixing ratio of the stratosphere of the order of 10^{-5} gm/gm.

A low resolution spectrometer of the rapid scanning type described by Brown and Roberts (1953) has been flown in a Lincoln aircraft by Jones and Roberts (1956) and

information regarding absorption by several minor atmospheric constituents was obtained at heights up to 30,000 ft.

The first high resolution solar spectra above the tropopause were obtained by Houghton, Moss, Seeley and Hawkins (1957) using a grating spectrometer in a Canberra aircraft. As pointed out by Houghton, Moss and Chamberlain (1958), the accuracy of spectroscopic measurements of the amount of water vapour and other minor constituents present in the stratosphere can be increased tenfold if the spectrometer is capable of resolving individual lines of the spectrum. Preliminary measurements by Houghton et al. (1957) on some lines in the 1.9 μ band indicated about 5×10^{-4} ppt cm of water above 45,000 ft. Complete solar spectra from 1 to 6.5 μ, taken at a number of different altitudes, have since been recorded by the same workers. These, together with laboratory spectra for comparison and tables of line identifications, have now been published in the form of an Atlas (Houghton, Hughes, Moss and Seeley (1961)).

A fuller description of some of the spectra in terms of water vapour content of the stratosphere has been given by Houghton and Seeley (1960). Portions of the 2.7 μ band were selected for analysis and the integrated absorption in these regions was measured from spectra taken at a number of

heights between 25,000 and 48,000 ft. Theoretical curves of growth for groups of lines were calculated from data on relative line strengths and positions published by Benedict and Plyler (1951) and laboratory spectra taken in an altitude chamber were used to calibrate the curves in terms of absolute quantities.

It was then possible to interpret absorptions measured in the solar spectra in terms of the mean mixing ratio of water vapour between the various heights at which spectra were recorded. A mean value in the stratosphere of about 3×10^{-6} was obtained both for these layers and as a value for the remainder of the stratosphere above 48,000 ft on the assumption of a constant mixing ratio. Equivalent frost-points deduced from results in the lower stratosphere were found to show good agreement with actual measurements made during the ascents.

Recently, high altitude solar spectra in the 2.7 μ water vapour band have been recorded from an aircraft by the Canadian Armament Research and Development Establishment. Gates, Calfee and Hanson (1963) have computed the spectral profile of the 2.7 μ band using theoretical values of line positions and strengths. By incorporating a triangular slit function into the calculation they were able to produce degraded spectra of the type which would actually be obtained with a spectrometer. These were calculated for a

variety of slit widths and amounts of water vapour and the results compared with one of the C.A.R.D.E. spectra taken at 13.7 km with a solar zenith angle of 71^{o}. The pressure used in the calculation was 0.069 atmospheres, which is half the pressure at which the aircraft spectrum was taken. The best fit was obtained with an effective slit width of 1.75 cm^{-1} and a path length of 3×10^{-3} ppt cm of water. This corresponds to a mean mixing ratio above 13.7 km of about 7×10^{-6} gm/gm.

Solar absorption measurements from balloons have been made by a number of American teams. Murcray, Brooks, Murcray and Shaw (1958) and Gates, Murcray, Shaw and Herbold (1958) recorded low resolution spectra of the water bands at 1.4 μ and 1.9 μ. Unfortunately, these bands are too weak to enable any accurate measurements of absorption to be made in the stratosphere and results are not quoted for heights much above the tropopause. Gates et al. give a value of 10^{-3} ppt cm for the water above 12.8 km, corresponding to a stratospheric mixing ratio of 6×10^{-6}. The value given by Murcray et al. is an order of magnitude higher.

More recent work by Murcray, Murcray, Williams and Leslie (1960) and by Murcray, Murcray and Williams (1962) has extended the range of balloon measurements to include the much stronger 6.3 μ water vapour band and has made

possible measurements to greater heights. In both cases substantial amounts of water above 30 km were indicated, amounting in the case of the former to about 3×10^{-3} ppt cm. This corresponds to a mixing ratio above 30 km of about 3×10^{-4}. The water vapour distribution profile deduced by Murcray et al. (1962) was similar to that obtained by Mastenbrook and Dinger (1961) although absolute values were wetter by a factor of 2 or 3. By comparison with the results of Houghton and Seeley (1960) the mean mixing ratio of the stratosphere obtained by Murcray et al. was at least an order of magnitude greater.

It is not impossible that some of the large water vapour concentrations found at high altitudes by the American workers were due to the presence of water within the spectrometer itself. One would expect considerable de-gassing of the apparatus to occur at low atmospheric pressures, especially under the action of direct solar heating. No precautions appeared to have been taken to overcome this and it would be quite easy to explain all the measured absorption in terms of contamination from within the instrument.

Nevertheless, there is a considerable weight of evidence (see Gutnick (1961)) in favour of a water vapour mixing ratio which increases in the middle stratosphere. Houghton (1963) has attempted to reconcile this with the

results obtained from the high resolution aircraft spectra. All the lines considered by Houghton and Seeley (1960) are strongly absorbing at their centres and this results in their absorption being dependent as much on pressure as on the amount of absorber. As a result, quite a large amount of water could exist at high altitudes where the pressure is low and still contribute little to absorption by strong lines, which are far more sensitive to water vapour present at lower levels. Weak lines, on the other hand, are not pressure dependent in this way, their absorption being directly proportional to the total amount of absorber in the path, irrespective of its pressure. Measurements were therefore carried out by Houghton on some weak lines in the aircraft spectra. These were taken from the 6.3 μ band where a much higher resolution was obtained, thus making it easier to isolate individual lines. Some of the lines corresponded to absorption by H_2O^{18}. The absorptions measured from these lines were compared with values calculated on the assumption of different atmospheric water vapour profiles.

It was found that results were consistent with a stratospheric mixing ratio, which increased above 20 km to reach 5×10^{-5} at 30 km, provided that the value in the lower stratosphere was assumed to be 1.5×10^{-6}, a value

somewhat lower than that indicated by frost point measurements. This profile is still at least a factor of 10 drier than many of the ascents obtained over the American continent in similar latitudes and, while it is not impossible that quite large zonal variations in stratospheric humidity could occur, heavy concentrations of water vapour at high levels are difficult to explain on the basis of general circulation theory (see section 2.4).

2.3 Miscellaneous measurements of Stratospheric Humidity

There have been attempts to estimate the humidity of the middle stratosphere by direct sampling. These were made by Brown, Goldsmith, Green, Holt and Parham (1961) using a cooled vapour trap carried on a large balloon to heights of between 80,000 and 90,000 ft. The apparatus was maintained at a constant height for a period of about 3 hours, during which time a large quantity of air was pumped through a liquid nitrogen trap. This was then sealed and recovered by parachute. The contents were analysed and the amount of carbon dioxide collected was used to determine the total quantity of air sampled. The results of seven ascents gave a mean value of 4×10^{-5} for the mixing ratio of water vapour at 80,000 ft - a value consistent with the American results.

Goldsmith (private communication) has made an ascent using an electrochemical hygrometer of the type described

by Brewer (1958). This consists of a glass rod wound with electrodes of fine platinum wire and coated with a thin film of a hygroscopic phosphorus pentoxide mixture. The conductivity between the electrodes can be regarded as dependent on the humidity of the air in contact with the hygrometer and as such the instrument can be made sensitive to very small concentrations of water vapour. After successful efforts to prevent water from reaching the instrument from inside the apparatus, an ascent was recently made over the south of England showing stratospheric mixing ratios less than 3.5×10^{-6} up to a height of 29 km. (see fig. 2.1).

2.4 Theoretical considerations of stratospheric humidity

Some of the attempts which have been made to explain the water vapour distribution of the stratosphere, in the light of results available, are described in this section. A summary of the stratospheric humidity measurements made to date is presented in fig. 2.1.

Theoretical justification for a dry stratosphere was first put forward by Brewer (1949) in an attempt to reconcile the abrupt change in atmospheric humidity above the tropopause, with the observed uniform mixing of non-condensable gases such as helium and carbon dioxide. This theory was later extended by Dobson (1956) to account for

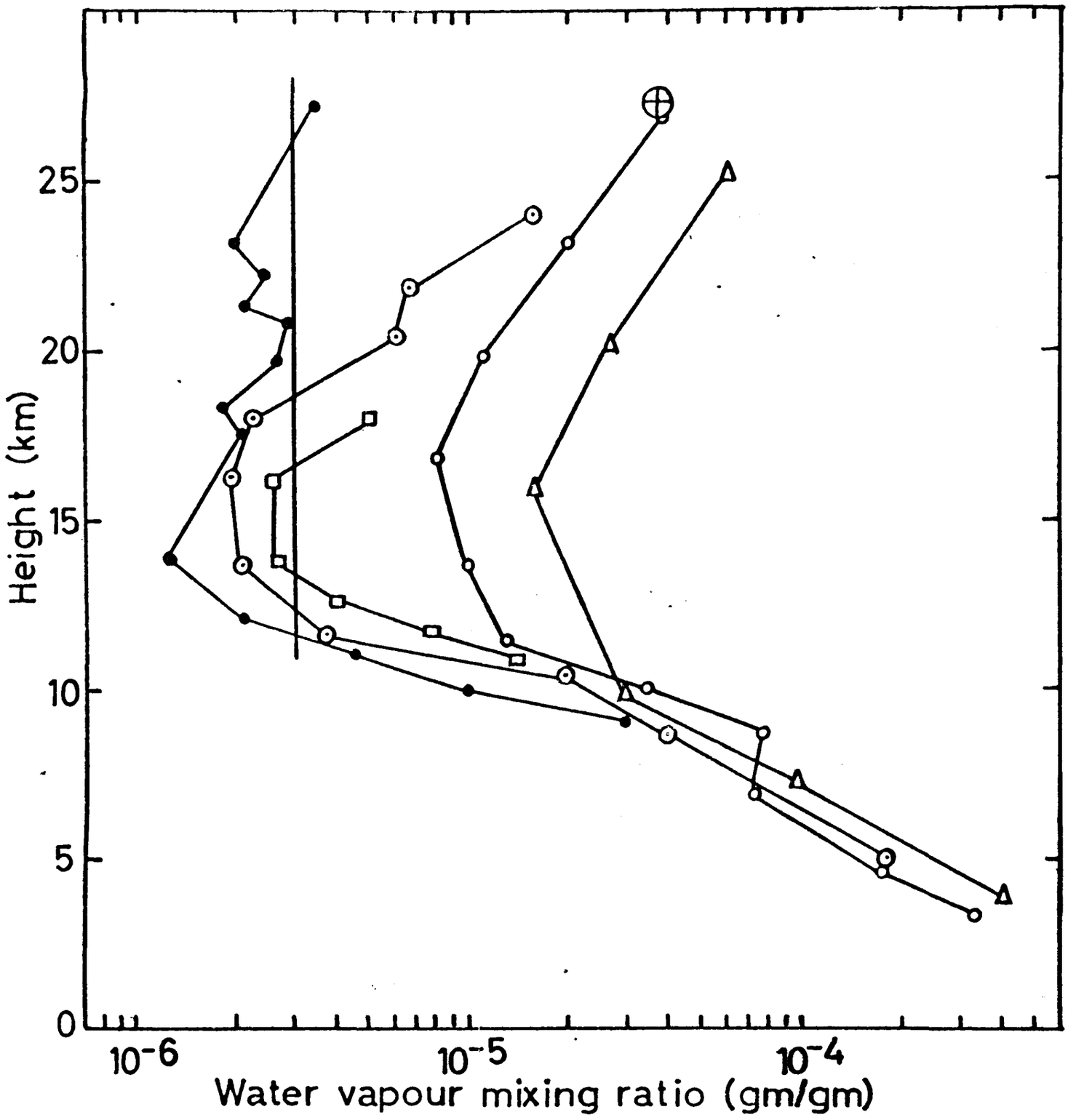


Fig. 2.1. Summary of stratospheric water vapour measurements.

△——△ Barrett et al (1950), mean summer profile. Automatic frost-point hygrometer.

⊕ Brown et al (1961). Cooled vapour trap.

●——● Goldsmith (unpublished). P_2O_5 hygrometer.

——— Houghton and Seeley (1960), mean value. Solar spectroscopy.

□——□ M.R.F. mean, Tucker (1957). Aircraft frost-point hygrometer.

⊙——⊙ Mastenbrook and Dinger (1961), 8.4.60. Automatic frost-point hygrometer.

○——○ Murcray et al (1962). Solar spectroscopy.

the seasonal variation in ozone distribution above temperate and polar regions. The Brewer-Dobson model postulates a general circulation of the atmosphere in which air rises at the equator, is transferred by horizontal advection in the upper layers of the stratosphere, and descends in temperate and polar latitudes. In passing through the cold equatorial tropopause the air is dried by precipitation until it is left saturated at a temperature of about 195°K. It would seem significant that the minimum values of frost-point which have been observed above the tropopause by the Meteorological Research Flight correspond very closely with the temperature of the equatorial tropopause. The humidity discontinuity observed above the tropopause in temperate latitudes is identified with the boundary between the dry air sinking in the stratosphere and the moist air being carried upwards by turbulent transfer in the troposphere. Thus, if all the water vapour in the stratosphere is assumed to have passed through the equatorial tropopause, its mixing ratio cannot exceed about 2×10^{-6} gm/gm.

Goldsmith and Brown (1961) have proposed a modified circulation model which permits the existence of water at levels above 80,000 ft. It is also consistent with recent measurements of the distribution of radioactive tracers such as tritium (Brown et al. (1961) and tungsten 185 (Feely and Spar (1960)). These substances, which have

originated as a result of certain nuclear bomb tests, were found to remain in the middle stratosphere long after they would have been removed had a Brewer-Dobson circulation existed (see also Sheppard (1963)). Goldsmith and Brown showed that these features could be explained if it is assumed that the main circulation takes place at levels immediately above the equatorial tropopause and does not extend above about 70,000 ft. This would provide the necessary source of dry air for the lower stratosphere. Above 70,000 ft little bulk movement of the air takes place and small scale turbulent diffusion is the only important means of transfer. Thus, comparatively large concentrations of water vapour could exist at these levels and it would be quite reasonable to expect a fairly abrupt transition from the extremely dry air below to wetter regions above. Also, the transition height could be subject to a seasonal variation.

There still remains the question as to what might be the source of water in the upper stratosphere. Goldsmith and Brown suggest a possible upcurrent from the summer pole, but this now appears to be unlikely in the light of recent frost-point measurements in polar latitudes. De Turville (1961) showed that if all the protons intercepted from the solar wind by the earth's magnetic field were oxidised, the upper atmosphere would be gaining water at the rate of

about 1.5 ton/sec. Indeed, the total mass of water on the earth, 1.42×10^{24} gm, is consistent with the total amount which would have been acquired in this way, 1.53×10^{24} gm, in the estimated lifetime of the earth, 1.04×10^{17} sec. However, little is known at present of photochemical equilibrium processes at great heights and it would be necessary to takemany more factors into account before such a theory could be considered acceptable.

Chapter 3

The development of a practical gold-doped germanium detector and chopper assembly

3.1 Introduction

The original idea for an emission measuring radiosonde was stimulated by the recent availability of single crystal gold-doped germanium. This semiconducting material, when cooled to liquid air temperature, can be used as a photo-conductive infra-red detector of high inherent sensitivity. With a natural long-wave cut-off at 8 μ, the material can be combined withacold indium antimonide filter to remove wavelengths below 5.5 μ, producing a detector which is ideal for the measurement of emission from the 6.3 μ water vapour band.

The following sections are an account of the development of a practical infra-red detector for use in a balloon-borne radiometer-sonde. The properties of gold-doped germanium are first of all briefly described, followed by the method adopted for the preparation of samples for use as detectors and the design of a suitable chopper. The complete sonde is described in Chapter 4.

3.2 Photoconductive properties of gold-doped germanium

The first account of gold-doped germanium was given by Dunlap (1953). On the basis of Hall-effect measurement he established the existence of two acceptor levels due to

gold. One of these was found to be 0.2 eV below the conduction band and the other 0.15 eV above the valence band. These results were later confirmed by Newman (1954) and by Kaiser and Fan (1954) on the basis of photoconductivity data. The infra-red properties of gold in germanium have also been described more recently by Johnson and Levinstein (1960).

Photoconductivity results from the production of carriers in the material by the absorption of photons. The 0.15 eV lower level gives rise to P-type conduction by capturing electrons excited from the valence band. The quantum of energy required for this must be greater than 0.15 eV, corresponding to a maximum wavelength for the incident radiation of about 8 μ. The upper acceptor state appears only through compensation when the lower level is completely filled and the 0.2 eV level partly filled with electrons from a suitable donor impurity. The cut-off wavelength in this case is in the region of 6 μ.

Measurements by Johnson and Levinstein (1960) showed that, whilst the N-type material was superior as a photoconductor in the intrinsic region, 0.5 - 1.4 μ, P-type gold-doped germanium was more sensitive beyond 5 μ. For this reason the latter type was chosen for the present work.

At normal ambient temperatures it is not possible to

observe impurity photoconductivity in gold-doped germanium as the impurity centres are completely ionised by thermal excitation. This can be overcome by cooling the material to liquid air temperature. Under these conditions the gold levels are practically empty and are capable of being excited by the absorption of incident photons of sufficient energy. The quantum efficiency of this mechanism, i.e. the number of carriers produced per photon absorbed, depends on the energy of the photon and results in a spectral response with a long wave cut-off.

The temperature dependence of the density of impurity carriers in a semiconductor causes the electrical conductivity to decrease rapidly with temperature in the extrinsic region. The change in conductivity amounts to about three orders of magnitude, for P-type gold-doped germanium, over the range of temperature which can be achieved by pumping liquid air. This property proved to be a valuable asset of the detector as is described later.

3.3 Preparation of samples for use as detectors

The gold-doped germanium used to construct detectors for the radiometer-sonde was produced in this country by the Mullard Research Laboratories, Salfords, Surrey. Crystals were grown by the seed-in-melt method from high purity germanium after compensation of residual acceptor levels with antimony and the addition of the appropriate

quantity of pure gold. The initial compensation is a difficult process to control accurately and greatly affects the quality of the final product. The material supplied by Mullards had a room temperature resistivity of 5 ohm-cm and contained about 7×10^{14} gold atoms per cm^3.

For the purpose of making detectors, a slice was first cut from the crystal perpendicular to the axis of crystal growth, using a 0.01" thick aluminium oxide saw. The disc was then cut into separate pieces which were ground and polished with fine alumina to produce specimens measuring 2 x 2 x 8 mm. These were etched in CP4 (see, for example, Bridgers, Scaff & Shive (1958)) and washed in distilled water.

Ohmic contacts were made at two points on each specimen as shown in Fig. 3.1. The material used for this was a 95% indium/5% gallium alloy supplied by Messrs. Johnson-Matthey Ltd. The procedure used was to melt a small bead of the alloy on to the surface of the germanium, using a miniature soldering iron with an arsenic free copper bit. The specimen was then heated to 400°C in an atmosphere of hydrogen and allowed to cool slowly. Under these conditions the alloy diffused about 0.1 mm into the surface of the germanium, producing a non-rectifying ohmic contact.

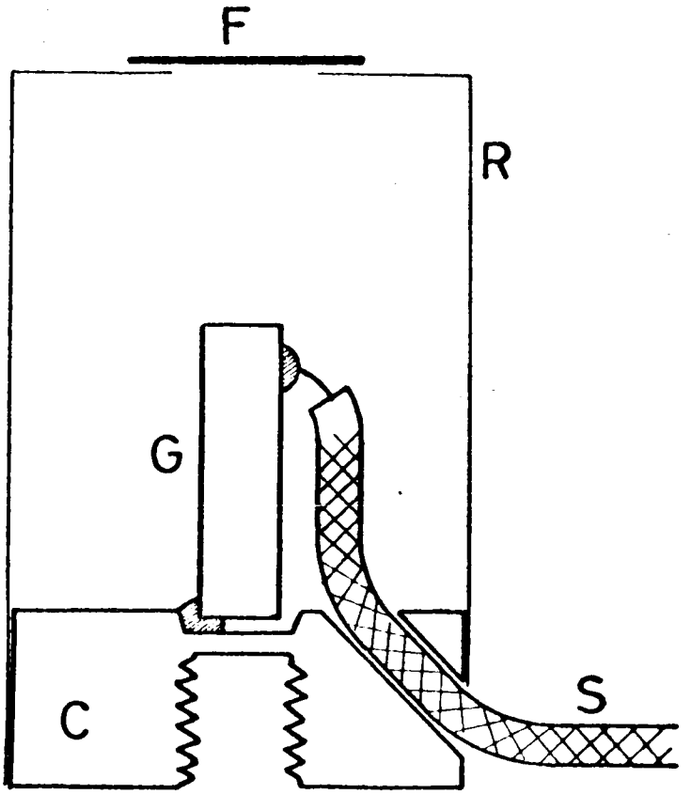


Fig. 3.1. The gold-doped germanium detector

C Copper mounting block

F InSb filter

G Specimen of gold-doped germanium

R Radiation shield

S Screened output lead

Detectors were soldered at one end to a small copper block to provide good thermal contact for cooling. The junction was restricted to one side of the base of the detector and did not extend over the entire surface. The latter was left polished to reflect back radiation which passed down the specimen without being absorbed. The absorption coefficient of the material in the extrinsic region is, in fact, only of the order of 10^{-2} cm^{-1} so the specimen should provide as long an absorption path as possible. However, the length of the detector was limited by the necessity of preventing its resistance from becoming unmanageably large at low temperatures.

The base of the detector acted as one electrical connection, the second being made to the contact at the top and brought out through a hole in the copper block (Fig. 3.1). After mounting, the detector was washed in de-ionised water for not less than 15 minutes. A polished german silver cap which fitted over the copper base served as a radiation shield and also acted as a mount for the indium antimonide filter. Plate 2 is a photograph of a finished detector with its cap and filter.

3.4 Limitations of a simple D.C. measuring system

The easiest way of employing a gold-doped germanium detector for the measurement of infra-red radiation is in conjunction with a D.C. measuring system. It was in this

form that the plan for a radiometer-sonde was first envisaged. Such a system would comprise a means for measuring conductivity changes in the detector due to the incident radiation and a transmitter for relaying this information to the ground. A zero radiation measurement can be achieved by moving a mirror into the field of view of the detector to reflect its cold surroundings, and calibration can be performed by observing radiation from a black body at a known temperature. The sky emission received would be proportional to the difference in conductivity of the detector with and without the mirror in place.

Further investigation and some preliminary measurements revealed the following difficulties which would have to be overcome before the simple arrangement described above could be employed.

1. The change in conductivity due to a flux of radiation of the order of magnitude of that anticipated in the stratosphere was vanishingly small compared with the steady conductivity of the specimen at liquid air temperature. A D.C. amplifier of considerable stability would therefore be required in order to detect and measure this change to the degree of accuracy required.

2. Because of the change with height of atmospheric pressure the boiling point of the liquid air coolant will

fall by up to 20°C during an ascent. This will result in a change of about three orders of magnitude in the electrical conductivity of the detector. A balanced D.C. system would probably be required, incorporating a second specimen shielded from the radiation to compensate for the rapidly changing conductivity. Once again this would require very high stability on the part of the electronics.

3. Semiconductors suffer from 1/f noise. A D.C. measurement would therefore be expected to give a poor signal to noise ratio.

Points 1 and 2 place formidable requirements on the stability of the amplifier required. Such requirements would be difficult to meet without resorting to somewhat complicated techniques. Further, it was intended that transistor electronics should be used wherever possible in order to economise on weight and power supply requirements. The inherent temperature sensitivity of transistors would be a further difficulty to overcome in the design of stable D.C. circuits.

In view of these considerations it was decided to investigate the possibility of employing a chopper to interrupt the incident radiation, in conjunction with an A.C. amplifier and rectifier. Although lacking the basic simplicity of a D.C. measurement such a system would overcome the above difficulties.

3.5 General considerations of an A.C. system

A fundamental problem associated with the construction of any cooled detector is that of preventing the formation of ice on cold optical surfaces. Conventional practice is to mount the detector in an evacuated enclosure fitted with a suitable window, the latter remaining at ambient temperature. In this way both the detector and the window are protected. When used with an external chopper the effect of radiation from the window is removed.

When an absolute measurement of radiation flux is required, however, it is necessary to know the temperature of the chopper as well as its emissivity and reflectivity. This would be difficult to achieve in a balloon-borne apparatus, especially as all these quantities would be liable to change with time. One solution is to employ a reflecting chopper which, when interrupting the radiation stream, causes the detector to observe a surface at a temperature sufficiently low that radiation from it is negligible. However, experience showed that it was very difficult to produce a mirror of sufficiently low emissivity. With a value of only 0.1%, a chopper at the ambient temperature of the apparatus would emit radiation comparable in magnitude to the downward emission from the 6.3 μ water band in the middle stratosphere. The size of the chopper would present an additional problem. It would

have to be the first item in the optical system, which means that its size could not be reduced below that of the entrance window. This would place heavy power requirements on the driving mechanism.

The effect of chopper emissivity can be eliminated if the chopper itself is maintained at a low temperature. In this case, of course, it is not possible to have it exposed to the air; it must be kept dry in the same way as the detector. If the chopper is mounted with the detector at the same temperature, there is the additional advantage that the cross section of the incident radiation is least at this point: but now radiation from the window will be chopped and again this might be many times greater than sky radiation. There is also the problem of constructing a chopper which will operate at liquid air temperature. The solution of these difficulties will be discussed in the next two sections.

3.6 The vibrating vane chopper

The possibility of utilising a rotary, motor driven chopper of conventional design was soon discarded. In the first place, a conventional motor would not operate at liquid air temperature and, even if it would, the relatively large amount of power dissipated would cause rapid evaporation of the liquid air coolant. Also some means

would have to be devised for accurately controlling the speed of the motor. This would present a problem in a small balloon apparatus. An alternative method was therefore sought.

Richards (1955) has described vibrating choppers which take the form of a reed, rigidly mounted at one end and carrying a soft iron armature. Small currents are induced in a pick-up coil mounted close to the armature, which are amplified and fed to a driving coil correctly phased to maintain the oscillation of the reed. Power consumption of the valve amplifier used in conjunction with a chopper operating at 250 c/s was 350 milliwatts.

The mathematical analysis of electrically forced oscillations in a mechanical system has been dealt with by Butterworth (1914, 1915). He showed that a coil (of negligible inductance) magnetically coupled to a mechanically resonant system, behaved electrically as if it were a simple tuned combination of L, C and R. At a frequency corresponding to that of the mechanical resonance, the reactive components cancelled out and the coil appeared as if it were a pure resistance. Following the demonstration of a valve driven tuning fork by Eccles (1919), Butterworth (1920) carried out the analysis of such a system and calculated the value of the minimum loop gain necessary to maintain oscillations. He also considered the effect of

making the pick-up and drive coils into tuned circuits by the addition of fixed capacitors. He was able to show that, in this case, there are three possible modes of oscillation depending on the tuning of the electrical circuits relative to the frequency of the mechanical resonance. If the correct mode was chosen, the efficiency of the system could be increased by the addition of the capacitors although the tuning was liable to be critical.

Some experiments were carried out with a vibrating chopper of the type described by Richards. It was quickly realised that for the system to work satisfactorily the reed had to be very rigidly clamped. The slightest yielding of the support dissipated energy from the vibrating system, reducing the amplitude of oscillation or causing oscillations to cease altogether. More power was therefore required to maintain the vibration. This problem would be difficult to overcome in the case of a small apparatus. However, it was found that a great improvement in performance could be achieved by using a mechanically balanced vibrating element in which the centre of gravity remained at rest. A tuning fork arrangement was one possibility, but this would have been bulky at all but high frequencies.

A compact device was constructed using a balanced chopper mounted on a torsion suspension. It was designed to operate at 40 c/s and in conjunction with a simple

transistor driving circuit consumed only 5 milliwatts of power. The chopper assembly is shown diagrammatically in Fig. 3.2.

The chopper itself is a piece of 0.003" thick copper foil soldered to a small magnet which is mounted at the centre of a length of 0.009" diameter piano wire stretched between two supports. The ends of the magnet vibrate between the pole pieces of two coils, one of which acts as a pick-up and the other as a driver. The coils are each wound with 10,000 turns of 48 swg wire and the cores are made from Stalloy stampings specially shaped to decrease the reluctance of the magnetic circuit as much as possible and to provide the maximum coupling with the magnetic field of the vibrating magnet.

The external circuit is shown in fig. 3.3. A 47 kΩ resistor in the base circuit is provided to bias the transistor into conduction so that oscillations will start. The loop gain is initially quite large and it was found that capacitively tuned coils, as described above, were unnecessary. The amplitude of the oscillations will increase to a point at which the current induced in the base circuit is sufficient to cause the transistor to operate between saturation and cut-off. The maximum collector current is determined by the resistance R in series with the internal resistance of the drive coil. As in any

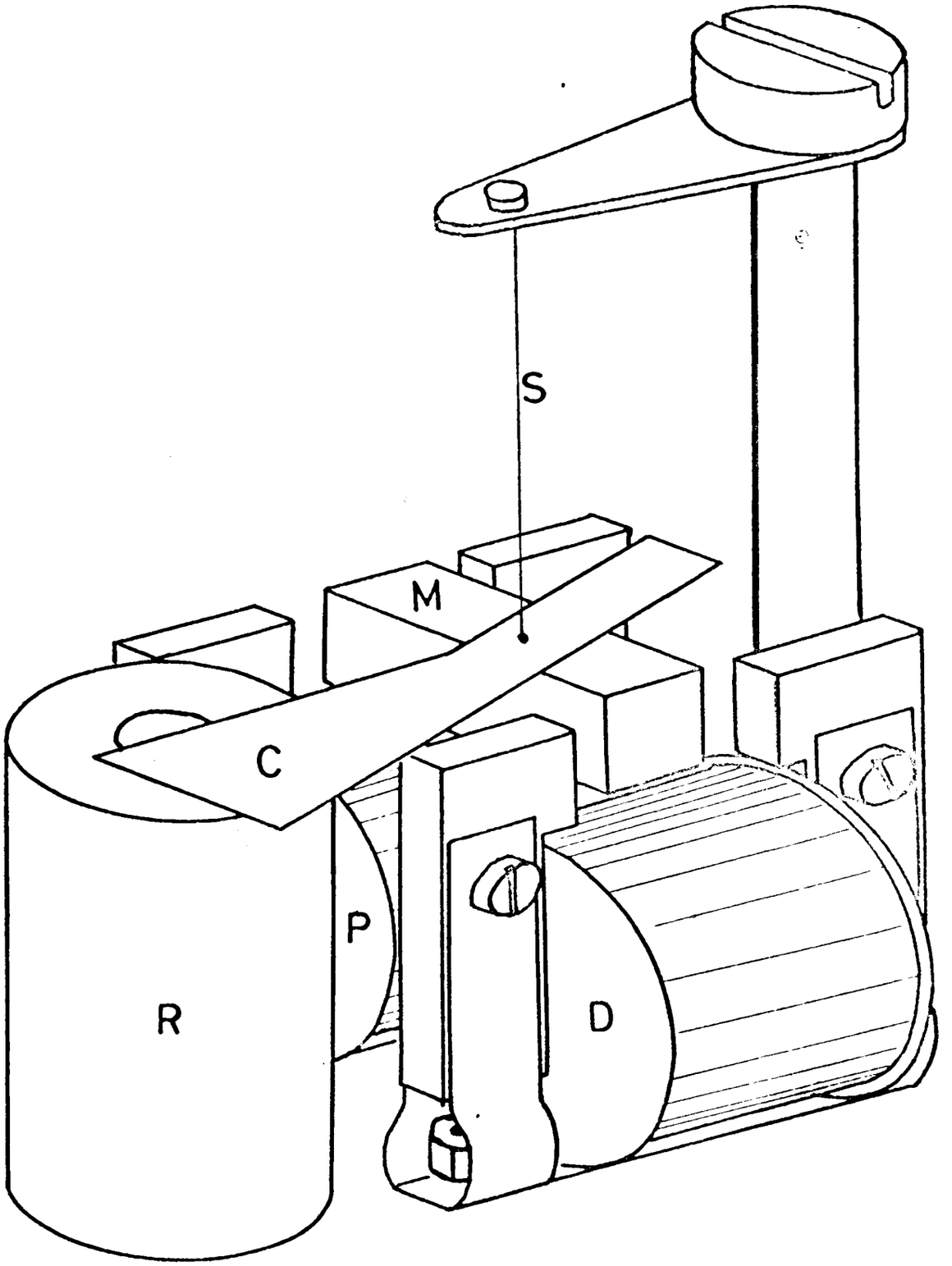


Fig. 3.2. The vibrating vane chopper.

C Chopper vane

D Drive coil

P Pick-up coil

M Magnet

R Detector radiation shield

S Suspension wire

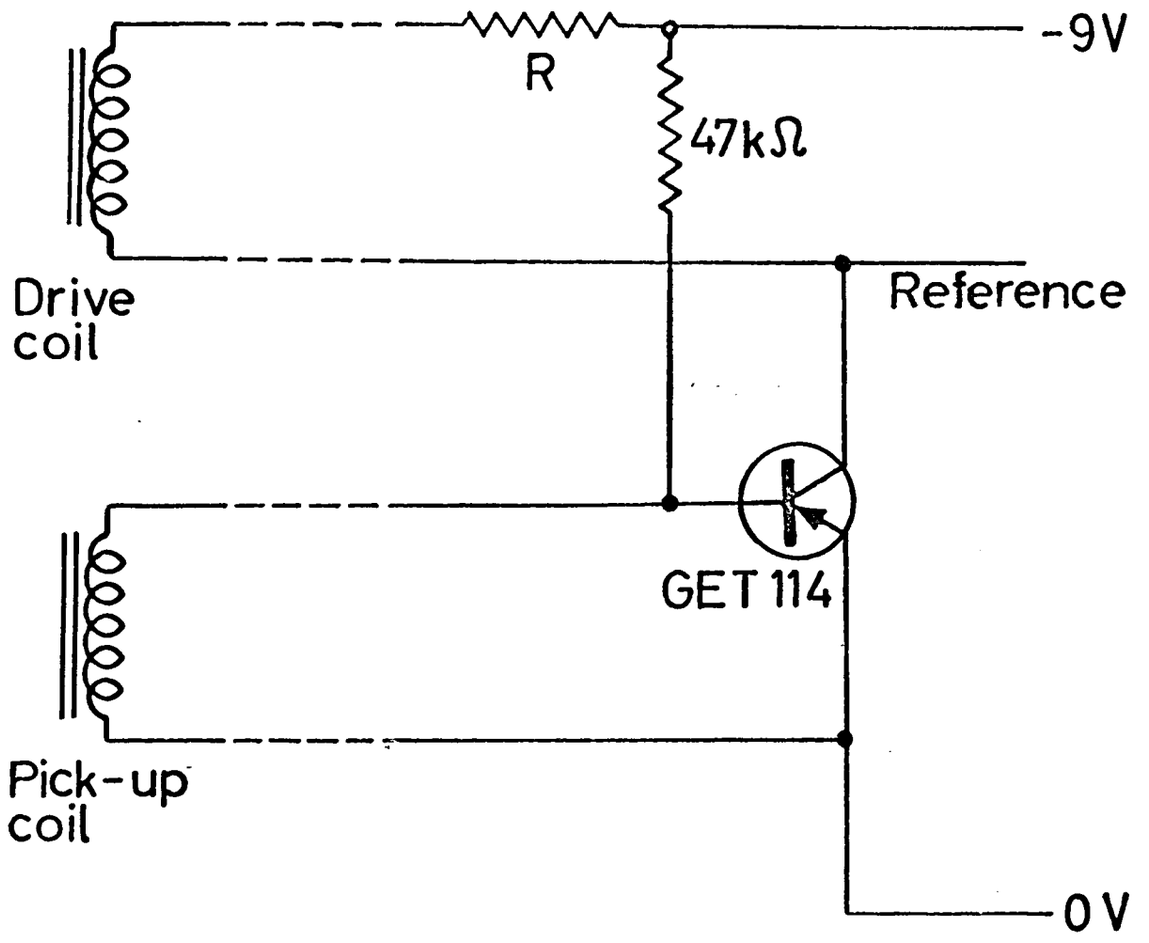


Fig. 3.3. Chopper driving circuit.

feedback oscillator, the amplitude of oscillation remains constant when the loop gain becomes unity. For maximum amplitude stability, the loop gain of the circuit should be highly amplitude dependent. This is the reason for the tight magnetic coupling of the coils with the magnet. Unit gain is reached when the transistor operates as a switch, as described above, and the value of R can thus be used to control the amplitude of oscillation.

The efficiency of the system is further improved by the fact that the coils are at liquid air temperature, resulting in a reduction in their resistance by about a factor of 6. Most of the power consumed by the circuit, is, in fact, dissipated in R which is many times larger than the coil resistance, This is important because any power generated by the coils contributes to the evaporation of the liquid air cooling the detector.

The chopper was found to operate perfectly well at liquid air temperature and to withstand the effects of repeated cooling down and warming up. One torsion wire broke during laboratory tests, after several weeks use, but this was found to be due to the action of rust. All subsequent suspension wires were tinned with solder to prevent rusting and no further trouble was encountered.

3.7 The complete detector

Having devised a chopper which was capable of operating in the cold environment of the detector, there remained the problem of radiation from the window of the vacuum enclosure. This can be removed by simply eliminating the window but, in this case, an alternative method is required for preventing the formation of ice on the detector.

The first approach to this problem was to submerge the detector in liquid air. The latter, being transparent to radiation in the region of 6.3 μ, would not affect the performance of the detector and any ice forming on the surface of the liquid would sink to the bottom, being the more dense. An experimental detector was built on this principle and is illustrated diagramatically in Fig. 3.4. The detector and chopper were mounted on a plate some 10 cm in diameter and the whole enclosed in a copper container submerged in liquid air. Radiation entered the top of the enclosure through a wide bore german silver tube which served also to support the assembly. Liquid air was admitted via a valve in the bottom of the container, the flow being controlled by a float which was adjusted to maintain the level of liquid air inside the vessel so that the detector was kept covered. The chopper operated just above the level of the liquid.

Although the system worked quite well, the valve and

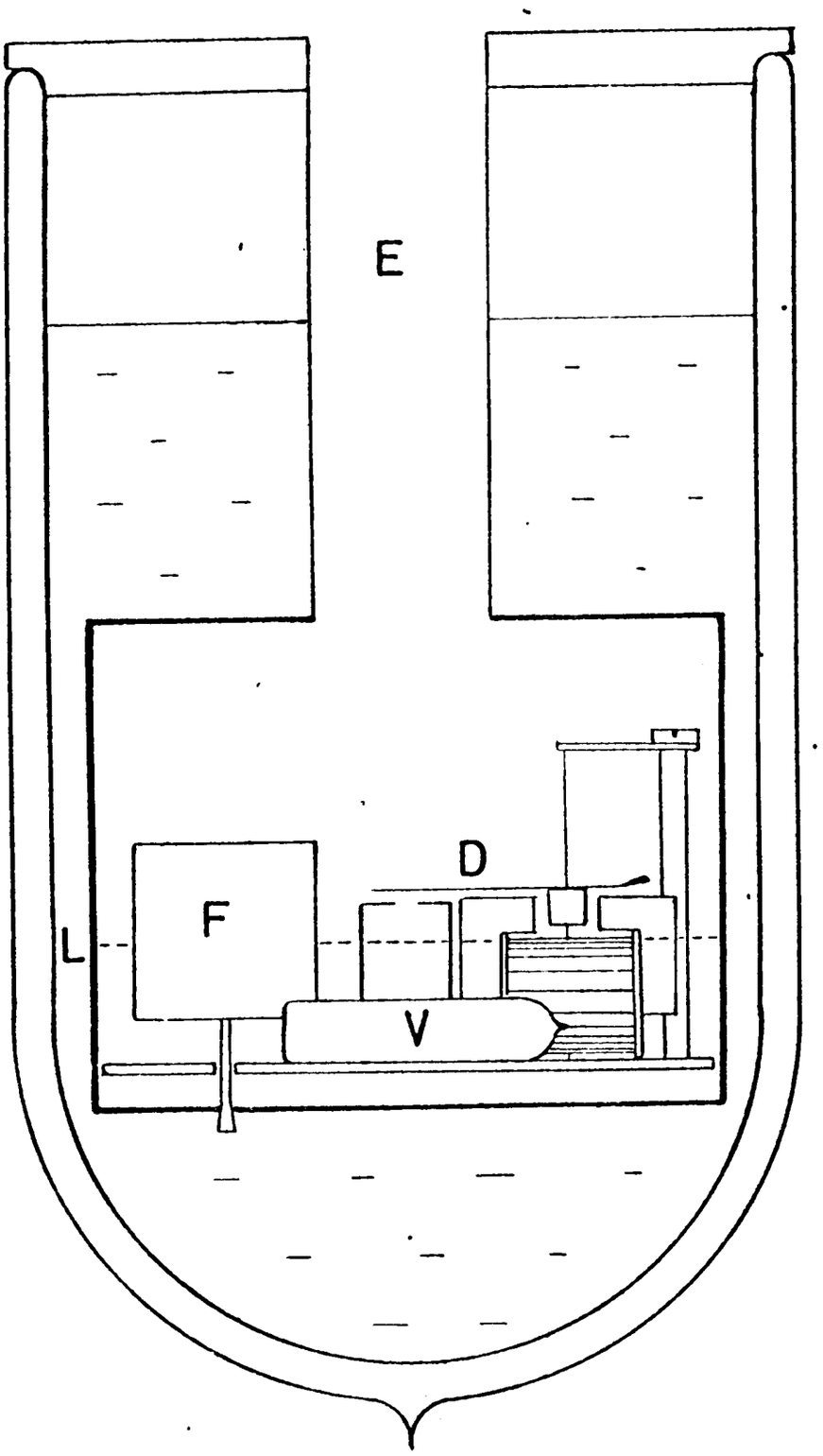


Fig. 3.4. An early detector and chopper assembly.

E Entrance aperture

D Detector and chopper

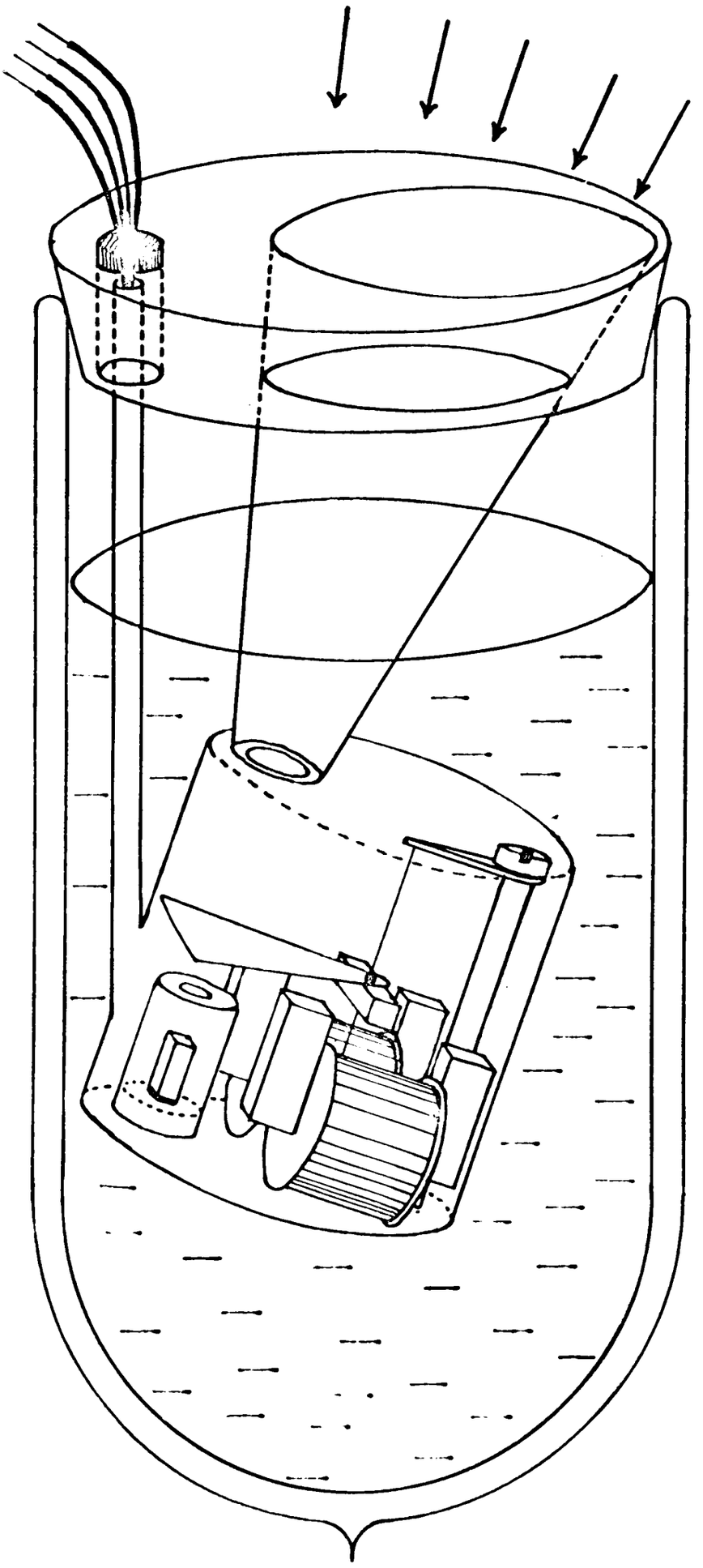
F Float and valve mechanism

L Level of liquid air inside container

V Cathode follower valve

float mechanism tended to be unreliable. Occasionally, the valve would stick so that the whole container filled with liquid air and the chopper would become submerged.

An alternative solution to the problem proved to be more satisfactory. It was found that the formation of ice inside the detector vessel could be prevented by continuously flushing it with dry air. This method was adopted in the final design (fig. 3.5). The container was completely sealed and the detector mounted in good thermal contact with the base plate. As the valve and float mechanism had now been dispensed with, the construction could be made more compact. The detector was positioned at one side of the base instead of at the centre as in the previous model. It was therefore necessary to tilt the axis of the whole assembly in order to accommodate it in as small a space as possible. The tube at the top through which the radiation entered was made conical in shape to permit an angle of view of 25°. The whole was mounted in a dewar with a tight fitting bung. When filled to within an inch of the top the apparatus contained 300 ccs of liquid air which was found to last for several hours in the laboratory. As the liquid evaporated the dry air was forced to flow down a tube into the detector container and out through the entrance aperture. In this way atmospheric air was prevented from entering the apparatus and the detector and



GOLD DOPED GERMANIUM DETECTOR AND CHOPPER ASSEMBLY

Fig. 3.5

chopper were found to remain free of ice as long as the supply of dry air was maintained.

A 1.75" length of copper tube with an internal bore of 2" and a wall thickness of 1/16" was used to construct the container for the detector and chopper. The two end plates were machined from 1/16" copper sheet, the one which formed the top of the container being permanently hard soldered to the tube. The unit was attached to the conical entrance tube and to the pipe through which the dry air entered. Both of these were of german silver, the former being fabricated from 0.004" sheet. The air supply tube served also as a means for taking out the electrical connections to the chopper and detector. The german silver cone was mounted in a bung made from balsa wood which was a tight fit in the mouth of the dewar vessel. The apparatus was filled with liquid air through a hole in the bung which was afterwards sealed.

The detector and chopper were mounted together on the base plate. This was then soldered on to the bottom of the container, using Wood's metal, an alloy with a melting point of 65°C. As an extra precaution against leaks, the outside of the container was afterwards coated with shellac varnish. The complete assembly with the base plate detached is shown in Plate 3.



Plate 2

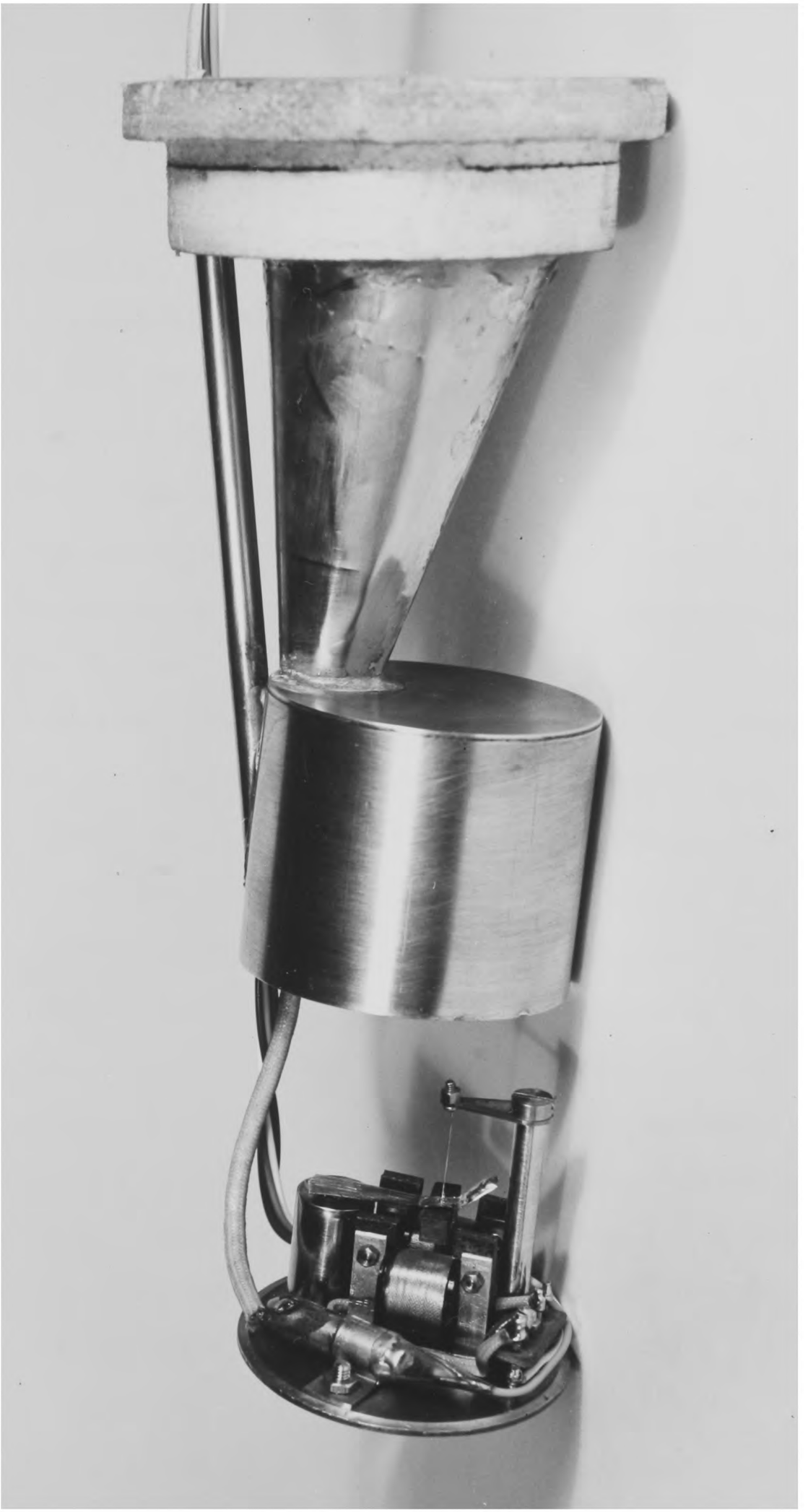


Plate 3

Chapter 4

The Radiometer-sonde

4.1 Introduction

The mechanical and optical problems which arose in connection with the use of gold-doped germanium as a practical form of infra-red detector have been dealt with in Chapter 3. There now follows a description of the way in which the detector was used as the basis for a balloon-borne radiometer-sonde suitable for the measurement of atmospheric thermal emission.

The complete instrument was designed to form part of the payload of a conventional radiosonde balloon and, as such, the total weight was limited to a few kilogrammes. In addition to the detector and chopper assembly, the apparatus had to include circuits to amplify and rectify the A.C. signal from the detector and a means for calibrating the detector against a black body at regular intervals. It also required a telemetry system to transmit information to the ground. Two prototypes were designed for use in conjunction with Kew sonde transmitters, but later models incorporated their own transmitters. A block diagram of the complete apparatus is given in fig. 4.1 and a circuit diagram in fig. 4.2.

For the purpose of description the complete sonde can be divided, broadly, into 7 sections, viz:

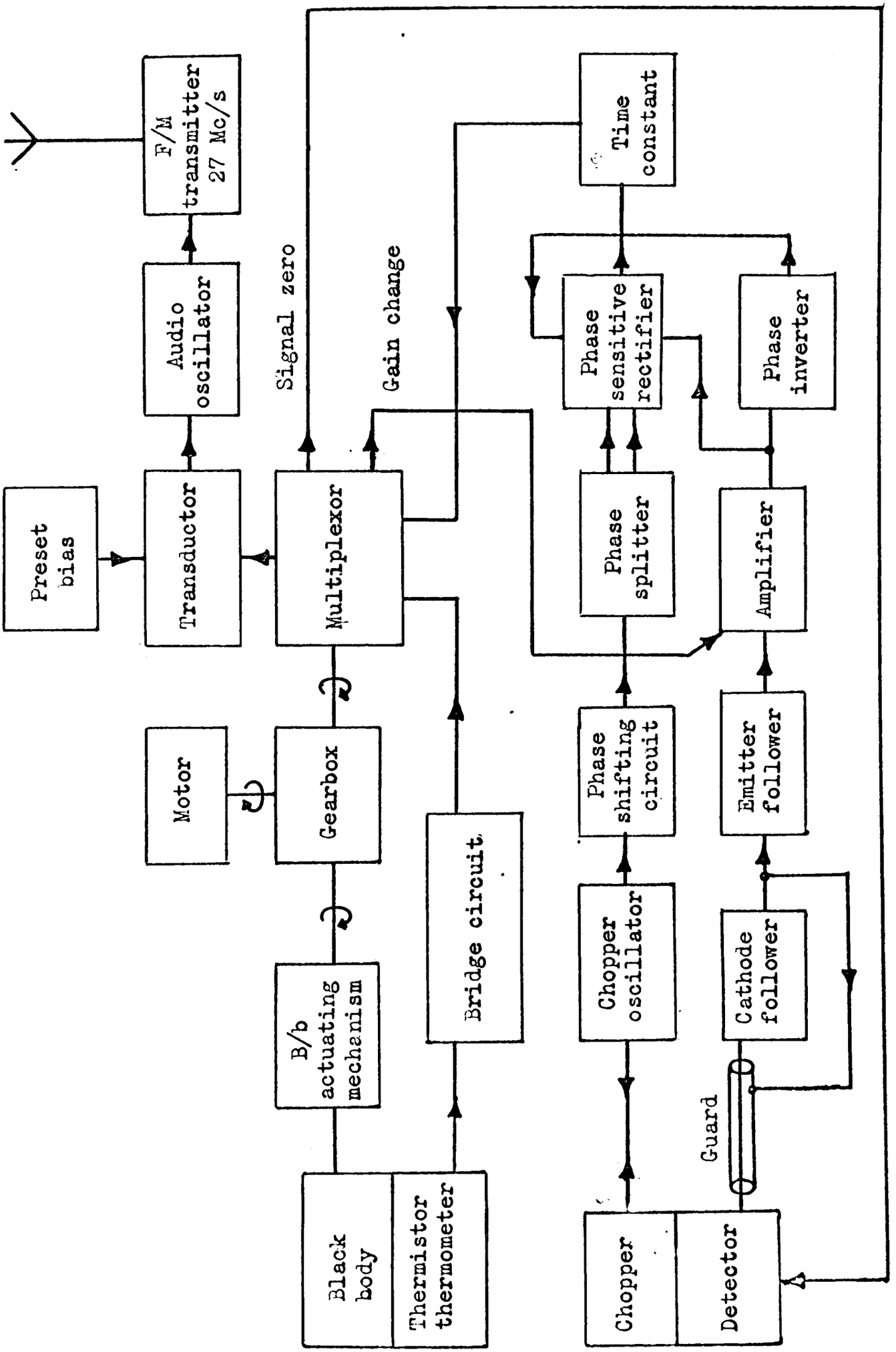


Fig. 4.1. Block diagram of radiometer- sonde.

CIRCUIT DIAGRAM OF RADIOMETER SONDE

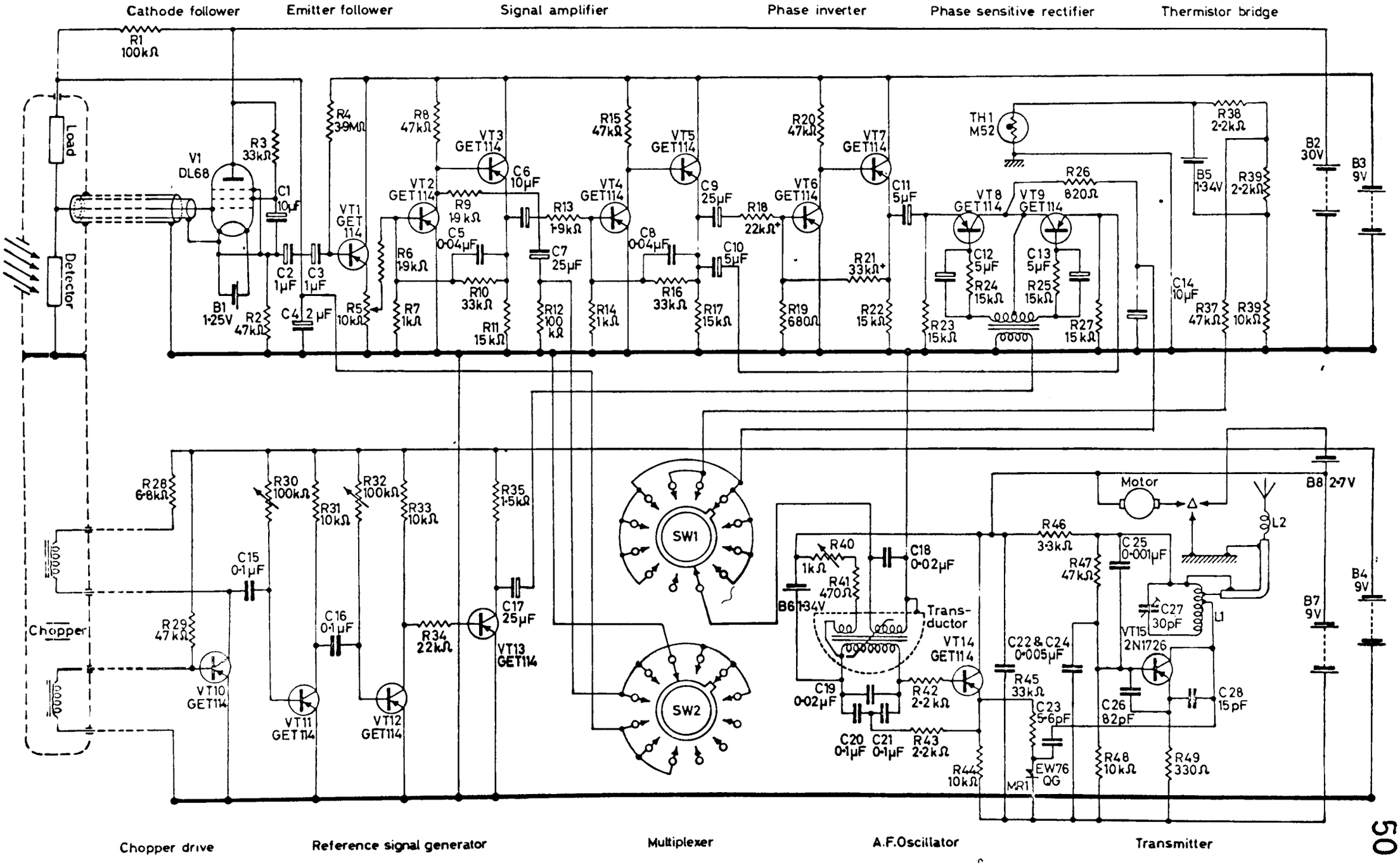


Fig. 4.2

1. Detector and chopper assembly.
2. Cathode follower and associated circuits.
3. Signal amplifier and phase sensitive rectifier.
4. Chopper drive and reference signal generator.
5. Black body and thermistor temperature element.
6. Multiplexing switches and black body mechanism.
7. Telemetry.

Of these, the detector and chopper and the chopper drive circuit have already been described: the remainder will be dealt with in turn. Many modifications to the design of the apparatus have been made since the first ascent in June 1961. While most attention will be paid, in the following account, to a description of the instrument in its final form, some of the problems which arose during early ascents will be discussed, together with the subsequent improvements which were made to the apparatus.

4.2 Circuits associated with the detector

4.2.1 Electrical properties of the detector

It was stated in the previous chapter that the electrical conductivity of gold-doped germanium changes very rapidly with temperature. This is a property of considerable importance when one comes to make use of the material as a balloon-borne detector of infra-red. The detectors which are described in Section 3.3 have a room temperature resistance of between 90 and 110 ohms. This becomes about

5×10^6 ohms when cooled to liquid air temperature and further increases by a factor of up to several thousand as the boiling point of liquid air falls during an ascent.

Interrupted incident radiation has the effect of producing small changes in the electrical conductance of the detector. By connecting the latter in series with a suitable load to D.C. supply, these changes appear as a small alternating component of the voltage across the detector. The magnitude of this voltage is proportional to the flux of incident radiation, at any given wavelength, and depends also on the resistances of both the detector and load. With the latter quantities equal, a liquid air cooled detector of the type which has been described, if operating in the laboratory from a D.C. supply of 30 V, produces a signal of about 1 mV r.m.s. when receiving room temperature radiation.

The amplitude of the A.C. signal v appearing at the detector, is given by an expression of the form:

$$v = \frac{k R^2 \uparrow}{(\uparrow + R)^2}$$

where R and $\uparrow$ are respectively the resistance of the detector and load and k is a constant. For a given detector resistance this has a maximum value when $\uparrow = R$, but for a given load resistance the signal approaches a maximum value as R tends to infinity. Thus from the point

of view of maximum output, τ and R should be equal and as large as possible. Under these conditions the sensitivity of the detector, i.e. the voltage output for a given incident flux, is proportional to the value of R.

Because the detector resistance varies by such a large factor during an ascent, it is necessary to continually vary the value of the load resistance to maintain it equal to that of the detector. This is conveniently accomplished by using a second specimen of gold-doped germanium as a load and locating it in the detector container at the same temperature as the detector. The second specimen was sealed inside a polythene tube and placed inside a μ-metal screen to shield it from the incident radiation and to prevent electrical pick-up from the chopper circuit.

4.2.2 The cathode follower

The high output impedance of the detector and load made it necessary to employ a cathode follower as the first stage of the signal amplifier. Two types of subminiature pentode, DL72 and DL68, were obtained as suitable for the purpose. Both had a filament consumption of 25 mA at 1.25 V and operated satisfactorily from an H.T. supply of 30 V. The latter voltage was chosen as being suitable for both valve and detector and could conveniently be obtained from hearing-aid batteries.

Initial experiments were carried out using the type

DL72 pentode. The valve was mounted beside the detector to reduce the length of the interconnecting lead to a minimum. It appeared to operate perfectly well at liquid air temperature. Pentode connection was found to be unnecessary and the valve was strapped as a triode, which obviated the need for a separate screen supply. A cathode load resistor of 47 kΩ was used, the overall gain of the valve being about 0.8 and the output impedance 1,600 Ω.

While the circuit worked quite well, the valve was found to suffer badly from microphony, due to vibration of the filament. This was induced by bubbling of the liquid air. The only solution to this problem was to mount the valve outside the detector container. This necessitated a screened connecting lead about one foot long, but a rough calculation suggested that very little signal would be lost as a result of the extra capacity introduced across the detector.

The circuit was used in this form for the first two flights. However, the second type of valve, DL68, was used, as it was found to be impossible to obtain further supplies of the first type. The DL68 had the advantage of being slightly smaller in size, whilst having similar electrical characteristics.

4.2.3 The emitter follower

Subsequent measurements in the laboratory indicated that a substantial loss of signal was occurring in the cathode follower as a result of loading by the comparatively low input impedance of the signal amplifier. This, together with the poor initial gain of the cathode follower, was resulting in an attenuation of signal of about a factor of 5, measured from grid to cathode of the valve. It was not possible to reduce further the output impedance of the cathode follower as this was limited by the low galue of g_m, which is a property of subminiature valves. The problem was tackled by incorporating an emitter follower stage between the valve and the signal amplifier. This effectively increased the input impedance of the signal amplifier by about a factor of 50. In addition, the capacitor which was used to couple the cathode follower to the next stage could now be reduced in size from 25 μF to 0.5 μF. The emitter follower was directly coupled to the input of the signal amplifier which avoided the use of a large capacitor at this point.

4.2.4 Reduction of input capacitance by the use of a guard

After two further ascents following the incorporation of the emitter follower, the input circuit was further improved. There was evidence that the capacitance of the detector lead was having a greater effect than had

originally been anticipated. Measurements made on a detector assembly mounted in an atmospheric chamber showed that a large phase shift was being introduced into the output of the detector when the resistance of the latter became large at low pressures. As a phase sensitive rectifier was being employed, the phase shift was resulting in a considerable reduction in the rectified signal.

The net current appearing at the output of the phase sensitive rectifier, as a function of detector resistance, can be calculated as follows. It is assumed that a given incident flux of radiation results in a constant change in the conductance of the detector. This assumption is valid provided the mobility of the impurity carriers in gold-doped germanium remains constant. This will be approximately true over the small range of temperature which is being considered. The voltage signal appearing at the detector will be proportional to the detector resistance R. The D.C. output from the phase sensitive rectifier for a given amplitude of applied A.C. voltage will depend on $\cos\phi$, where ϕ is the phase angle between the reference and signal voltages. Combining these two effects, the rectified output for a given flux will be proportional to the factor

$$\frac{R}{1+\omega^2C^2R^2}$$

where C is the total capacity across the detector and ω the angular frequency of the chopper. This has a maximum value when $R = 1/\omega C$. Putting in a value for C of 100 pF, which was the measured capacitance of the input lead, it can be seen that maximum sensitivity occurs when $R = 40 M\Omega$ During an ascent, the detector resistance would reach this value at a height of about 7 km, which is long before maximum sensitivity is required.

As the length of the detector lead could not conveniently be made any less, its effective capacitance was reduced by connecting the screen round the lead to the cathode of the valve. By feeding back a voltage which was nearly the same as the signal voltage on the centre conductor of the lead, the effective capacity to earth of the lead was reduced to a value $(1-A)C$ where C is the actual capacity of the lead and A the gain of the cathode follower. The latter was made as near as possible to unity by reverting to pentode connection. This increased the amplification factor of the valve by about a factor of ten and put up the gain of the cathode follower to a value of 0.93. Thus the capacity of the lead was reduced from 100 pF to an effective value of 7 pF. Fig. 4.3 shows the results of measurements made with the detector assembly in the atmospheric chamber and illustrates the difference between the performance of triode and pentode

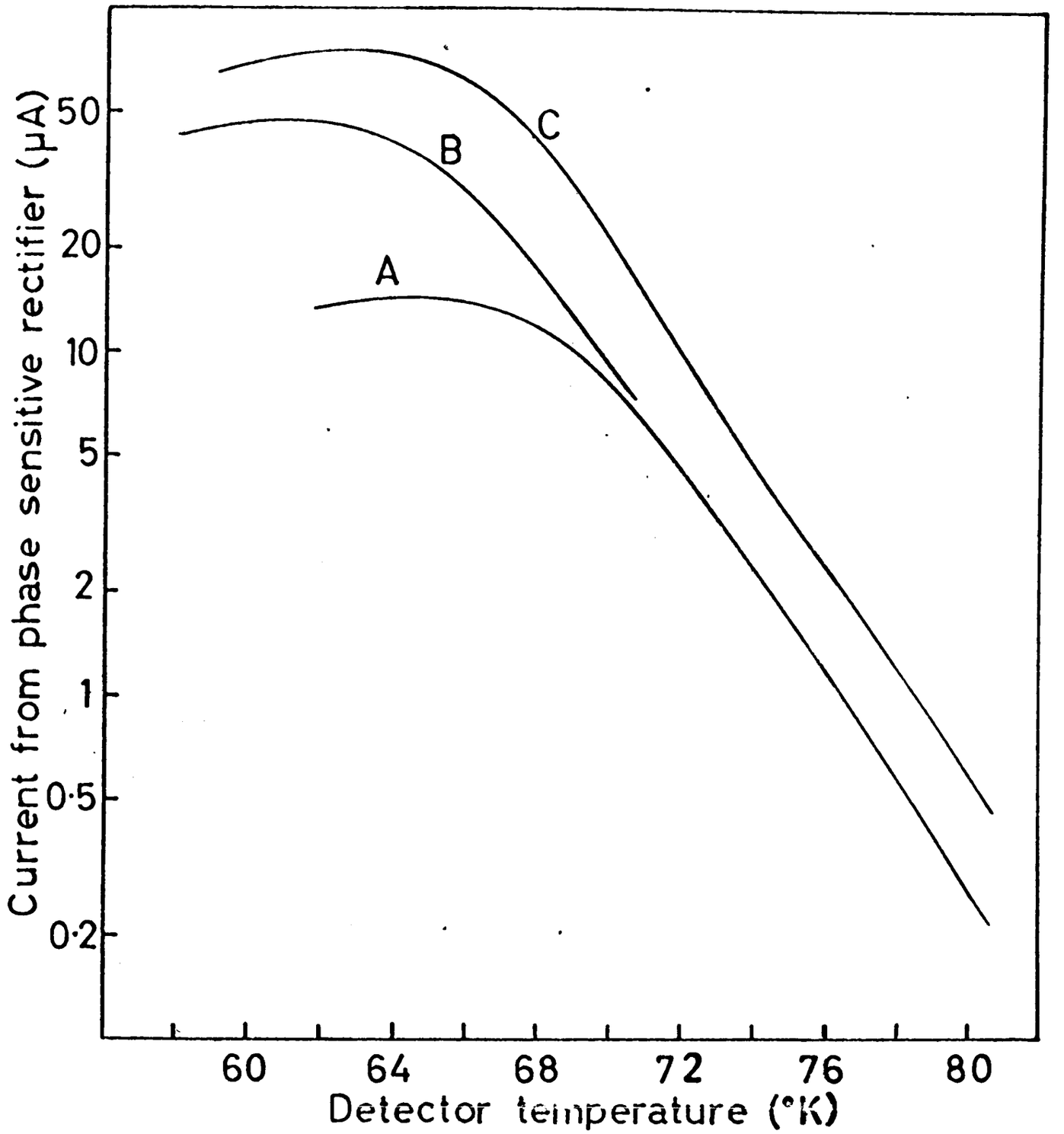


Fig. 4.3. Performance of detector in conjunction with various cathode follower circuits.

A. Simple triode connection

B. Triode connection with guard

C. Pentode connection with guard

cathode followers and the effect of the guard on the input lead.

It was found that it was still necessary to have an earthed screen around the signal lead, as the impedance to earth of the guard was not sufficiently low to prevent pick-up from occurring, especially owing to the close proximity of leads associated with the chopper circuit. A length of double screened lead was therefore used, the inner screen acting as the guard, the outer one being earthed. The final form of the detector and amplifier input circuit can be seen in fig. 4.2.

4.2.5 Automatic Gain Change

Owing to the large difference in magnitude between the flux of radiation received from the sky and that from the black body employed for the purpose of calibration, it was necessary to reduce the gain of the signal amplifier when the latter was being measured. It was also considered desirable to make a measurement of the sky radiation on two gain settings to guard against the risk of the signal becoming too large. On the first two ascents the gain change was achieved by shunting the output of the cathode follower with a suitable resistance in series with a large capacitor. The latter was included to avoid disturbing the D.C. conditions of the circuit. The capacitor was of a sufficient size to ensure that its impedance at 40 c/s

was negligible compared with that of the shunt resistance. The arrangement is illustrated in fig. 4.4. For practical reasons it was necessary that the gain change should be accomplished by a switch, one side of which was earthed.

After the guard screen had been added to the detector lead, the above method of achieving the change in gain was unsuitable, as it prevented the action of the guard from taking place. This problem was overcome by incorporating the gain change in the first stage of the signal amplifier, by loading the collector of the first transistor in the same way as had previously been done on the cathode of the valve. This method proved quite satisfactory in all subsequent ascents.

4.2.6 Zero signal measurement

In order to allow for the fact that the absence of radiation on the detector might not necessarily correspond to zero output from the phase sensitive rectifier, it was necessary to provide a separate zero signal measurement. The best possible way of achieving this would be to cut off the incident radiation by means of a shutter at the same temperature as the chopper. This would be difficult to achieve in practice and the following method was adopted. The D.C. supply to the detector was connected via a 100 kΩ resistor and a 2 μF decoupling capacitor (fig. 4.4). By

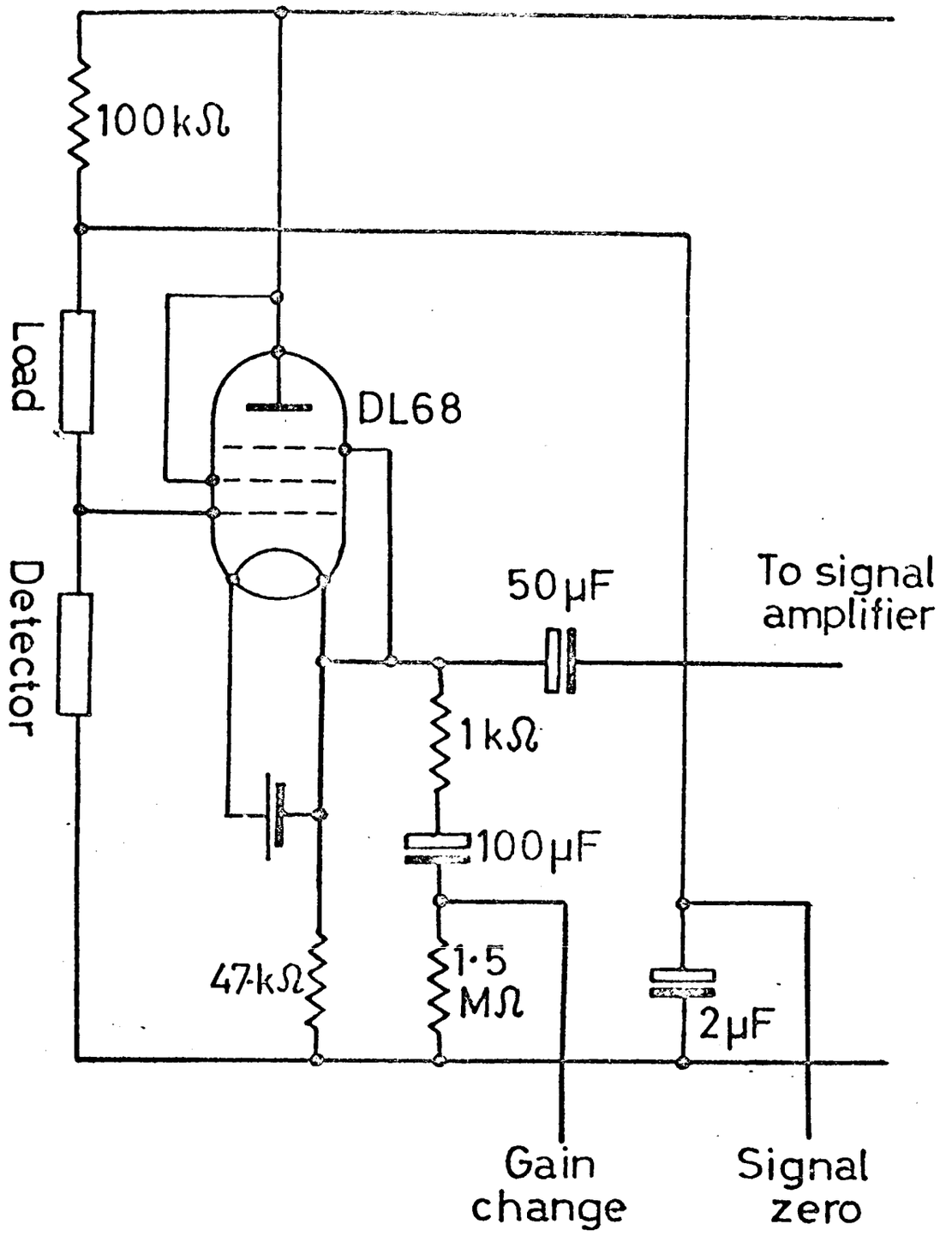


Fig. 4.4. Circuit of cathode follower in its original form illustrating the method of obtaining a zero signal measurement and an early type of gain change.

short circuiting the capacitor the supply to the detector could be removed without unduly loading the 30 V battery. Thus the detector could be rendered inoperative without breaking any electrical connections in the input circuit. This was important, as it was found that a certain amount of electrical pick-up from the chopper circuit occurred at the detector and contributed to the net output from the phase sensitive rectifier. It was essential that this pick-up should be present in exactly the same form when the zero measurement was being made.

The validity of the electrically simulated zero was checked by comparing it with the true zero in the atmospheric chamber at pressures ranging down to 20 mb. The true radiation zero measurement was made by covering the entrance aperture of the detector container with a small copper disk at liquid air temperature. The output from the phase sensitive rectifier was measured in each case and the results are shown in fig. 4.5. It can be seen that the net output is, in general, not zero. At low pressures the departure from zero amounts to about 1.3 μA which represents nearly 10% of the whole working range of the phase sensitive rectifier. However, the difference between the outputs corresponding to the two zeros was nowhere greater than 0.3 μA which, in fact, is of the same magnitude as the error which arises in the telemetry of

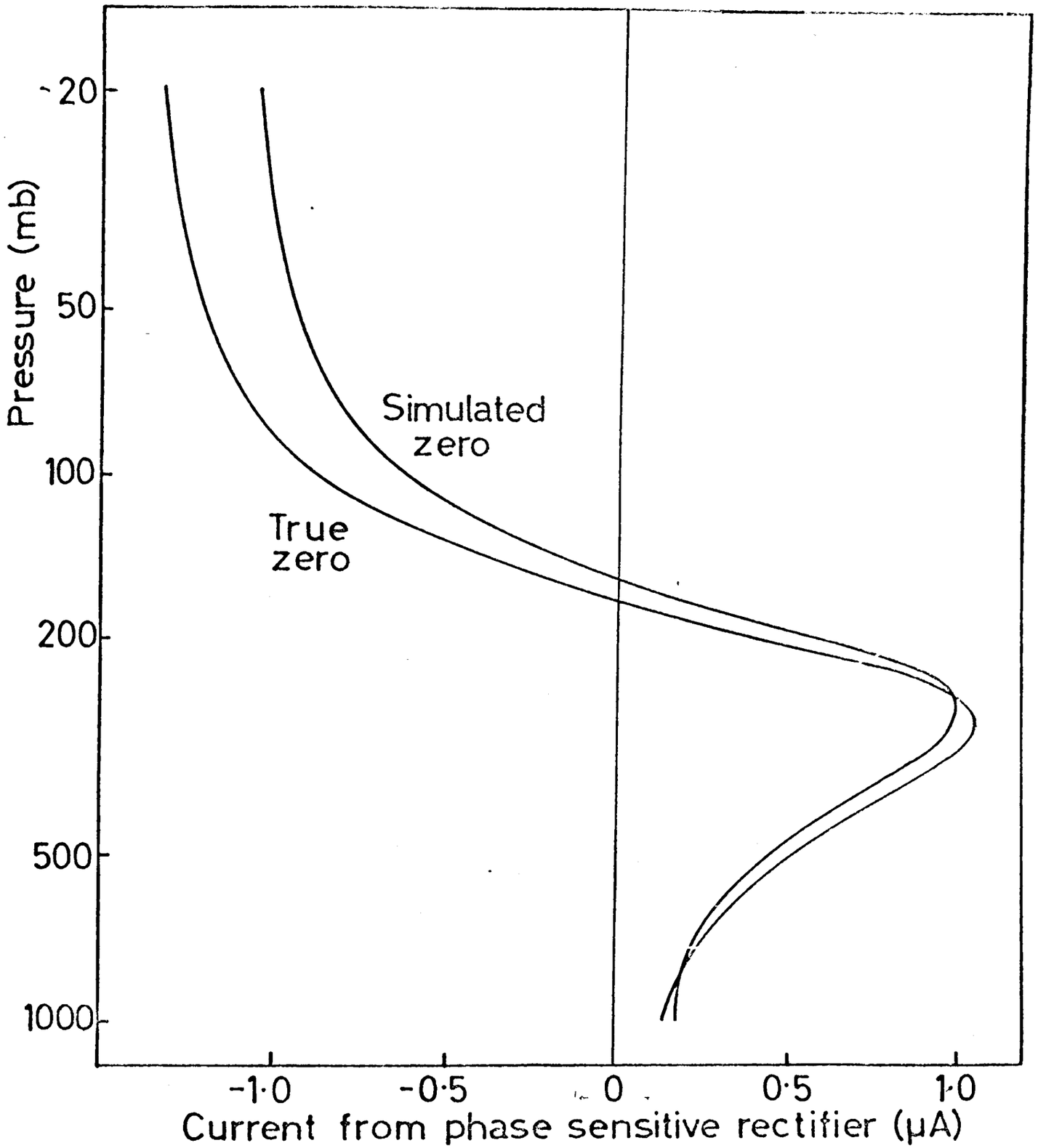


Fig. 4.5. Comparison of zeros.

detector signals.

It will be noticed that the zero is also operated by means of a switch, one side of which is connected to earth. Both the zero and the gain change are, in practice, operated by a common rotary switch. This is described in more detail in a later section.

4.3 Signal amplifier and phase sensitive rectifier

4.3.1 Basic amplifier circuit

When faced with the problem of designing a signal amplifier, it was only possible to make a rough estimation of the degree of amplification required. The effective emissivity of the stratosphere in the 6.3 μ band at about 16 km was anticipated to be only a few percent. Further, it was judged that the detector sensitivity at this height would be some 50 times greater than at ground level, whereas the rate of emission of energy from a black body at ground level would be 10 or 20 times greater than from one at stratospheric temperature. Thus, the net signal produced by the detector at 16 km would perhaps be 20% of its value at ground level. It was therefore considered that the degree of amplification should be such that the rectified signal, due to room temperature radiation at ground level, represented the upper limit of the telemetry. This would necessitate a signal amplifier with a gain of about 100. According to this estimation, stratospheric

signals would be readily measurable. However, to give added flexibility, it was decided to incorporate a gain control on the amplifier input.

The most important consideration in the design of the signal amplifier was good linearity. For this reason considerable negative feedback was incorporated in the circuit.

The basic unit of the amplifier is a direct coupled two transistor combination of grounded emitter and emitter follower which incorporates the advantages of the high gain of the former with the low output impedance of the latter. The circuit is shown in fig. 4.6 and is similar in many respects to one described by Avery and Bowes (1958). A.C. and D.C. negative feedback are provided by the network consisting of R_1, R_2 and R_4, whilst the capacitor C_1 increased the feedback at high frequencies. The capacitor C_2, which provides coupling to the next stage, results in attenuation at low frequencies. By a suitable choice of component values the circuit can, in effect, be broadly tuned to a centre frequency of 40 c/s.

Two stages of the basic circuit provide a gain, at signal frequency, of about 100, the value decreasing outside the pass band at 12 db/octave to give the frequency response curve which is shown in fig. 4.7. The linearity

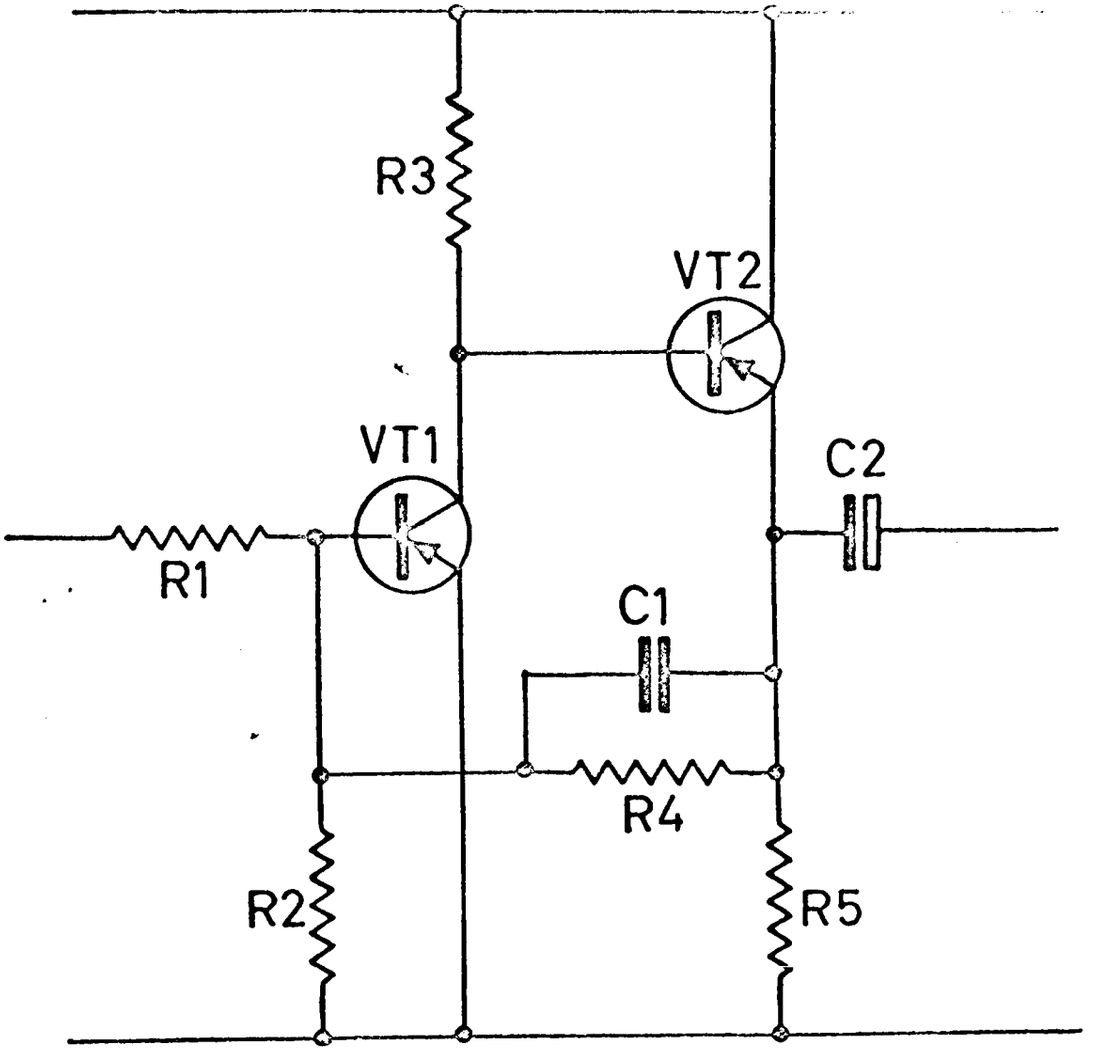


Fig. 4.6. Basic circuit of signal amplifier.

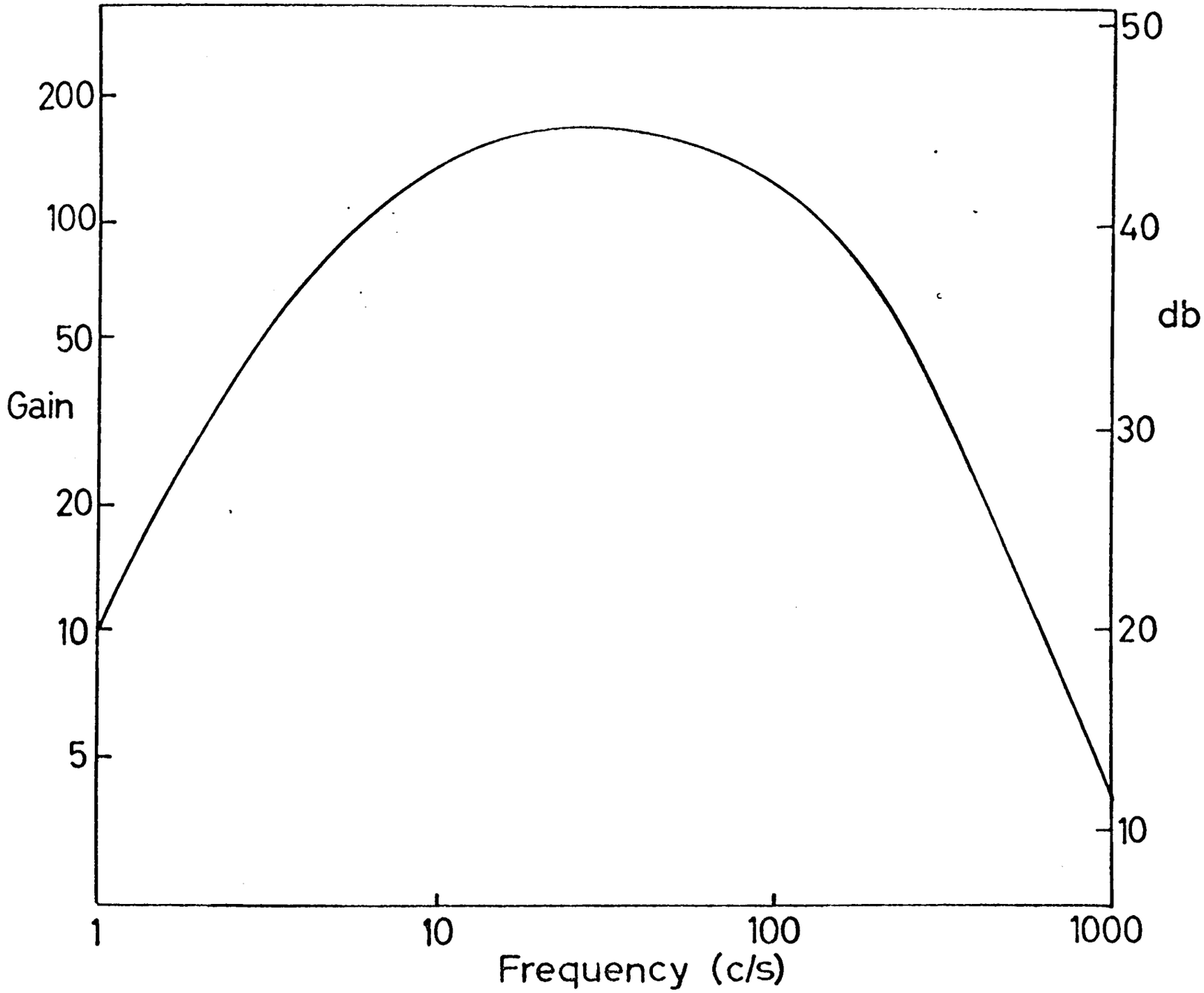


Fig. 4.7. Frequency response of complete signal amplifier.

of the circuit was found to be very good up to an output of 1 V r.m.s. This was about ten times larger than the maximum signal anticipated.

4.3.2 The phase inverter

After amplification, the detector signal was synchronously rectified to produce a direct current of a few microamperes which was subsequently telemetered. The first prototype sonde employed a half-wave rectifier, but this was later modified for full-wave operation. The latter type only will be described.

An anti-phase signal is derived from an inverter which is similar in design to the basic circuit described above. The degree of negative feedback, in this case, is increased to provide a stage gain of unity. The exact figure is achieved by adjusting the value of R_1 or R_4, depending on whether the gain is too large or too small. By filing away a portion of the appropriate resistor, its value can be increased. The feedback capacitor is omitted and the circuit is coupled to the signal amplifier with a capacitor of a sufficiently large value to ensure that no extra phase shifts are introduced. The anti-phase signal is fed to one input of the full wave rectifier, the other being connected directly to the signal amplifier.

4.3.3 The phase sensitive rectifier

Avery and Bowes (1958) describe a half-wave phase sensitive rectifier using a pair of transistors operating as switches. A circuit of similar design was used on the first prototype sonde. It was realised, however, that the efficiency of rectification could be improved by a factor of two and a smoother rectified output obtained if a full-wave circuit was employed. Such an arrangement is illustrated in fig. 4.8 and is the form used on all subsequent sondes.

The transformer T_1 is driven by the output stage of the reference circuit and supplies anti-phase square waves to the bases of the two transistors. Alternately, this causes one transistor to be brought into conduction whilst the other half is cut off. Each input is thus connected in turn to the rectifier output circuit. The phasing of the reference signal is such that the negative half cycles are selected. A direct current is thereby produced. This is smoothed by the resistance-capacity combination R_1C_1 and flows into the telemetry circuit which has a resistance of 4.5 kΩ. The value of the current i μA produced by the rectifier for a given applied r.m.s. voltage v mV is given by

$$i = \frac{2\sqrt{2}}{\pi} \times 10^3 \cdot \frac{v}{R}$$

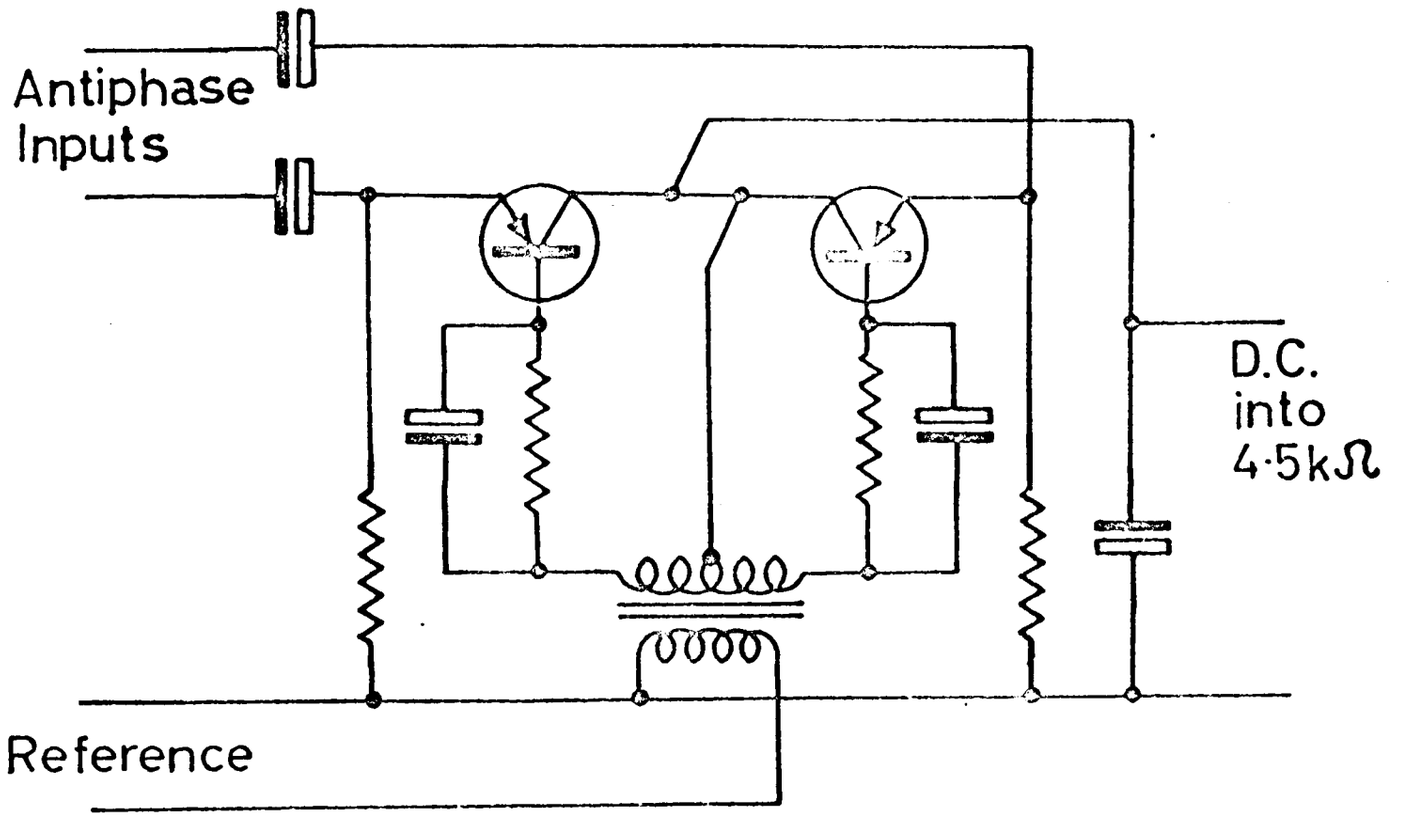


Fig. 4.8. Full wave phase sensitive rectifier.

where R is the total resistance of the load in the output circuit of the rectifier. In the circuit shown, the value of R is about 5.3 kΩ and the effective conductance is, therefore, 0.17 μA/mV.

Considerable effort was made to ensure that the rectifier circuit was linear. The transistors were selected for low collector leakage current and were employed with the roles of emitter and collector reversed. Under these conditions the current gain is only slightly greater than unity, but the leakage current is reduced to a negligible amount. The gain is, in any case, unimportant as the transistors are only required to act as switches. The resistor-capacitor combinations in the arms of the transformer secondary were added to increase the dynamic range of the rectifier. In an earlier circuit, the base of each transistor was directly connected to the transformer secondary. During the half cycle when the base is driven positive with respect to the collector, the transistor is cut off, provided the signal applied to the emitter does not drive the latter positive by an amount which exceeds the excursion of the base. If this does happen, the transistor will come into conduction again and will begin to nullify the effect of the other input.

This effect occurred in the early circuit and gave rise to non linearity when large signals were applied.

It was not, however, possible to increase the output of the secondary without employing a larger transformer. The following proved to be a satisfactory solution to the problem.

A capacitor was connected between the transformer and the base of each transistor. During the half cycle when the base was driven negative with respect to the collector, the capacitor became charged to half the peak-peak voltage of the transformer secondary. On the positive half cycle, the capacitor was effectively in series with the output of the transformer, with the result that the base was driven positive to the extent of the full transformer output instead of only half the value as in the original circuit. However, without a leakage path for the capacitor, the latter remained charged and the base of the transistor was consequently not driven into conduction during subsequent negative half cycles. A resistor was therefore connected in parallel with the capacitor and the time constant of the combination adjusted to about four times the half period of the reference square-wave. The linear range of the rectifier was thus slightly less than the full peak-peak value of the transformer output, but this proved to be quite adequate.

The measured non-linearity of the combined signal amplifier, phase inverter and phase sensitive rectifier was

less than 1% over the full working range. The complete circuit diagram can be seen in fig. 4.2.

4.4 The reference signal generator

4.4.1 The circuit in its original form

The operation of the vibrating vane chopper has been described in section 3.6. One advantage of this type of chopper is the fact that a reference signal at chopper frequency is directly available from the driving circuit. It is therefore not necessary to employ a pick-up. This, in any case, would have been difficult, owing to the particular design of the chopper.

The waveform at the collector of the drive transistor is approximately square, but is 90^{o} out of phase with the corresponding signal from the detector. It is therefore necessary to incorporate a phase shifting circuit in order to provide the correct reference signal for the phase sensitive rectifier. Because of the comparatively low frequency it was considered that a delay circuit would be the best approach to the problem. The required delay was about 6 milliseconds.

The first type of circuit used is shown in fig. 4.10. The chopper waveform (fig. 4.11 (i)) is applied to an integrating circuit R_1C_1 which has a time constant of the same magnitude as the period of the oscillation. The resulting waveform at A is that shown in fig. 4.11 (ii)

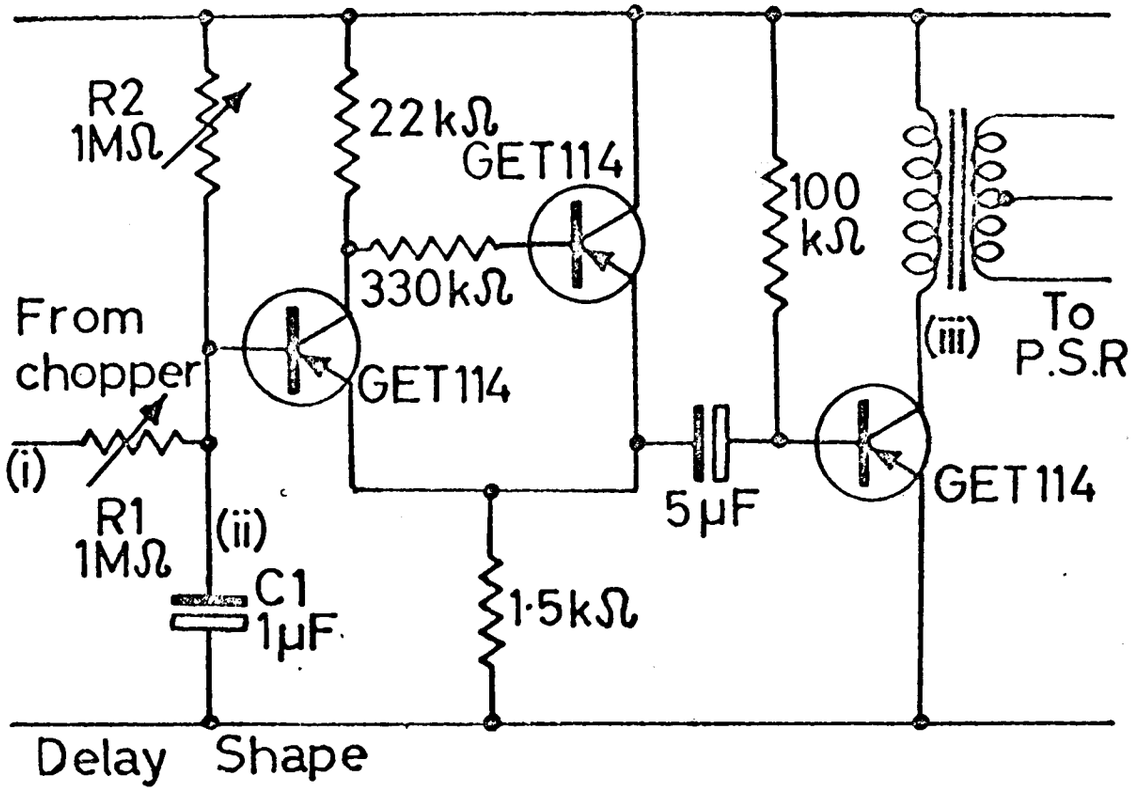


Fig. 4.10. The original phase shifting circuit.

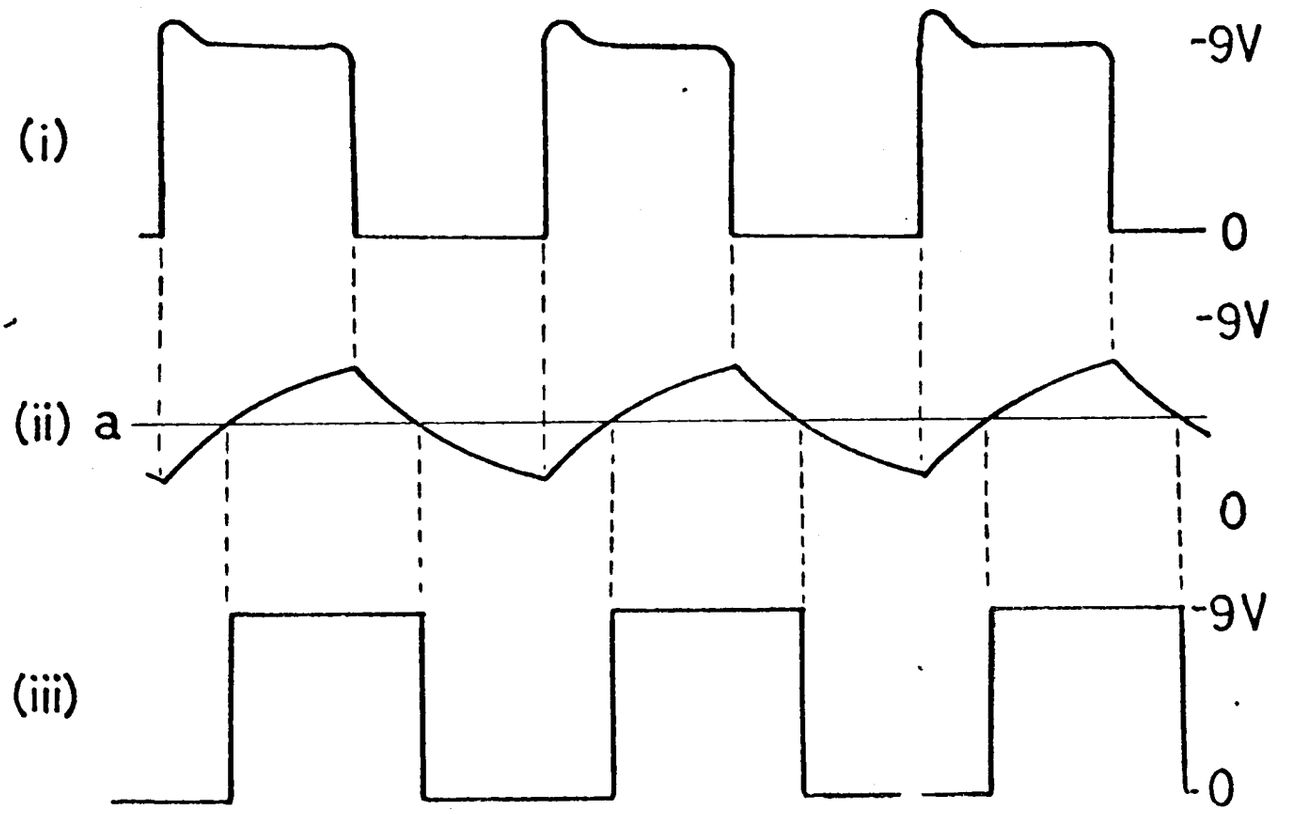


Fig. 4.11. Waveforms associated with the original phase shifting circuit.

and is used to control the operation of an emitter coupled Schmitt trigger circuit. This type of circuit has two stable states and can be made to switch from one to the other by altering the voltage level at the base of the first transistor. This is adjusted by R_2 and corresponds to (a) in fig. 4.11 (ii). The circuit switches whenever the input voltage crosses the level (a). Strictly speaking, the levels at which the switching occurs are different for the two directions of operation and this results in a certain amount of 'backlash'. However, in practice this can be made so small that it can be neglected. The output is taken from the common emitter point of the trigger circuit and is amplified by the output transistor which drives the transformer, providing anti-phase outputs to the phase sensitive rectifier.

The waveform at the collector of the output stage is shown in fig. 4.11 (iii). It can be seen that it is delayed with respect to the chopper waveform. The level of (a) is set with R_2 so that the output waveform is square. Alteration of R_1 will affect the time constant of the integrator and thereby alter the delay. In this way, a reference signal of correct phase can be obtained.

The circuit appeared to perform its function satisfactorily although it was sometimes rather difficult to set up. However, it was employed, basically in the

form described, in sondes used for the first eight ascents.

4.4.2 Reasons for abandoning the original circuit

The malfunctioning of some of the early ascents, notably ascents 4 and 5, was difficult to explain at the time. At a certain point during the flight the sensitivity of the detector appeared to rapidly diminish and, at the same time, the zero signal level began to drift from its normal position. The effect occurred after about 30 minutes on ascent 4 and after only 8 minutes on ascent 5. There were also some unusual digressions of the zero signal level on ascents 6 and 8 at about 35 and 45 minutes from launch, respectively. In each case, one or more of the signals appeared to fall below the zero level.

It was difficult to explain the cause of this sudden and consistent malfunctioning of the apparatus. The possibility of its being an effect of temperature was investigated. There was good reason for believing that the thermal insulation provided on the apparatus was effective. The transductor, a component of the telemetry (see section 4.6), possessed a temperature coefficient, the value of which was known (see Jones, Maddever and Sanders (1959)) and which resulted in a steady drift of the telemetered signals with temperature. Examination of the records of a number of ascents showed that the ambient temperature inside the sonde did not fall by morethan 3°C during the

first 25 minutes of the flight and that the total cooling was, at the most, 15°C after 50 minutes. In every case of malfunctioning the unusual effects occurred within this time. However, tests were carried out in the laboratory on various component parts of the circuits, notably transistors, to see whether or not this amount of cooling was important. In the case of the amplifier and phase sensitive rectifier no significant effect was observed, but the phase shifting circuit was found to be sensitive to a very small change of temperature. The first effect of this was to alter the mark-to-space ratio of the reference signal and further cooling caused the circuit to stop triggering altogether.

This could have explained the unexpected behaviour of the early ascents. An improved delay circuit was subsequently devised which did not exhibit these undesirable characteristics and was used on the last four ascents.

4.4.3 The second phase shifting circuit

The second circuit is shown in fig. 4.12. At first sight it appears to be a conventional two stage transistor amplifier with fixed bias, but it operates in rather an unconventional fashion which is best described by reference to fig. 4.14. This shows one half of the main circuit. In the quiescent state the transistor is held in a bottomed condition by current flowing from the base through R. The

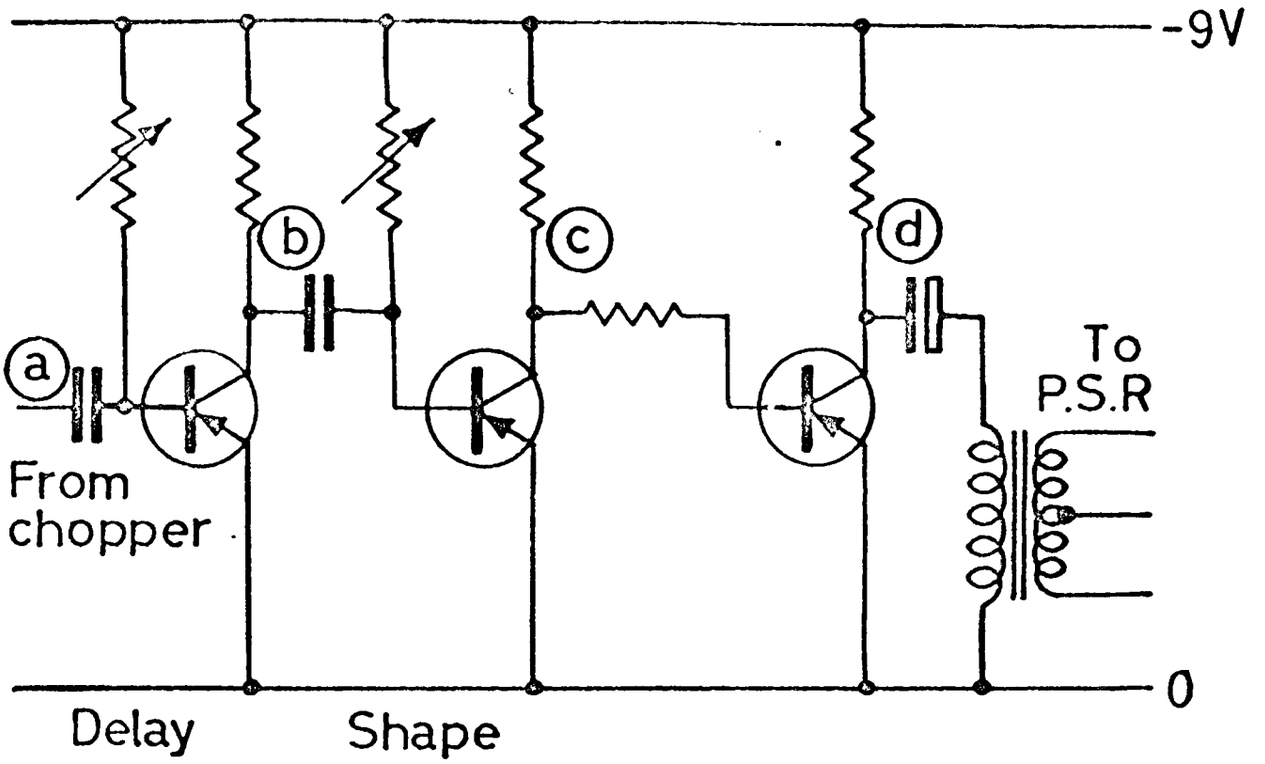


Fig. 4.12. The improved phase shifting circuit.

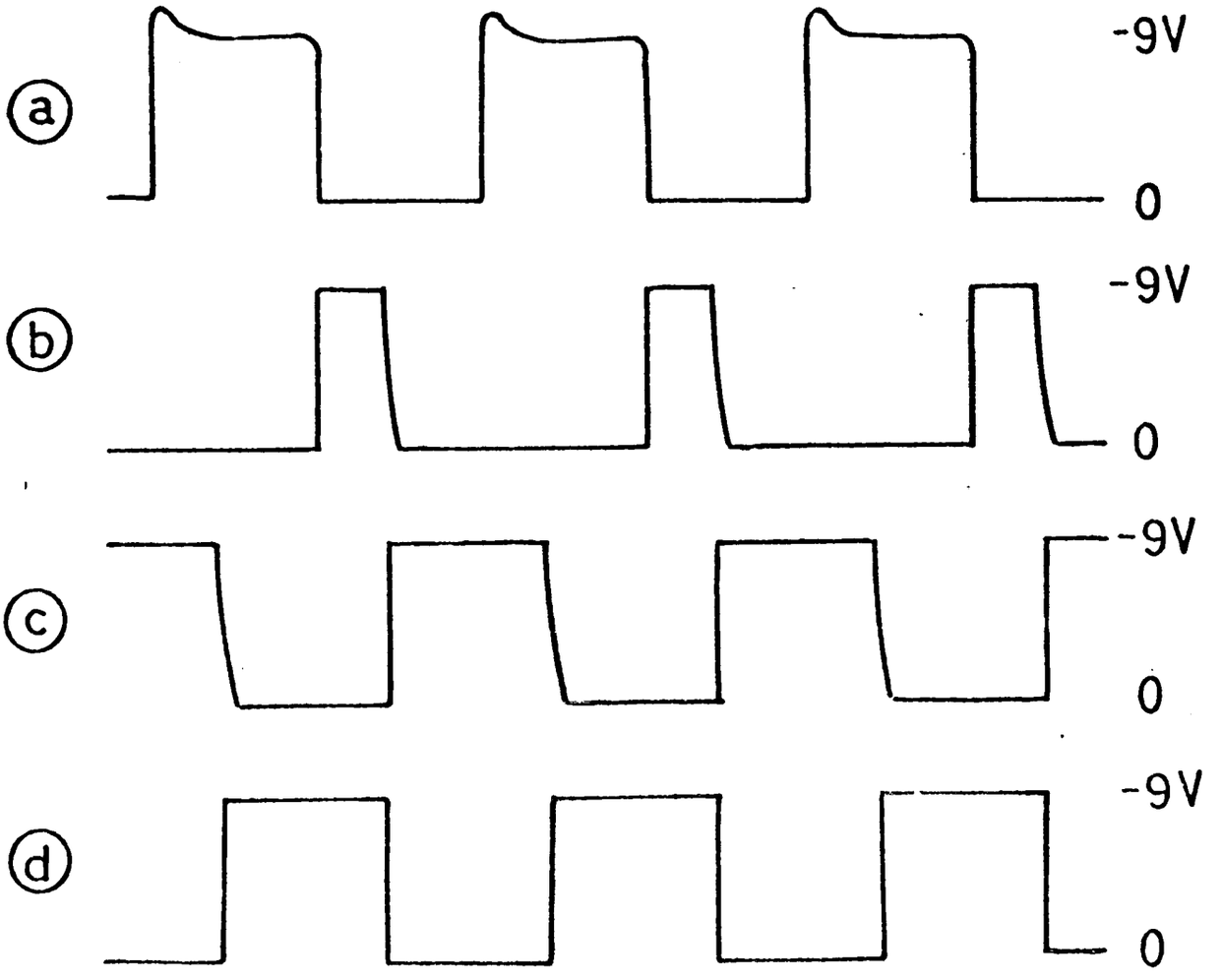


Fig. 4.13. Waveforms associated with the improved phase shifting circuit.

collector is thus at a low potential. If the point X is now driven negative, the capacitor C is charged through the base-emitter path of the transistor. No effect will be observed at the collector as the transistor is already conducting heavily. When the point X is brought down to ground potential the base will be driven positive to the extent of the excursion in X, and the transistor cut off. In this condition, the base-emitter impedance is very high. The capacitor therefore begins to discharge through the resistance R, so that the base potential begins to rise towards the negative supply voltage with a time constant CR. When this potential approaches that of the emitter, the transistor will begin to conduct once again and will quickly reach bottoming condition, being held there by current through R. Conditions are now as they were at the beginning and may be repeated continuously by the application of a square wave to the input X.

Provided the time t during which the capacitor discharges is less than half the period of the square wave applied to the input, the output Y from the collector will be a series of negative pulses of width t, whose leading edge corresponds to the positive going edge of the square wave (fig. 4.15). If t is greater than half the square wave period, the transistor will be driven into conduction by

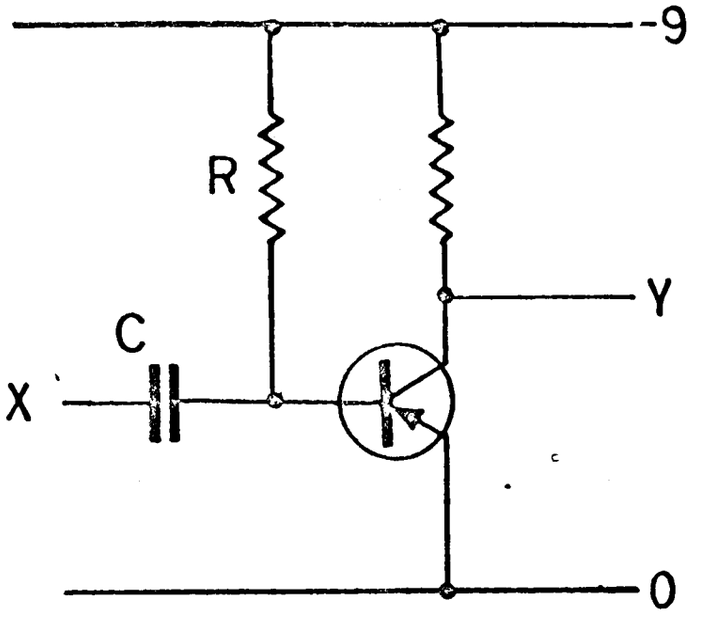


Fig. 4.14. Basic delay circuit.

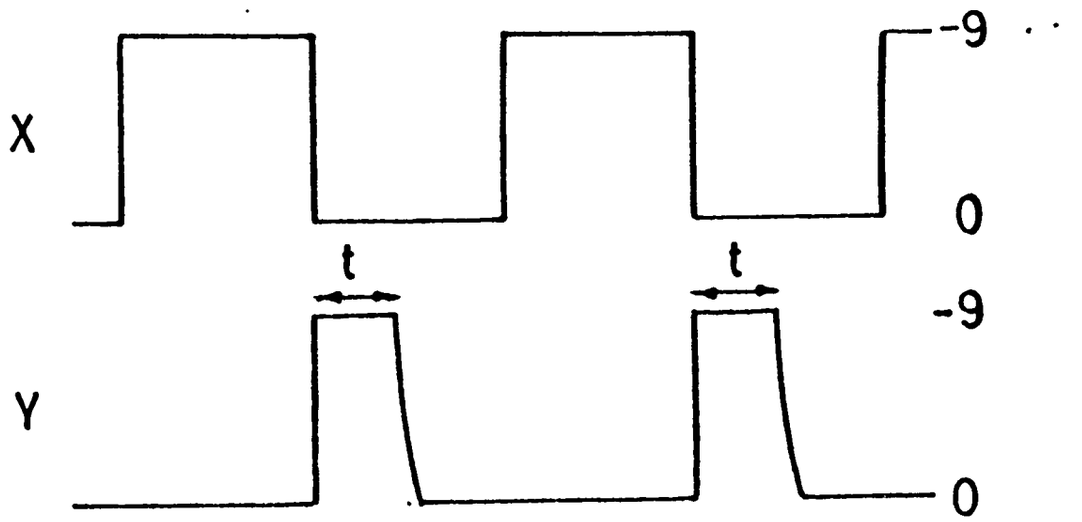


Fig. 4.15. Waveforms associated with the basic delay circuit.

the negative going edge of the input, with the result that the output will simply be an anti-phase version of the input. In fact, the circuit now behaves as a conventional resistance-capacity coupled amplifier.

The trailing edge of the collector output when a short time constant is used, is a small portion of an exponential curve with a time constant CR and an amplitude twice the supply voltage (assuming that X has a peak-peak amplitude also equal to the supply voltage). This is indicated in fig. 4.15. Owing to gain in the transistor, however, the curvature is so small that the trailing edge can be regarded as vertical. Thus, the circuit behaves as a delay to the negative input edge.

To provide an effective delay circuit of the type required, two such circuits are coupled together. The second provides a delay T between the negative edge from the previous stage and its own negative edge. If T is made equal to the half period of X, the result will be a square wave of the same period as X, but delayed by an amount t. The sequence of events is illustrated in fig. 4.13.

The circuit is virtually insensitive to temperature variations, because the delay times are determined by time constants independent of transistor parameters such as collector leakage current.

The delayed square wave was fed to an output stage as in the original phasing circuit. The output stage differed from the previous one in that the transformer was capacitively coupled to the collector instead of directly forming the collector load. Steady current flowing in the transformer primary considerably reduced its inductance. This resulted in a deterioration of the low frequency performance of the transformer and caused distortion of the square wave.

4.5 Black body and temperature element

For the purpose of providing calibration during an ascent, use was made of a local black body at a known temperature. This was moved into the field of view of the detector for about ten seconds each minute and the resulting signal, together with a knowledge of the black body temperature, enabled the sensitivity of the detector to be calculated.

Fig. 4.16 illustrates the black body and the mechanism which is used to actuate it. The former, in the shape of a hollow cone 2.5" in diameter and 2.25" high, is constructed of 0.004" thick copper foil mounted on a stout ring attached to a 6" pivoted arm. It is mounted on the top of the apparatus and is operated by a small crank which protrudes through the top plate. The crank is driven at

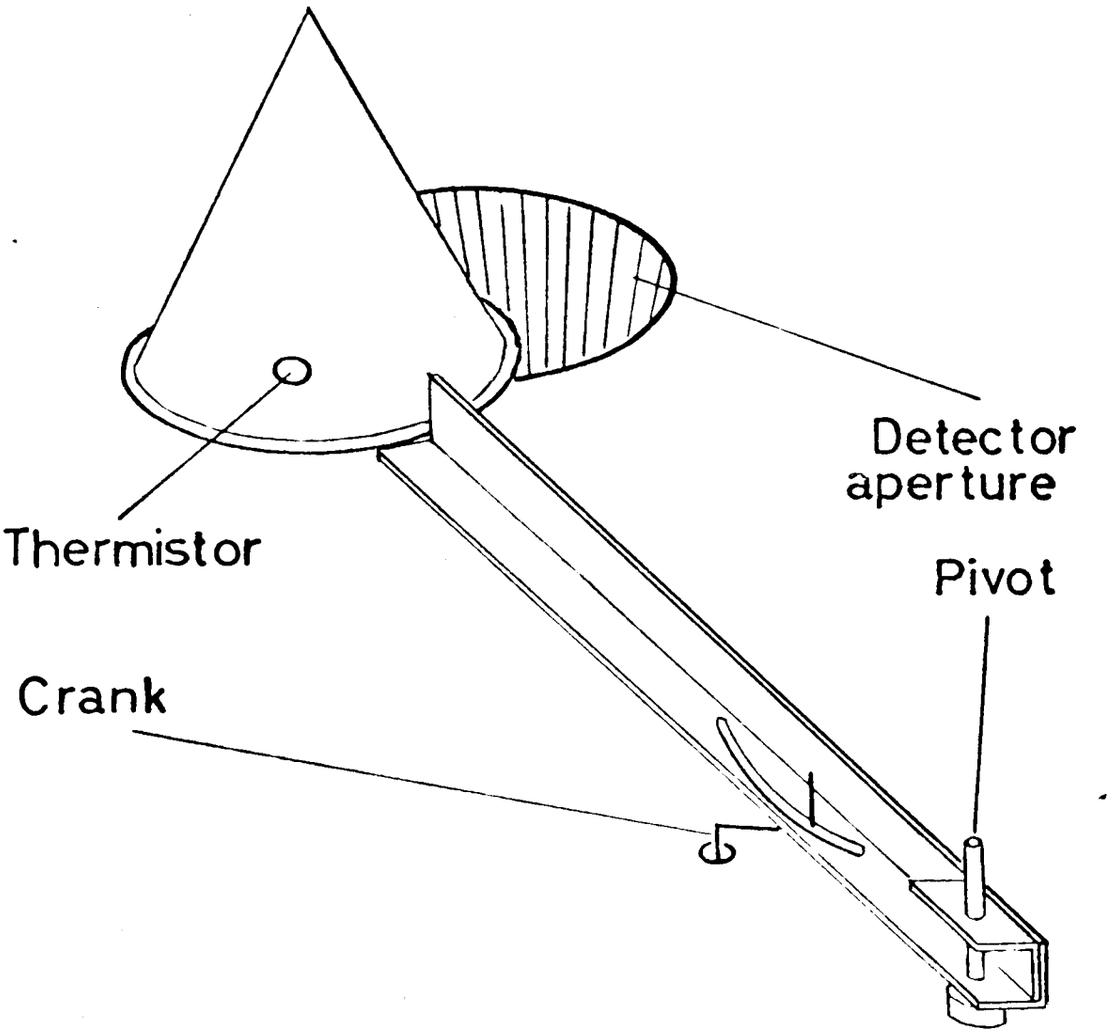


Fig. 4.16. Black body and actuating mechanism.

one revolution per minute by a small motor and gearbox and moves in a curved slot cut in the black body arm so that the latter is driven from side to side once during each revolution. The shape of the slot is such that the black body does not move symmetrically about its centre position, but rests for most of the time at one side, moving rapidly across to cover the detector aperture for the required period. Nevertheless, a certain time is required by the mechanism to move the black body in and out of position and use is made of this time to transmit two other signals which do not require the operation of the detector.

Although the black body cone is open to the air, it is not safe to assume that it is always at air temperature. It is therefore necessary to provide some means of measuring its temperature during an ascent. For this purpose, a small thermistor of the type designed for surface temperature measurement was soldered to the outside of the black body cone. The type used had a resistance at 290°K of about 500 Ω which increased more or less exponentially as the temperature was reduced, becoming about 10 kΩ at 220°K.

The thermistor is incorporated in the simple Wheatstone bridge circuit shown in fig. 4.17. The bridge is powered by a Mallory cell type RM 625 which has an e.m.f. of 1.34 V. These cells maintain their e.m.f. constant to within a fraction of a percent during discharge, providing the 100

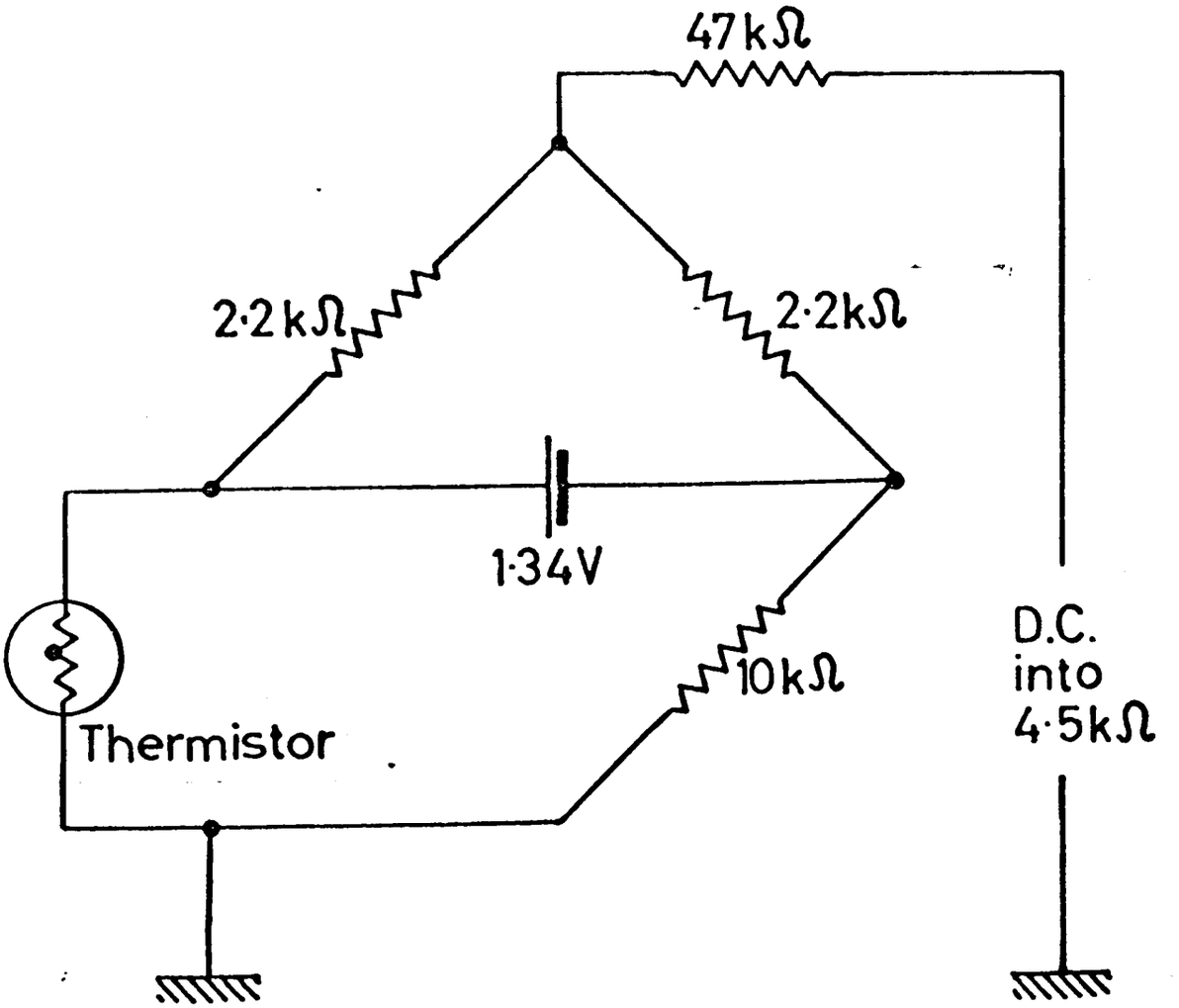


Fig. 4.17. Thermistor bridge circuit.

hour rate is not exceeded. The capacity of the D 625 is 250 mAh and the maximum current taken by the bridge is about 0.25 mA, which allows a good margin of safety.

As the resistance of the thermistor varies with temperature, it changes the out-of-balance current of the bridge, which is the quantity telemetred.

The relationship between the out-of balance current i in a Wheatstone bridge and the resistance R in one arm is of the form

$$i = \frac{aR - b}{cR - d}$$

where a, b, c and d are constants dependent on the resistance in the other arms of the bridge, the load resistance and the driving voltage. The gradient of this expression, which represents the sensitivity of the circuit to changes in thermistor resistance, is a maximum when $R = 0$ and tends to zero as R increases. The shape of the curve is approximately logarithmic over a small range and by suitable choice of component values can be made to compensate, to a large extent, the exponential resistance-temperature law of the thermistor. The result is that the current produced by the bridge into the load is very nearly a linear function of temperature over a certain range. However, in order to produce maximum sensitivity at low temperatures, complete linearity over the whole range of

measurement was not possible.

Each temperature element was calibrated against a copper/constantan thermocouple mounted beside the thermistor. For this purpose, a 4.5 kΩ load replaced the telemetry circuit and the output current flowing into the load was measured as the temperature of the black body was varied over the range from 200°K to room temperature. A typical calibration curve is shown in fig. 4.18. It can be seen that the sensitivity at the low temperature end of the scale is about 0.3 μA/°K. The sensitivity of the telemetry is such that temperature measurement to an accuracy of 0.5°K can easily be achieved.

Immediately prior to an ascent, the telemetry was calibrated, using a series of accurately known currents. This enabled the telemetered signals corresponding to temperature measurements to be interpreted in terms of the currents produced by the bridge circuit. By reference to the original calibration curve it was then possible to obtain actual black body temperatures. Owing to zero drift in the telemetry it was necessary to transmit, in addition to the bridge current, a signal corresponding to zero current. Thus, altogether three telemetered signals were associated with calibration of the detector.

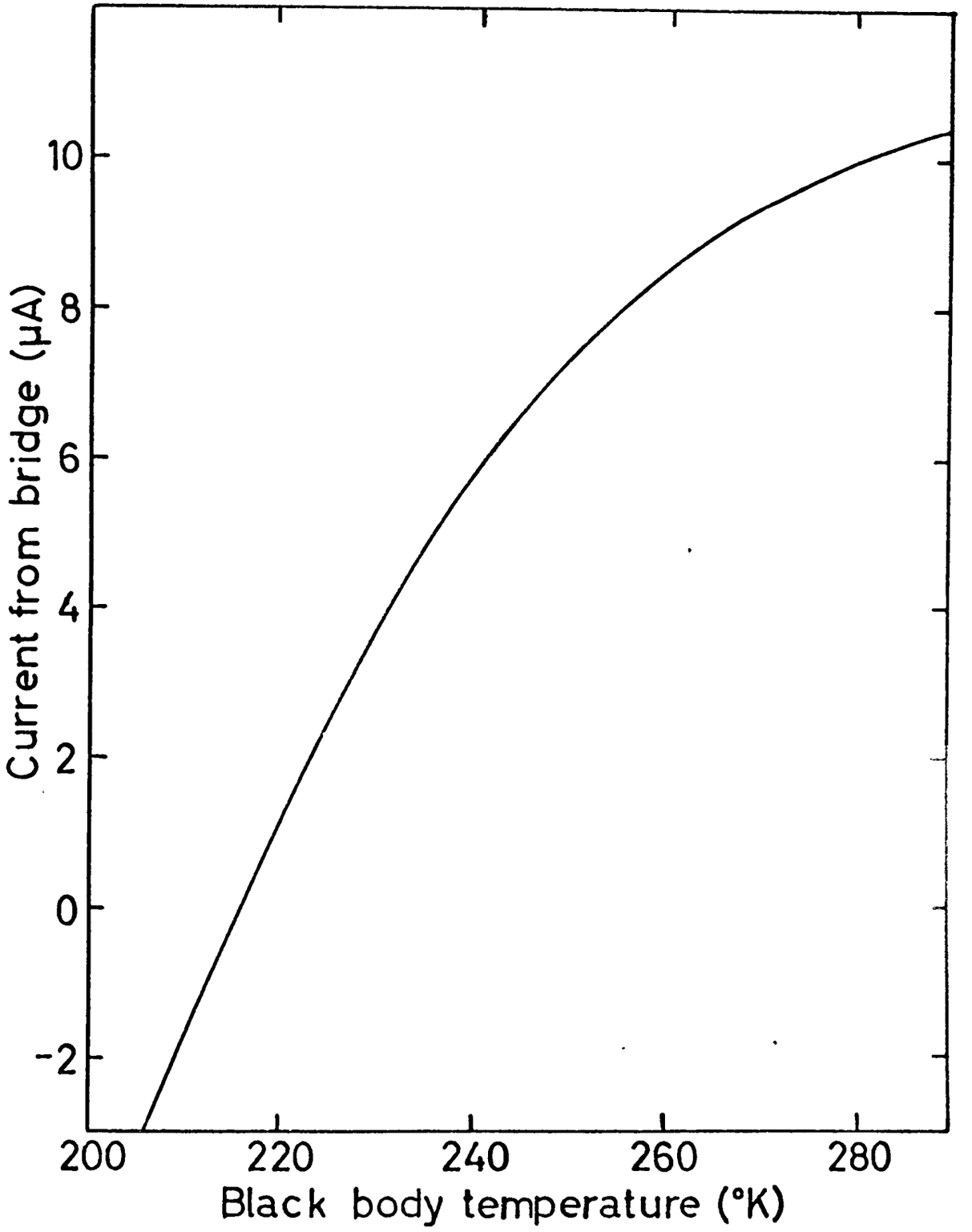


Fig. 4.18. A typical thermistor bridge calibration curve.

4.6 Multiplexing and telemetry

4.6.1 The multiplexor

Six signals in all had to be telemetered by the radiometer-sonde. These corresponded to:

1. Electrical zero (for temperature measurement)
2. Radiation zero
3. Emission from the black body
4. Black body temperature
5. Sky emission at reduced sensitivity
6. Sky emission at full sensitivity

The currents corresponding to these six quantities were selected for telemetry in turn by a six position rotary switch which took one minute to perform a complete revolution. At the same time the gain change and radiation zero controls (see section 4.2) were operated by a second rotary switch driven at the same rate as the first. The wiring of the switches is illustrated in fig. 4.19. In practice, 12 way switches were used, two positions being used for each signal. The switches were driven by a small 2.7 V D.C. motor via a gearbox giving a reduction of about 6000:1. The gearbox is of the same type as that described by Nickless (1962) and is of special interest in that it is constructed almost entirely of moulded plastic parts. Such an assembly is cheap, light in weight and easy to

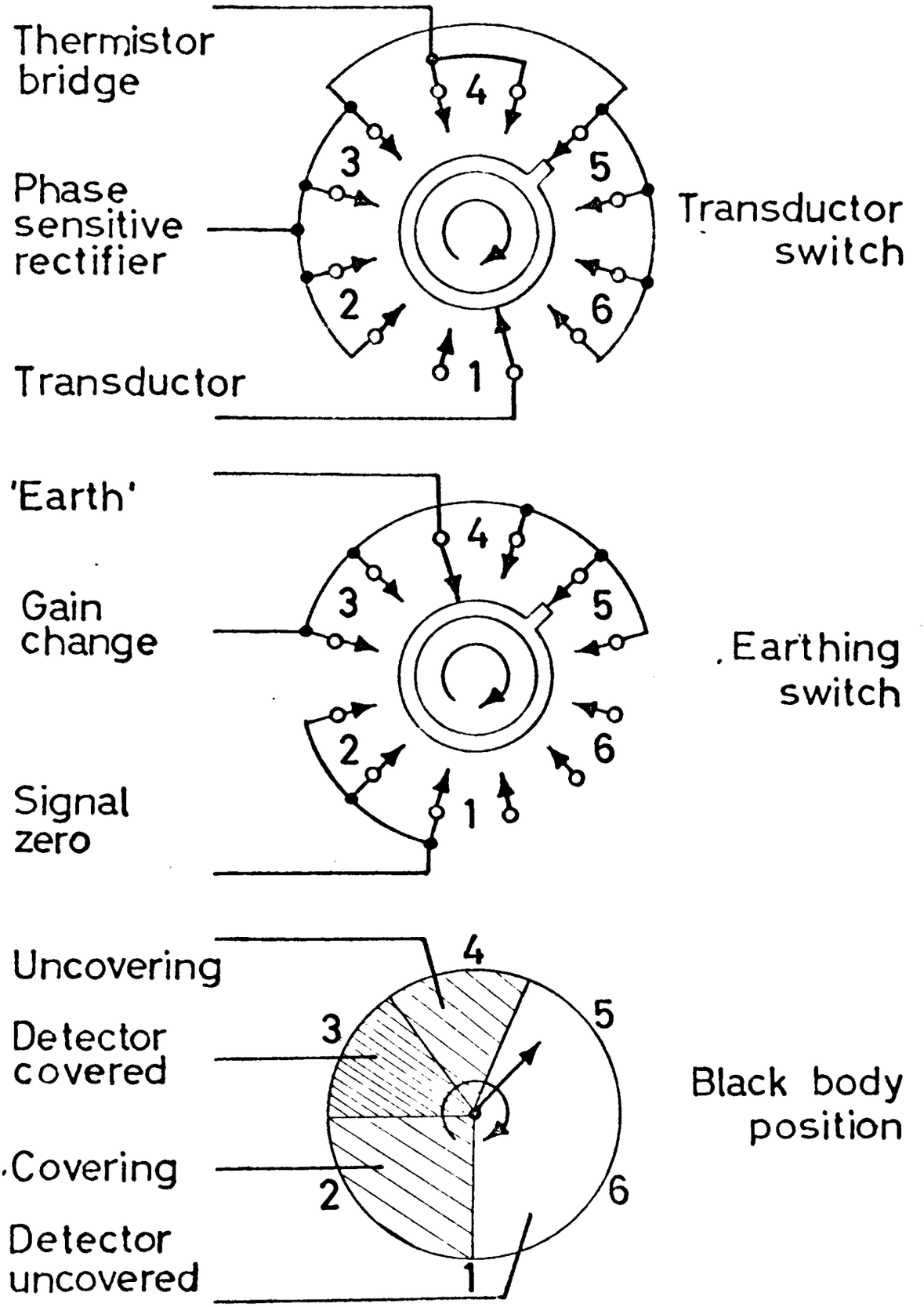


Fig. 4.19. The multiplexor

1 - Electrical zero
2 - Signal zero
3 - Black body signal
4 - Black body temperature
5 - Sky signal (reduced gain)
6 - Sky signal (full gain)

mass produce in the laboratory once moulds have been made.

The same drive was used to turn the crank which actuated the black body, the latter being correctly synchronised with the motion of the switches. As can be seen from the list of signals above, the black body signal was preceded by the radiation zero signal and followed by the temperature signal. Neither of the last two, both of which take place while the black body cone is in motion, require the operation of the detector.

The order in which the signals were to be transmitted was determined by two main factors. It was found that when the radiation zero switch was operated the D.C. conditions of the cathode follower circuit took several seconds to settle down. It was therefore arranged that the switch should operate while the electrical zero was being transmitted. This requirement, combined with the above consideration connected with the motion of the black body, predetermined the order of transmission given above.

4.6.2 Telemetry

The two quantities which are measured in the radiometer-sonde, namely infra-red flux and temperature, appear at the input of the telemetering circuit in the form of direct currents in the range -3 to +15 μA. The current is used to linearly control the frequency of an audio oscillator operating in the range from 700 to 1000 c/s by the use of a

current regulated inductance in a tuned circuit. The audio frequency is subsequently transmitted on a V.H.F. carrier at about 27 Mc/s in the channel allocated for radiosonde work. A brief description of the ground installation used for the reception and decoding of signals is given in Section 4.8.

The above method of telemetering a small current was first described by Jones, Maddever and Sanders (1959) and was further developed by Brewer and Milford (1960) and by Griggs (1961) for use in the Oxford ozone-sonde. In all these cases the current regulated inductance, or 'transductor', replaced one of the three inductive elements on a standard Kew Mk II radiosonde. A very much more compact ozone-sonde, complete with its own transistorised audio oscillator and F/M transmitter, has since been developed at Oxford by A. W. Brewer, E. L. Simmonds and C. A. Nickless and has been described in detail by Nickless (1962).

The first two radiometer-sonde ascents made use of the early telemetry system which employed a Kew sonde as a transmitter. This, however, was soon abandoned owing to the difficulties which were encountered in launching the composite apparatus. Later sondes were re-designed and incorporated the transistorised telemetry system mentioned above.

The transductor which is illustrated in fig. 4.20

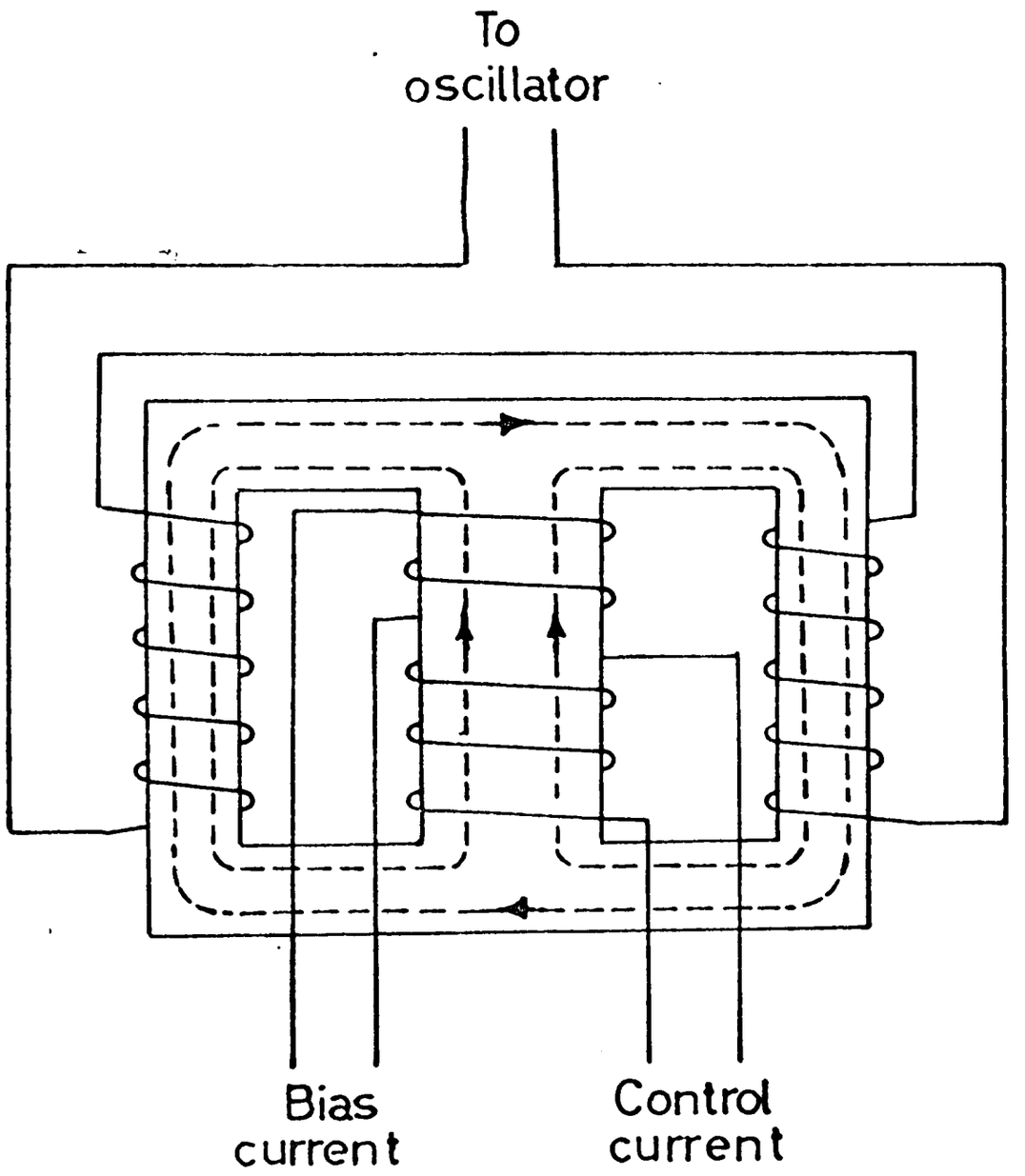


Fig. 4.20. The transductor

consists of a stack of μ-metal laminations which link four coils and form two distinct magnetic circuits. The outer one passes through the two oscillator coils L_1 and L_2 which are connected in series and form the inductive part of the tuned circuit of a Colpitts oscillator. The reluctance of the outer magnetic circuit, and hence the inductance of the oscillator coils, is controlled by a steady magnetic field which can be varied by a control coil wound on the centre limb of the transductor. The magnetic circuit which carries the magnetising field is split into two halves, as shown in the diagram, and passes in opposite directions through the two oscillator coils. This anti-phase coupling between the control coil and the two halves of the oscillator coil tends to reduce the magnitude of the voltage induced by the oscillator circuit in the control coil. Any signal which does appear is removed by a small capacitor connected across the latter.

The control coil consists of 15,000 turns of 47 s.w.g. wire and has a D.C. resistance of 4.5 kΩ. The sensitivity of the transductor is such that 1 μA through the control coil produces a change of between 10 and 15 c/s in the frequency of the oscillator. In order to achieve this sensitivity, and also to make the device linear over the whole range of operation, it is necessary to bias the μ-metal on to a suitable portion of the B - H curve by the

application of a steady magnetic field. This is provided by a bias coil of 400 turns which is wound on the same former as the control coil. The bias current required is about 1 mA and is provided by a Mallory cell. By controlling the bias current over a small range an adjustment of the zero frequency can be provided.

The transductor is enclosed by a μ-metal shield to protect it from the earth's field and other external influences which might otherwise affect its performance. Cooling the transductor caused a drift in frequency towards the lower end of the scale. Thermal insulation reduced this to a minimum but it was not possible to eliminate the effect altogether. The zero frequency was set at about 800 c/s and positive deviations used in the case of the first two sondes. This arrangement was reversed on subsequent sondes, the zero being set high and negative control currents used to decrease the transductor frequency. In this way the frequency was safeguarded from drifting off scale.

The complete telemetry circuit can be seen in fig. 4.2. Both the A.F. oscillator, which incorporates the transductor, and the R.F. oscillator are of the Colpitts type. The latter operates in the grounded base configuration, the tank coil being connected in the collector circuit. Frequency modulation is provided by means of a capacity diode and a small series capacitor. The latter is chosen

to give a carrier frequency deviation of about 7 kc/s.

The circuit described by Nickless (1962) made use of the varying emitter-collector capacitance of the audio transistor to provide frequency modulation by connecting the small coupling capacitor directly to the emitter of the audio oscillator. This arrangement was used on half the radiometer-sonde ascents but was later modified to incorporate the capacity diode. It was found that the direct coupling caused R.F. to be injected into the transductor circuit and was affecting the operation of the latter.

Power supplies to the telemetry were arranged so that it was possible to operate the transmitter on high or low power. The latter conserved the batteries during pre-flight testing as these were among the less conservatively rated ones in the sonde. The audio oscillator section was supplied with a constant 9 V, but the R.F. circuit was fed via a 3.3 kΩ resistor to provide low power operation. Full power was obtained by connecting the 2.7 V motor battery in parallel with the 3.3 kΩ resistor giving a total supply for the transmitter of 11.7 V. An intermediate power could also be obtained by shunting the resistor with the motor without connecting the battery.

4.6.3 Aerial tuning

Weak transmitter signals were experienced on some of

the early radiometer-sonde ascents when the transistorised circuit was first used. This was undoubtedly the result of bad aerial matching. It was found that the aerial connection had to be tapped well down on the tank coil otherwise the loading produced by the aerial caused the transmitter to stop oscillating. The situation was later improved by increasing the collector-emitter feedback capacitor from 4.7 pF to 15 pF to maintain oscillations while the aerial tapping was moved to the optimum position on the coil. Even so, the transmitted power was marginal.

A modified Kew sonde aerial was used on the apparatus. These aerials are cut to a quarter wavelength at 27 Mc/s but, because an effective ground plane cannot be provided, behave electrically as though they are too short. The impedance presented by such an aerial can be represented by a resistance somewhat less than the normal 75Ω in series with a capacitive reactance. In the case of the Kew sonde, the considerable mismatch which results at the aerial is unimportant, owing to the conservative rating of the transmitter. However, the power produced by the transistor oscillator was not so large and optimum aerial matching was essential. Regulations prevented the use of an aerial of greater length, or a dipole might have been an effective solution to the problem.

A considerable improvement in performance was

achieved by including a small inductance in series with the aerial. The object of this was to tune out the capacitive component of the aerial's impedance in order to achieve better matching. The correct value of the inductance had to be obtained empirically for each individual sonde. It was not possible to make any adjustments in the laboratory because the presence of the surroundings affected the characteristics of the aerial as did any other electrical connection to the circuit.

Adjustments were therefore carried out with the apparatus suspended from a line well away from the ground and away from the presence of buildings. The performance of the transmitter was estimated by measuring the signal received by an aerial mounted on the roof of a building some 150 ft away from the apparatus. The simple tuned circuit and detector shown in fig. 4.21 were used in conjunction with a microammeter to measure the current induced in the receiving aerial. Tests were carried out as nearly as possible to one frequency to avoid variable effects due to the presence of standing waves in the vicinity of the aerial. A value for the aerial inductance of about 0.5 μH was found to be suitable in all cases. The coil was mounted on top of the apparatus close to the transmitter. It was incorporated in sondes used for the last four ascents.

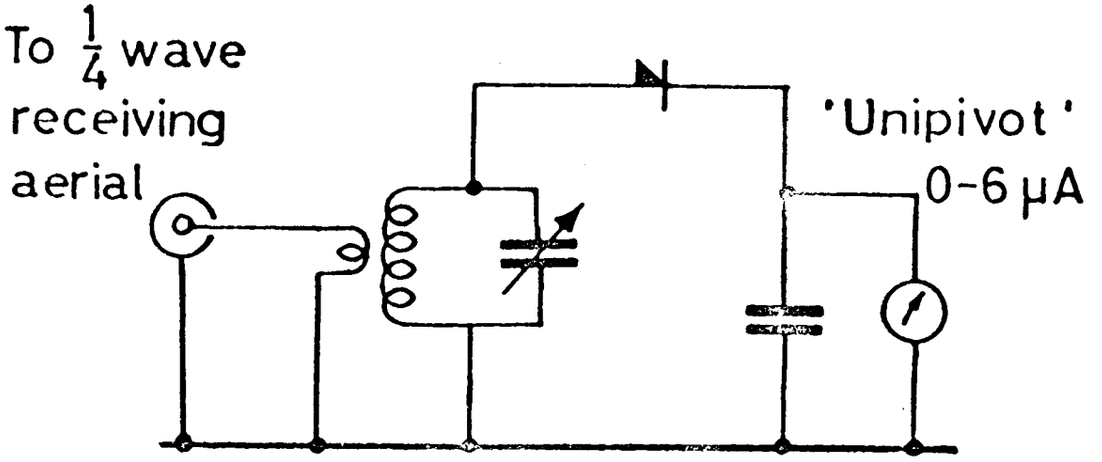


Fig. 4.21. Simple detector used in transmitter signal strength measurements.

4.7 General construction and layout of sonde

Photographs of the complete sonde are shown in plates 1, 4 and 5. Mechanically, the apparatus can be sub-divided into five main sections.

1. Top mounting plate and associated fittings
2. Dewar containing the detector and chopper assembly
3. Electronics section and power supplies
4. Motor, gearbox and switch unit
5. Black body

The top plate consists of a sheet of aluminium alloy strengthened with angled strips, measuring $12\frac{1}{2}$" x $10\frac{1}{2}$" and is supported on four 9" tubular legs. With the exception of the black body the remaining items are mounted below the plate. Fig. 4.22 shows the general layout of the apparatus.

The electronics section is illustrated in more detail in plates 6 and 7. It is made in two halves. One section comprises the cathode follower, signal amplifier, phase sensitive rectifier, chopper drive and reference circuits, while the other half consists of the telemetry, thermistor bridge circuit and power supplies. Eight batteries in all were used and are listed in Appendix I.

The motor and gearbox unit is secured on an anti-vibration mounting. The two switch wafers are mounted on top of the gearbox and connections to the electronics

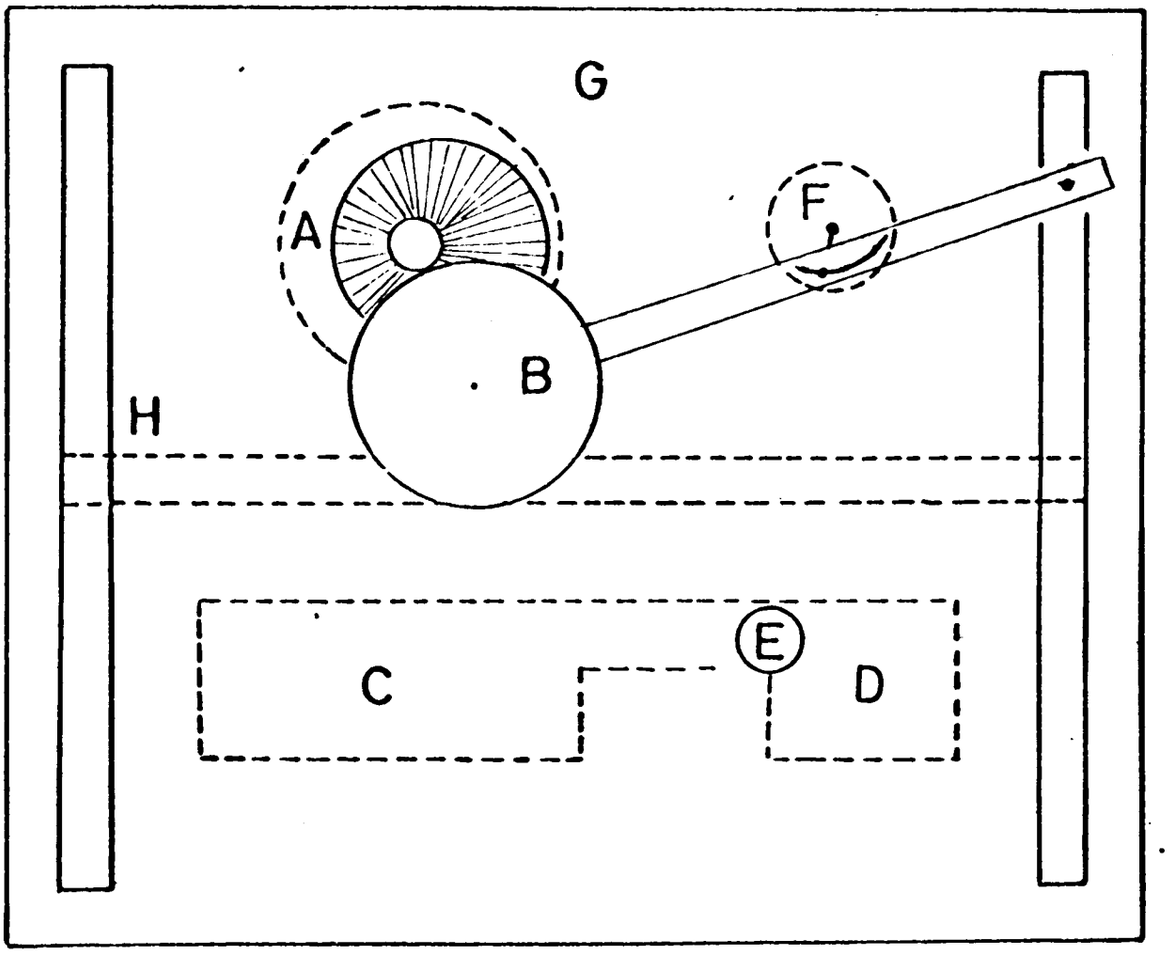


Fig. 4.22. General layout of radiometer-sonde (plan view)

A. Detector assembly
B. Black body
C. Electronics section
D. Transmitter
E. Aerial tuning coil
F. Motor unit
G. Top plate
H. Strengthening members

section are made via screened leads. An inductive suppressor circuit is fitted to the motor to prevent electrical interference.

For the purpose of thermal insulation, the units below the top plate are enclosed in a block of expanded polystyrene measuring 14" x 12" x 9". The mounting plate forms the top of the apparatus, the detector, electronics and motor units fitting into recesses cut in the polystyrene block. The four legs pass through holes in the block and screws and $1\frac{1}{2}$" washers, attached to the ends of the legs, serve to draw the insulation into close contact with the top plate. As an extra precaution against cold air entering the apparatus, the top plate is sealed around the edge with adhesive P.V.C. tape.

At least three inches of insulation was provided round the section containing the electronics. There is evidence that this succeeded in maintaining the inside temperature above $-10^{o}C$ during subsequent ascents.

4.8 The ground installation

The telemetry system, which has been described, was designed originally to be compatible with the standard receiving equipment employed at radiosonde stations. Until a few years ago, the method used to measure the frequency of the received radiosonde signal consisted of beating it

against the output of an accurately calibrated oscillator to produce a stationary pattern on a cathode ray tube. It was then necessary to read the frequency of the oscillator and the time and hand plot the two on a special sheet. This method has now been superceded by the Cintel automatic recording system. This equipment counts the number of cycles of a 100 kc/s crystal oscillator occurring during exactly 100 c/s of the radiosonde signal and plots the result, in $4\frac{1}{2}$ spans, on a pen recorder. The quantity measured is reciprocal frequency and, as such, the method is not directly suitable for use with the transductor telemetry as the latter is essentially linear in frequency. It was therefore necessary to continue to employ the 'beat' method, using the equipment which was still maintained as a standby at radiosonde stations.

The transistorised telemetry used in radiometer-sondes after the first two differed from the original only in that it employed frequency modulation of the carrier signal. As a suitable receiver was available, little change had to be made to the ground installation. It was clear, however, that hand plotting was not entirely satisfactory owing partly to the unsteadiness of some of the received signals and partly to the lack of practice on the part of the operator (E. J. W.). As a result, maximum accuracy was not always achieved.

In an effort to improve the situation, an automatic frequency recording system was built and was employed on the last four ascents. It is described briefly in Appendix II. The accuracy obtained was perhaps only 10% of that achieved by the Cintel equipment but was adequate. Provision was made for beating the incoming signal against the oscillator and feeding the latter to the recording equipment when the quality of the signal was too poor to enable direct reading to be made.

A knowledge of absolute frequency was not necessary. Only relative quantities were required as far as the infra-red measurements were concerned. For the purpose of making the temperature measurement, the telemetry and recording system were calibrated, as a whole, directly in terms of transductor currents just prior to the flight. A reproduction of part of the record of Ascent 9 is given in fig. 4.23.

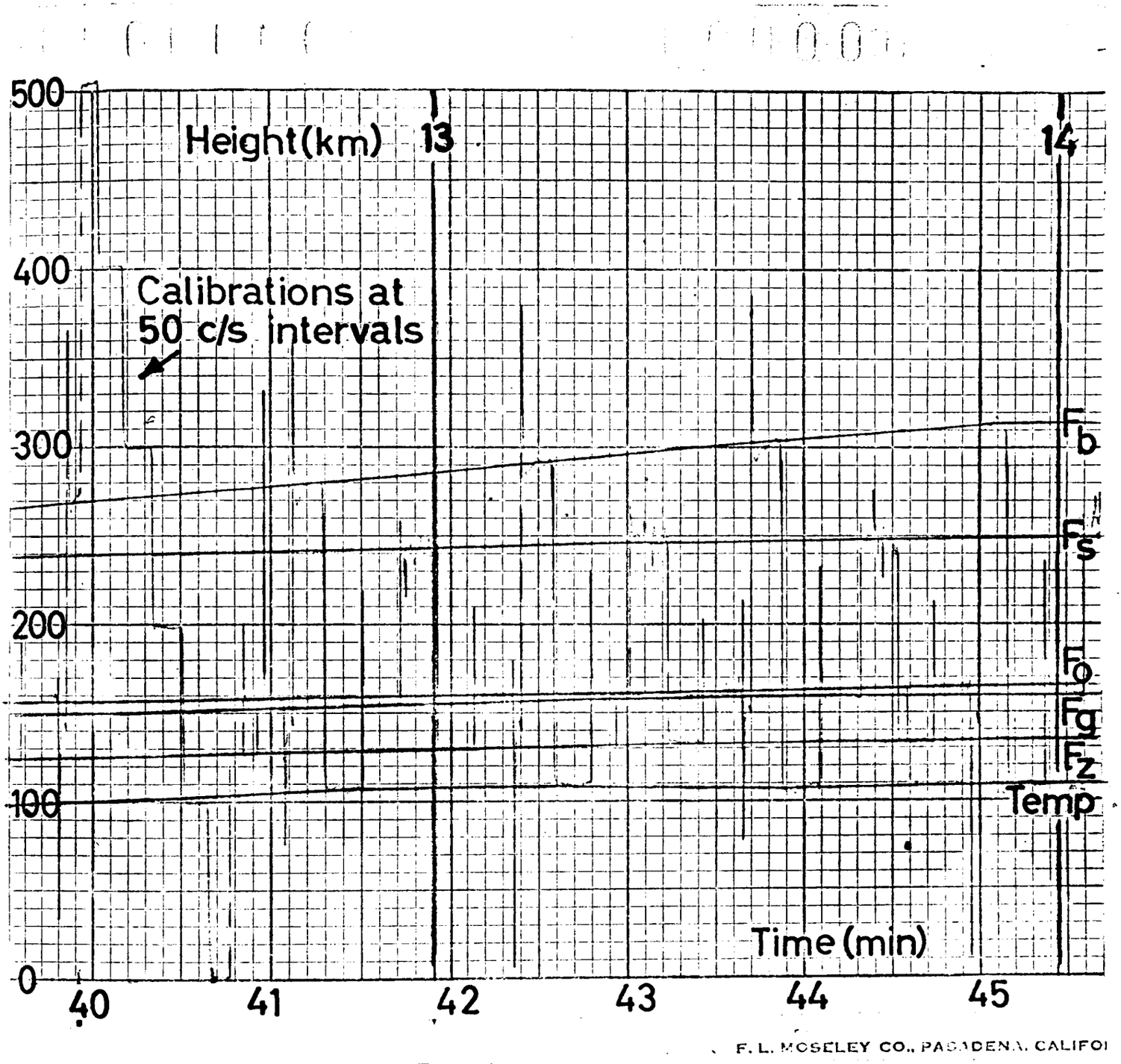


Fig. 4.23. Part of the original record of Ascent 9.

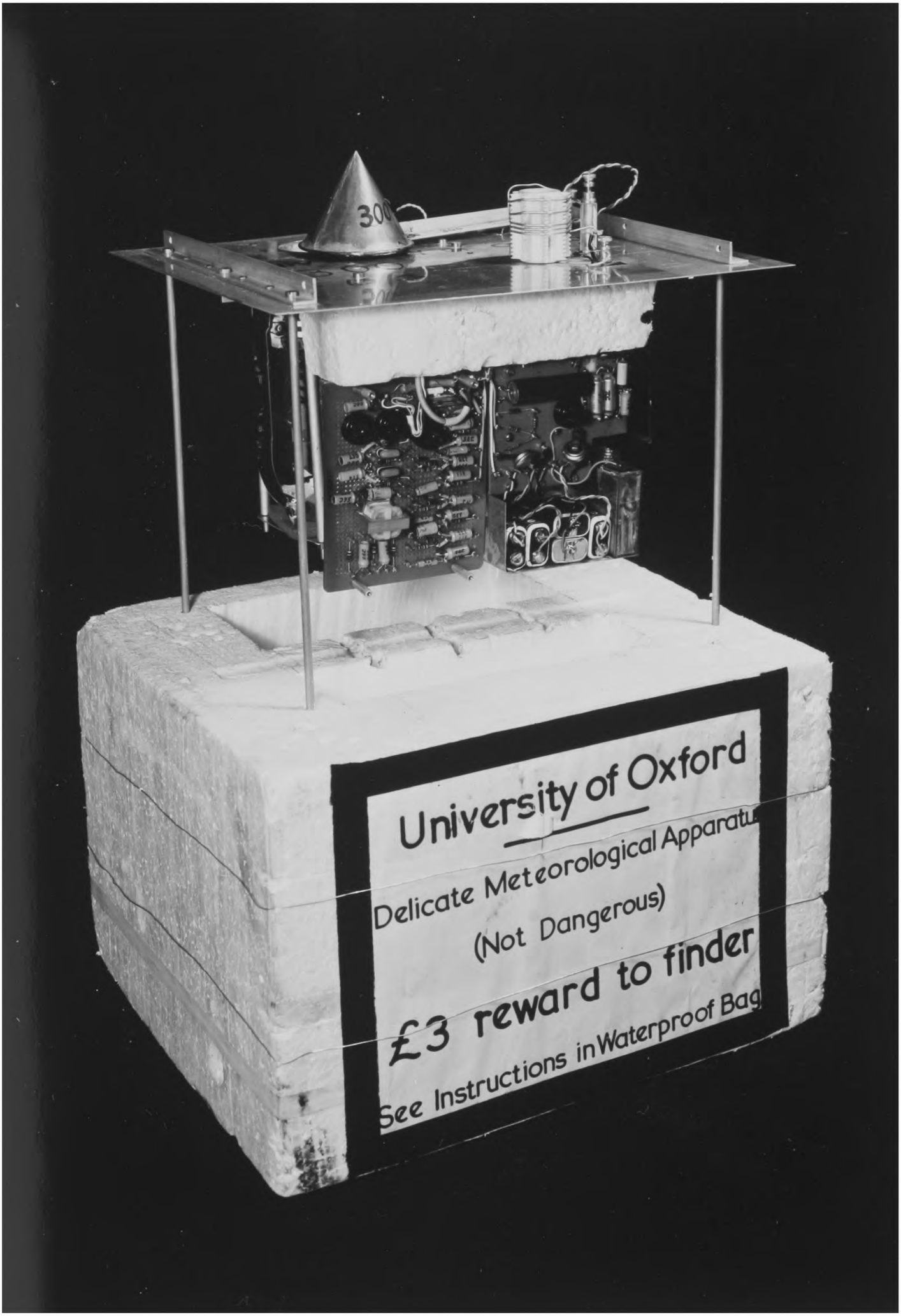

University of Oxford
Delicate Meteorological Apparatu
(Not Dangerous)
£3 reward to finder
See Instructions in Waterproof Bag

Plate 4

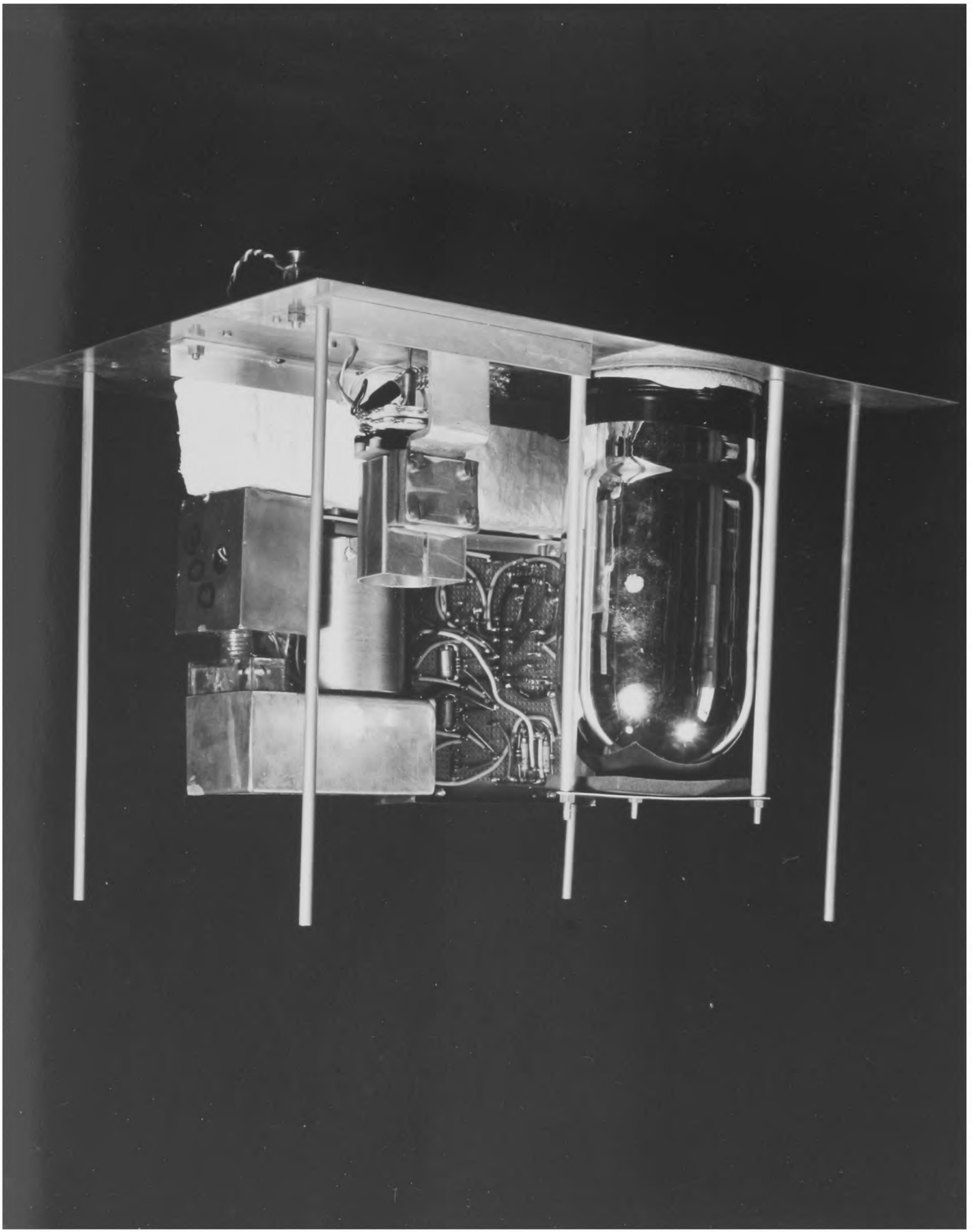


Plate 5

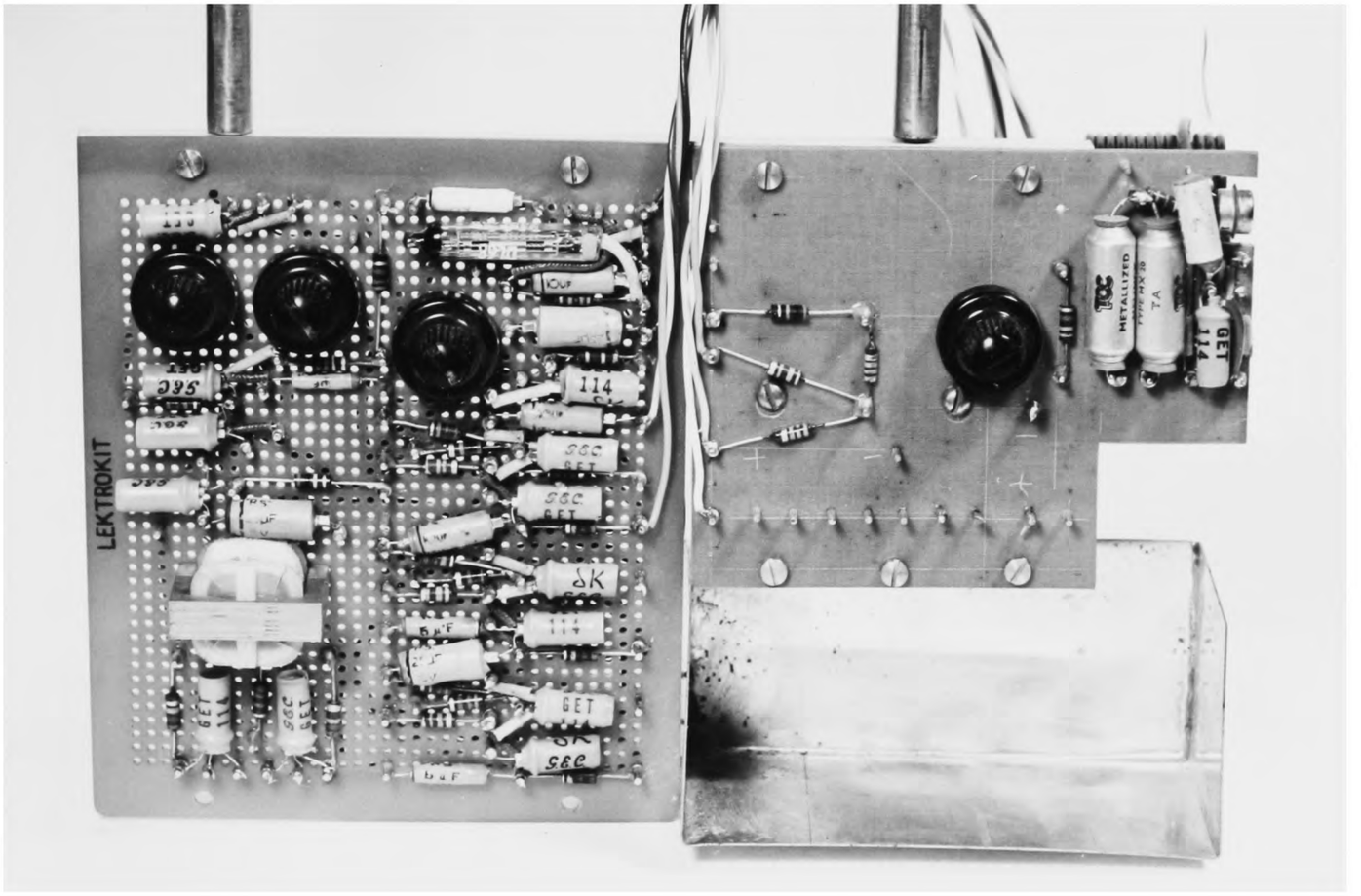


Plate 6

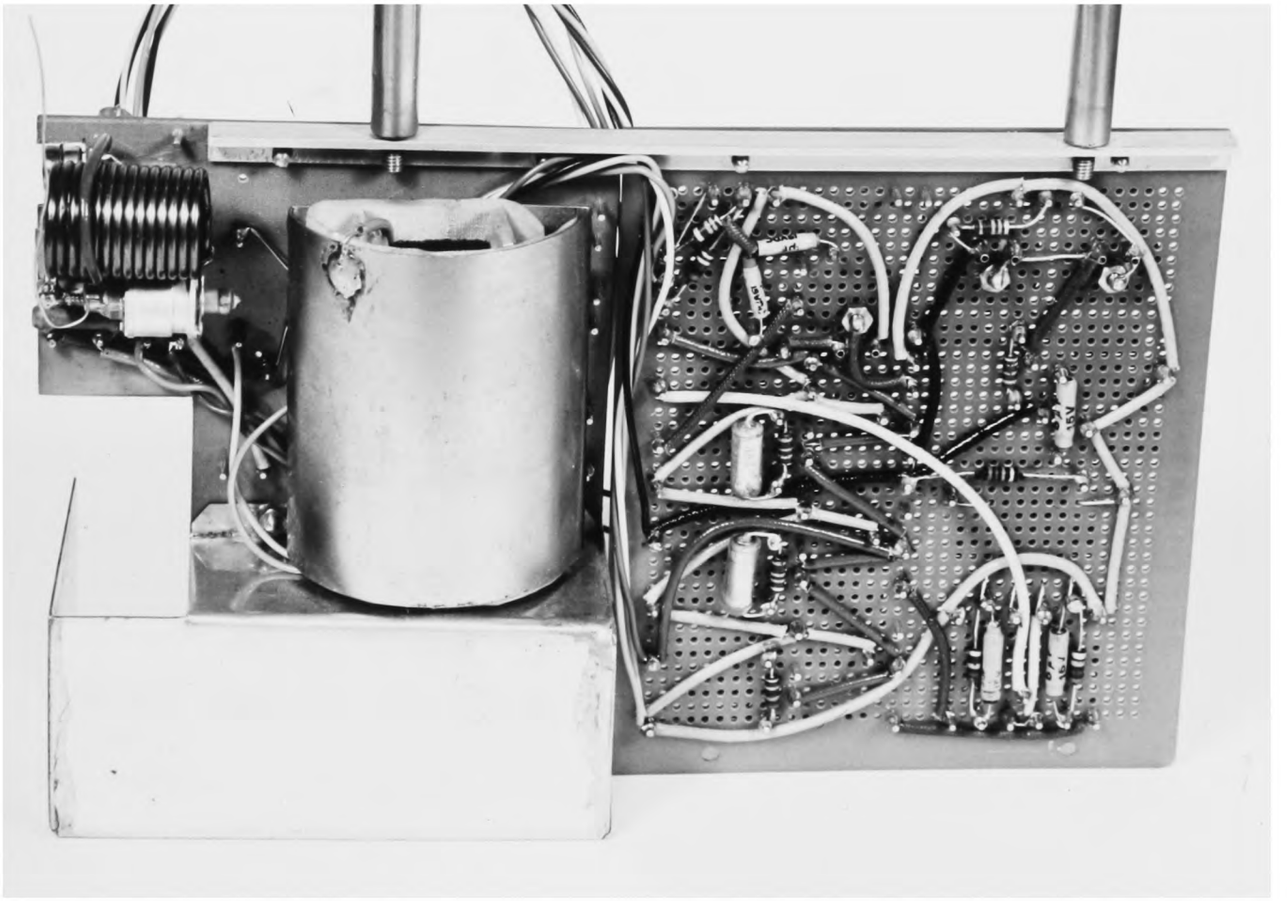


Plate 7

Chapter 5

Mathematics and radiation transfer

5.1 The extent of the problem

Some of the difficulties which occur in the mathematical treatment of radiative energy transfer in an absorbing atmosphere were mentioned in Chapter 1. The main problem stems from the large number of independently variable factors involved. Any complete calculation of radiation flux in the atmosphere would require four separate integrations, one over frequency, two over path length and one over angle. Further, in most cases the integrations would have to be performed analytically. A complete solution is, in practice, virtually impossible unless suitable approximations can be made.

Integration over angle is avoided in most cases by making use of the fact that a diffuse atmospheric flux can be represented by the vertical intensity multiplied by a suitable factor. Kaplan (1952b) has shown that, when radiation from all directions is being considered, very little error is introduced by the above approximation, in the case of carbon dioxide and water vapour if a factor of 1.66 is used. The same result has been shown to hold in the case of ozone (Hitschfeld and Houghton (1961)).

Simplification of the frequency and path length

integrals is rather more difficult. Some of the methods which have been proposed are described below.

5.2 Line shapes and transmission models

The construction of molecular absorption spectra is usually very complex. Each band consists of many thousands of individual lines whose strengths vary over several orders of magnitude. The spacing between lines, usually of the order of one wavenumber, is fairly regular in the case of certain molecules such as carbon dioxide, methane and nitrous oxide. Water vapour and ozone lines on the other hand show little regularity in spacing and, within any small interval, appear to be almost randomly distributed both in position and strength.

The shape of a pressure broadened spectral line can usually be adequately represented by the Lorentz formula

$$k_\nu = \frac{S}{\pi\left\{(\nu-\nu_0)^2+\alpha^2\right\}}$$

where k_ν is the absorption coefficient at a frequency ν, ν_0 the frequency of the line centre, α the half width of the line and S the line strength which is given by

$$S = \int_0^\infty k_\nu \, d\nu$$

The half width α is related to the mean time t between molecular collisions by the simple relation

$$\alpha = \frac{1}{2\pi t}$$

and, on the basis of the kinetic theory one would expect the half width to be dependent on the pressure p and temperature T according to the relation

$$\alpha = \alpha_o \frac{P}{P_o}\sqrt{\frac{T_o}{T}}$$

where α_o represents the half width at standard temperature T_o and pressure p_o.

The Lorentz formula neglects the effect of molecular distortion during collision and differs from more exact formulae in the shape predicted for the wings of the line. However, unless lines are widely spaced, the Lorentz formula is adequate for most applications.

Spectral lines are also subject to Doppler broadening, resulting from the motion of the radiating molecules. Doppler half widths can be calculated from Maxwell's law and depend on temperature. Above 30 km they begin to predominate, although below this they can generally be neglected. No account of Doppler broadening has been taken in this study.

The total absorption W by a single Lorentz line was

shown by Landenburg and Reiche (1911) to be given by

$$W = \int_0^\infty A_\nu \, d\nu = 2\pi\alpha x e^{-x}\left[J_0(ix) - i J_1(ix)\right]$$

where $x = \frac{Su}{2\pi\alpha}$ and J_0 and J_1 are respectively first and second order Bessel functions with imaginary arguments. A_ν is the fractional absorption at a frequency ν due to a path length u of absorber and is given by Beer's law

$$A_\nu = 1 - \exp(-k_\nu u)$$

Two important results follow from the Landenburg and Reiche formula. In the case of strong absorption for which $x > 3$ the total absorption of a line is given by

$$W \doteq 2\sqrt{S\alpha u}$$

On the other hand, if $x \ll 1$ the absorption is weak and

$$W \doteq Su$$

The first of these corresponds to the well known square root absorption law and follows from the fact that the line centre is completely absorbed. When this happens, any further absorption must take place in the wings where the extinction rate is less. It then depends on both pressure and path length.

The second case represents a linear absorption law

where the total absorption of a given line is proportional to the path length of absorber present. Both of these approximations have useful applications in the case of actual spectra, providing lines are sufficiently well separated.

When considering an interval containing several spectral lines, calculations have been greatly simplified by the introduction of band transmission models which smooth out the rapid variation of absorption coefficient in the neighbourhood of each individual line. They thus represent an effective transmission over the frequency interval in terms of quantities which vary only slowly over the whole band.

Perhaps the first such model was proposed by Elsasser (1942). He considered an infinite array of identical, equally spaced Lorentz lines and, by summing the effects of all the lines, was able to show that the absorption coefficient k_ν at a frequency ν was given by

$$k_\nu = \frac{S}{\delta} \frac{\sinh 2\pi\alpha/\delta}{\cosh 2\pi\alpha/\delta - \cos 2\pi\nu/\delta}$$

where δ is the spacing between line centres.

The mean transmission τ of the band when a uniform

path length of absorber u is present follows directly from Beer's law. It is

$$\tau = \int_{\delta} \exp\{-k_\nu u\}\, d\nu$$

by performing the integration over an interval equal to the line separation. The integration cannot be performed analytically in the general case, although well known approximations can be obtained in the cases of weak, strong and widely spaced lines. The last of these yields results which are similar to those for a single line.

The Elsasser model has been shown to give good results for carbon dioxide (Kaplan (1952a)), for nitrous oxide (Goody and Wormell (1951)) and for carbon monoxide (Goody (1961b)). In the case of water vapour and ozone, however, transmissions predicted by the Elsasser model are less accurate. Cowling (1950) compared numerical computations made for small portions of the water vapour rotation band with some early experimental results of Fowle (1912) and Adel (1941) and found good agreement. However, calculated transmissions differed somewhat from values predicted on the basis of the regular model, both for large and small path lengths of water.

It is hardly surprising that errors should arise when the Elsasser model is applied to the water vapour band.

Indeed, it is remarkable that results are as good as they are, for the distribution of water vapour lines is far from regular. It is, in fact, more nearly a random distribution. Goody (1952), by assuming that there was no correlation between line position and strength and that all line positions were equally probable, obtained, for the mean transmission τ of a large number of lines, an expression of the form

$$\tau = \exp\left[-\frac{1}{\delta}\int_0^\infty P(k)\{1-\exp(-ukS_h)\,dk\}\right]d\nu$$

where $P(k)$ is the line strength probability function, S_h is a line shape parameter and δ the mean line spacing.

In the case of a Lorentz line shape and assuming an exponential distribution of line intensities of the form

$$P(k) = \frac{1}{S}\exp\left[k/S\right]$$

where S is the average line intensity, the transmission can be represented by

$$\tau = \exp\left[-\frac{Su}{\delta}\left(1+\frac{Su}{\pi\alpha}\right)^{-\frac{1}{2}}\right]$$

Goody showed that transmissions predicted by the statistical model were in good agreement with Cowling's computations.

Godson (1954) has proposed a logarithmic distribution of line intensities based on an analysis of lines in several of the water vapour bands. Kaplan (1954) has further extended the theory with the so called quasi-statistical or regular-random model of band absorption. This model assumes a random overlapping of a number of Elsasser bands and has been shown to give a good representation of the 15 μ carbon dioxide band as well as the water bands.

5.3 Slant path approximations

In all the transmission models described above, the assumption of a Lorentz line shape has been made, which introduces the effect of pressure. When one comes to consider the case of transmission along atmospheric path-lengths the question arises as to what value of pressure to use when the latter varies from one end of the path to the other.

One attempt at a solution, which was much used in earlier literature, was the so-called pressure weighting method. The path is divided into a number of thin layers and the amount of absorber in each layer is weighted by a factor

$$\left(\frac{p(z)}{p}\right)^{1/2}$$

where $p(z)$ is the pressure of the layer at a height z. The path is then assumed to be at the constant pressure p and the line shapes Lorentzian at that pressure. This method can lead to serious errors, especially where the absorption is strong. In this case the linear scaling factor

$$\frac{p(z)}{p}$$

is more appropriate.

Undoubtedly the most powerful device which exists today for dealing with the problem is a method which was put forward originally by Curtis (1952) and later in a more general form by Godson (1955) and is now known as the Curtis-Godson approximation. In its simplest form, an effective pressure $\bar{p}$ for the whole path length is taken to be the mean of the pressures in individual layers, each weighted by the corresponding amount of absorber, viz

$$\bar{p} = \frac{\sum p(z)\, u(z)}{\sum u(z)}$$

This approximation is exact in the limiting cases of weak and strong lines and provides good accuracy for intermediate values, provided the ratio of the extremes of pressure is not greater than about 100.

5.4 The calculation of radiation flux

When considering the transfer of infra-red radiation through an absorbing atmosphere use is made of Kirchhoff's law which equates the radiation emitted by an element of an absorber to the product of its absorptivity and the black body radiation at the temperature of the element. This law assumes a Maxwellian distribution of velocities among the molecules of the absorbing gas. There is little doubt that this assumption is valid up to balloon altitudes and the law will be assumed to hold in the following discussion.

The energy emitted by a thin layer at height z' (fig. 5.1) where the absorber density is $\rho(z')$ and the absorption coefficient $k(z')$ is given by Kirchhoff's law as

$$dE(z') = B(z')\, k(z')\, \rho(z')\, dz'$$

where $B(z')$ is the Planckfunction at the temperature of the layer. The intensity reaching the level at a height z (below z') is

$$dI(z) = B(z')\, k(z')\, \rho(z')\, \tau(z,z')\, dz'$$

where $\tau(z,z')$ is the transmission of the path between z' and z. The total vertical intensity at z due to the atmosphere above that level is, thus, by integration

$$I(z) = \int_{z'=z}^{\infty} B(z')\, k(z')\, \rho(z')\, \tau(z,z')\, dz'$$

Now from Beer's law

$$\tau(z,z') = \exp\int_{z''=z}^{z'} -k(z'')\rho(z'')\,dz''$$

and it can be shown that

$$\frac{\partial}{\partial z'}\tau(z,z') = -\tau(z,z')\,k(z')\rho(z')$$

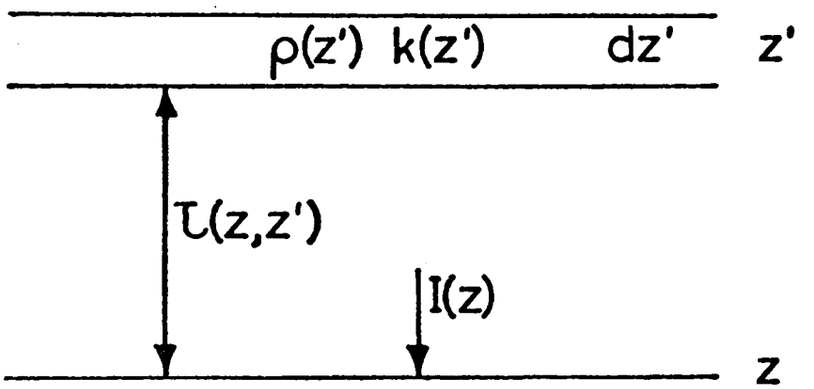


Fig. 5.1

The above expression for $I(z)$ therefore reduces to

$$I(z) = -\int_{z'=z}^{\infty} B(z')\,\frac{d}{dz'}\tau(z,z')\,dz'$$

The negative sign indicates that the energy is directed downwards.

This relation is for monochromatic radiation only

since both $k(z)$ and $B(z)$ are functions of frequency. To obtain the emission due to a whole band, or part of a band, a second integration must be performed. In general it is possible to represent $\tau(z,z')$ by a suitable transmission model which greatly simplifies the frequency integration. Use will be made of the above expression for the downward intensity when dealing with the analysis of data for the radiometer-sonde in Chapter 7.

Chapter 6

The ascents

For practical reasons, all radiometer-sonde ascents were made at Aughton, Nr. Liverpool, one of the eight radiosonde stations in the British Isles maintained by the Meteorological Office. These stations are fully equipped for the preparation, launching and tracking of radiosondes. Aughton produces the highest recovery rate of all, the theoretical figure being 91%. This value represents the average percentage of sondes launched which are judged to fall on land and are thus capable of recovery. The staff at Aughton provided much valuable assistance with the work and much of the success which was achieved is attributable to their willing co-operation at all times.

Routine meteorological ascents at radiosonde stations are made every six hours, two of these being pilot ascents for windfinding only; the other two, at 11.30 and 23.30 G.M.T. respectively, being radiosonde ascents. With one exception, all radiometer flights took place in conjunction with the 23.30 ascent. Twelve flights in all were made and are summarised in Table 1.

The procedure adopted was to mount the apparatus in tandem with the Kew sonde, the two sondes being separated by about 150 ft. This, together with the 150 ft suspension normally used above the Kew sonde, gave a clear 300 ft

Ascent no	Date	Launch time G.M.T.	Sonde	Balloon	Weather conditions	Height at burst km	Pressure at burst mb	Height of trop(s) km	Remarks
1	26.6.61	23.50	Mk I	Beritex 1250	bc $\frac{3}{8}$ Sc	24.62	25	8.86 14.05	Tx's on same frequency
2	19.1.62	23.50	Mk II	Beritex 1000	c $\frac{7}{8}$ Sc	Not known	Not known	11.09	Tx failed
3	13.4.62	23.30	213	Beritex 1000	Clear sky	24.00	49	11.42	No signals no b/b temps
4	25.4.62	23.40	214	Beritex 1250	Clear sky	22.56	37	12.10	Signal failed min. 30
5	8.9.62	23.30	214	Beritex 1000	c $\frac{7}{8}$ CuSc AcAs	22.30	67	12.12	Signal failed min. 8
6	9.10.62	23.30	213	Beritex 1000	Fog - sky obscured	18.50	78	11.11	? successful
7	19.6.63	17.30	214	Beritex 1000	c rain in past hour	Not known	Not known	Not known	Affected by sunlight
8	19.6.63	23.30	213	Beritex 1000	bc $\frac{4}{8}$ ScAc	20.59	52	10.98	? successful
9	11.9.63	00.00	300	Darex 1750	b $\frac{1}{8}$ Ci	32.50	Not known	10.70	V successful
10	11.9.63	23.50	213	Darex 1750	b $\frac{1}{8}$ Ci	27.29	Not known	9.74 13.94	Poor quality signals
11	12.9.63	23.30	214	Darex 1750	Clear sky	28.58	Not known	13.73	Motor failed min. 50
12	13.9.63	23.40	213	Beritex 3000	Clear sky	18.35	73	13.04	Premature burst

Table 1. The ascents

between the balloon and the radiometer. A three point suspension (Plate 1) held the radiometer-sonde with the direction of view of the detector at about 30° to the vertical. This ensured that at no time was the balloon visible to the detector. On all but the last four ascents, 1000 gm or 1250 gm Beritex seamless rubber balloons, manufactured by the Guide Bridge Rubber Company, were used. The larger balloon, surprisingly, did not produce any significant increase in the maximum height achieved.

The last four ascents made use of somewhat larger balloons in an effort to reach greater heights. The first three of these were made with Darex 1750 gm neoprene balloons, of American manufacture, which gave a notably better performance. A 3000 gm Beritex balloon was used on the last flight. The unusually low ceiling obtained on this occasion suggests that the balloon was faulty.

For practical reasons, it is inadvisable to attempt a tandem launch if the surface wind is much greater than 10 knots. It is quite probable that some of the early sonde failures were due to damage caused by rough launches. The larger balloons used on the last ascents made the difficulties even greater. On these occasions, it was necessary to shorten the suspension by about 100 ft to facilitate the launch, and to compensate for this by increasing the direction of view of the apparatus from 30° to 45° from the vertical.

Every apparatus was recovered promptly and, in most cases, without much damage: one sonde in particular made five ascents. A £3 reward to the finder no doubt provided the incentive in most cases.

The first test flight was made on 26th June, 1961. The apparatus used was of a fairly crude construction and was intended mainly as a flight test of the various component parts of the system. A simple rotating black body was used, coupled directly to the switch drive, but no temperature measurement was provided. A Kew sonde transmitter mounted 6 ft above the apparatus was coupled to the transductor by means of a long lead. Unfortunately, when launched, the two sonde transmitters were found to be on almost the same frequency, although they had originally been set well apart. This made reception of the signals very difficult. However, sufficient information was gathered to enable the following conclusions to be drawn:

1. There was insufficient thermal insulation of the electronics. This was clear from the fact that the zero frequency drifted off scale after 22 minutes.

2. Interference from the motor was badly affecting some of the signals.

3. The gain of the signal amplifier had been set too low. (This was increased to about 100 on subsequent ascents).

The equipment was recovered and considerably modified. Instead of an insulated box built around the electronics and batteries, as on the first sonde, a block of expanded polystyrene was used as an envelope for the entire apparatus, the various parts being set in holes cut in the block. The top was covered with an aluminium alloy plate below which the detector assembly was mounted. The new insulation was tested in an atmospheric chamber at the Radio Department of the Royal Aircraft Establishment. The sonde was cooled through 70°C over a period of two hours, during which time the zero frequency of the telemetry drifted about 30 c/s. The temperature coefficient of the transductor, which caused this drift, was known to be 1.5 c/s per °C, so the temperature change inside the apparatus was about 20°C. This was considered acceptable.

R.F. interference was removed by fitting small inductive suppressors to the motor. The anti-vibration mounting of the latter was also improved. It was found that vibration of the apparatus was causing microphony in the cathode follower valve.

The rotating black body of the original apparatus was replaced by the swinging arm type described in Chapter 4, and was fitted with a thermistor temperature element. The apparatus still made use of a Kew sonde transmitter as on the first ascent. The modified sonde was flown on

19th January, 1962 (Ascent 2), but, unfortunately, a failure occurred in the transmitter and no signals were received.

The failure was probably due to damage resulting from a certain amount of rough handling which is unavoidable in making a triple launch. It was therefore decided to completely redesign the apparatus to include its own transmitter. Two sondes (designated 213 and 214) were built on this new pattern, incorporating the transistorised transmitter which has been described in Chapter 4. The overall size, 14" x 12" x 9", and weight, 2500 gm, were slightly larger than was the case in previous models. Apart from minor alterations, the design was not changed further.

One of the new sondes was flown on April 13th, 1962 (3) but was unsuccessful as no useful detector signals were received. In addition, the temperature element failed to work. This fault was later traced to a short circuit in the thermistor lead.

The second sonde was flown a fortnight later, (4), with somewhat better results. Good signals were received for the first 30 minutes of the ascent, but failure again occurred. Later on, this was attributed to malfunctioning of the phase shifting circuit in the sonde.

A similar fault developed during the next ascent (5), made in September of the same year. This time failure occurred after only 8 minutes of the flight. In addition, the transmitter was very weak.

The ascent made on 9th October, 1962 (6) appeared, at first, to have been completely successful as good signals were obtained up to the point of burst at 19 km. It has since become clear that slight malfunctioning occurred on this ascent also, although some useful information was obtained.

Ascent 7, made at 17.30 G.M.T., was the only one which was not made at night. It was thought that, with the sun low in the sky, there would be little chance of sunlight affecting the detector. The filter used removed wavelengths below 5.5 μ, and it is known that scattered sunlight contains very little energy at any wavelength above 4 μ. Contrary to expectation, it was found that the sun had a very great effect. Probably as the result of scattering from the entrance aperture, direct sunlight found its way on to the detector and no useful results could be obtained.

A further ascent (8) made at midnight the same day, behaved satisfactorily.

At this stage the modified phasing circuit was incorporated into the existing sondes (213 and 214) and a further sonde completed (300). The remaining four ascents

were made on consecutive nights, September 10th to 13th, 1963. The first of these (9) reached a height of 32 km and was the most successful of all the ascents. Greatest confidence is attached to the data which were obtained on this occasion. The second (10) reached 28 km, but signals were of a much poorer quality due to a noisy detector and were virtually unusable between 17 and 22 km. Neither of the remaining two ascents (11 and 12) gave results much above the tropopause. Motor battery failure terminated the operation of the sonde during ascent 11, while a premature burst was responsible for the failure of the last flight.

Since complete success depends not only on the correct functioning of the apparatus but also on launching conditions and on balloon performance, only one ascent (9) could be described as entirely successful; a further five (6, 8, 10, 11 and 12) were partly successful, three (1, 4 and 5) only slightly so and three (2, 3, and 7 were complete failures. It is inevitable, with a complicated piece of equipment, that some failures will occur, especially in the developmental stage. The experience gained as a result of these ascents clearly demonstrates that the more complex an apparatus is, the more reliable each individual part must be. It is encouraging that, with one exception, the failures occurred early in the development of the equipment.

Data which were obtained from the ascents, are presented in figs. 6.1 to 6.7. The last ascent has been left out as little useful information was obtained from it due to bad quality signals, but Ascents 4 and 5 are included to illustrate the malfunctioning of the apparatus on these occasions.

Apart from the black body temperature which is in ^{o}K (top scale), all data are plotted directly in terms of telemetered frequencies. In the cases of Ascents 9 to 11, 100 recorder divisions corresponds to 50 c/s. The five signals shown are: electrical and signal zeros (F_z and F_o), sky signal on full and reduced gains (F_s and F_g) and calibration black body signal (F_b).

The position of the tropopause was determined from Kew sonde air temperatures which were invariably between 5 and $6^{o}K$ above black body temperatures. The difference was probably due to radiative cooling of the black body resulting from the close proximity of the cold detector.

The interpretation of ascent data is discussed in the next chapter.

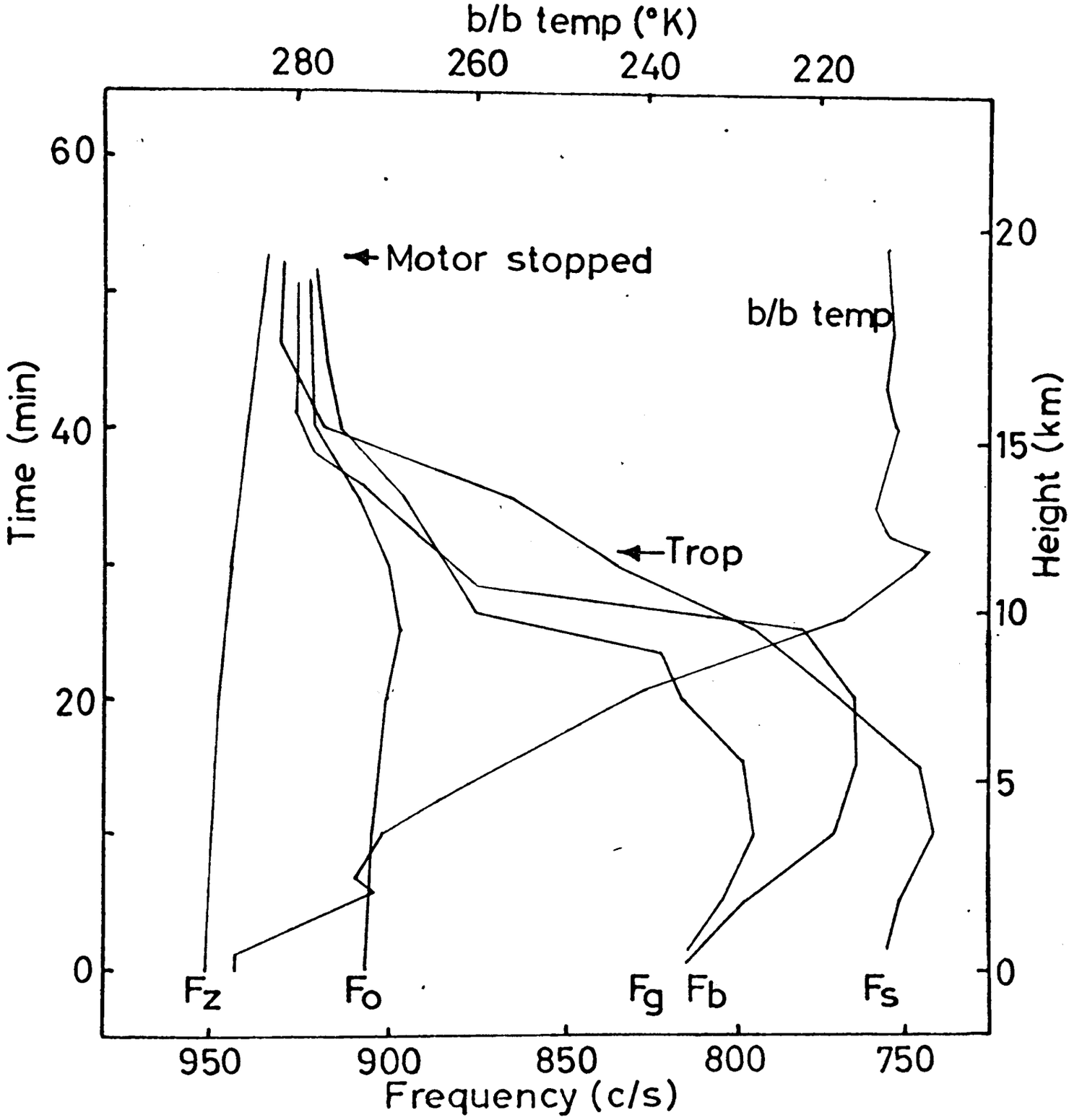


Fig. 6.1 Ascent 4 25-4-62

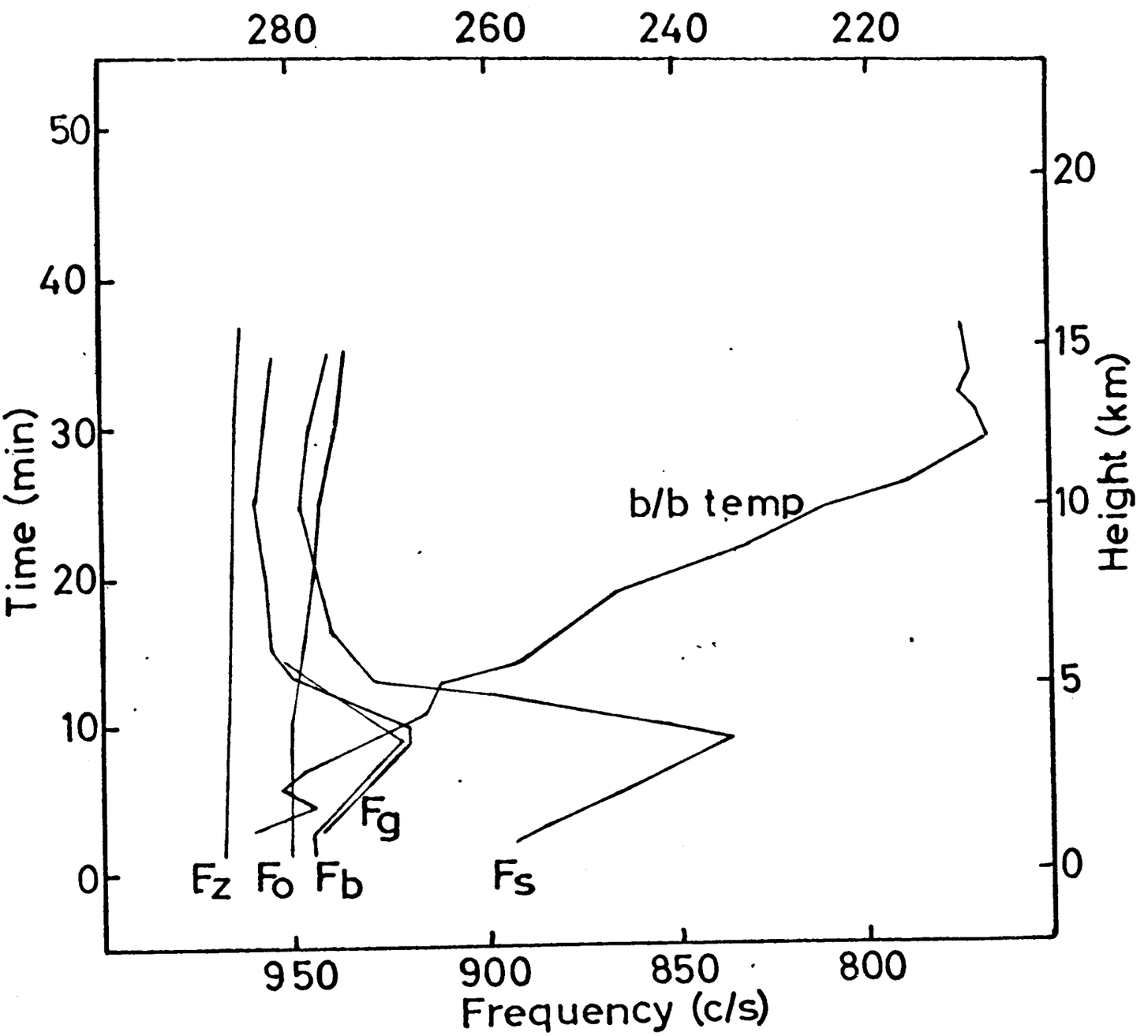


Fig. 6.2 Ascent 5 8-9-62

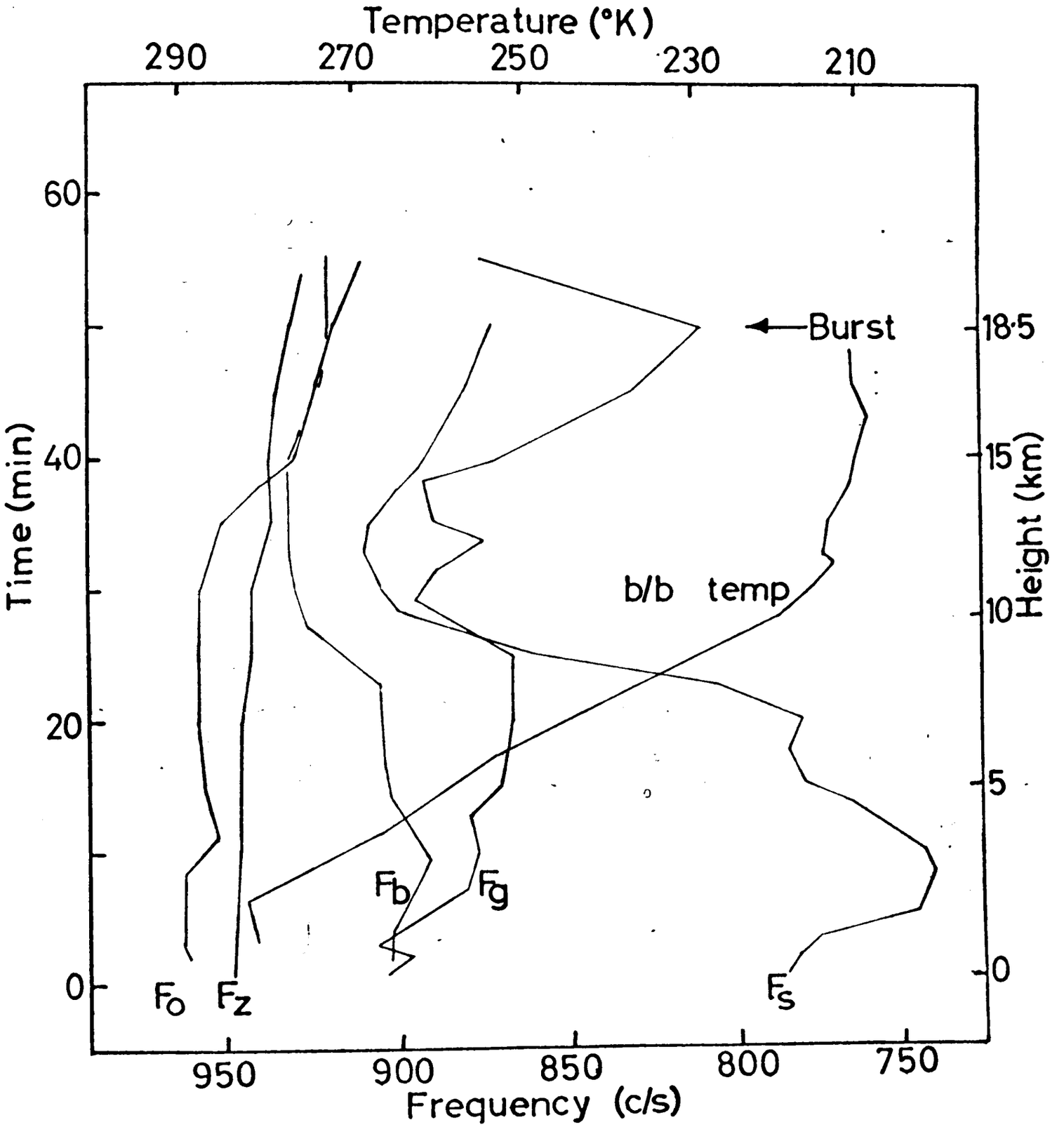


Fig. 6.3 Ascent 6 9-10-62

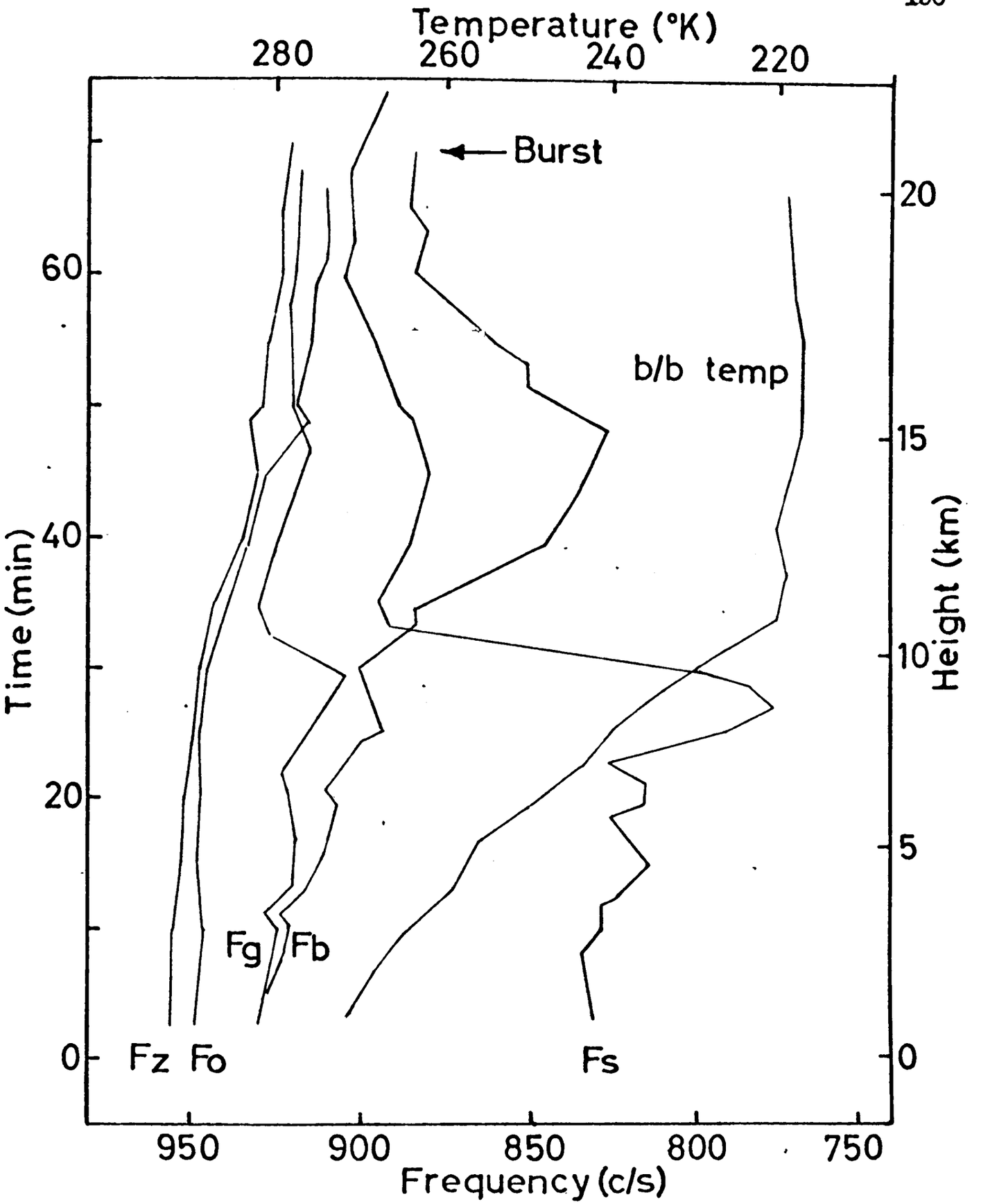


Fig. 6.4 Ascent 8 19-6-63

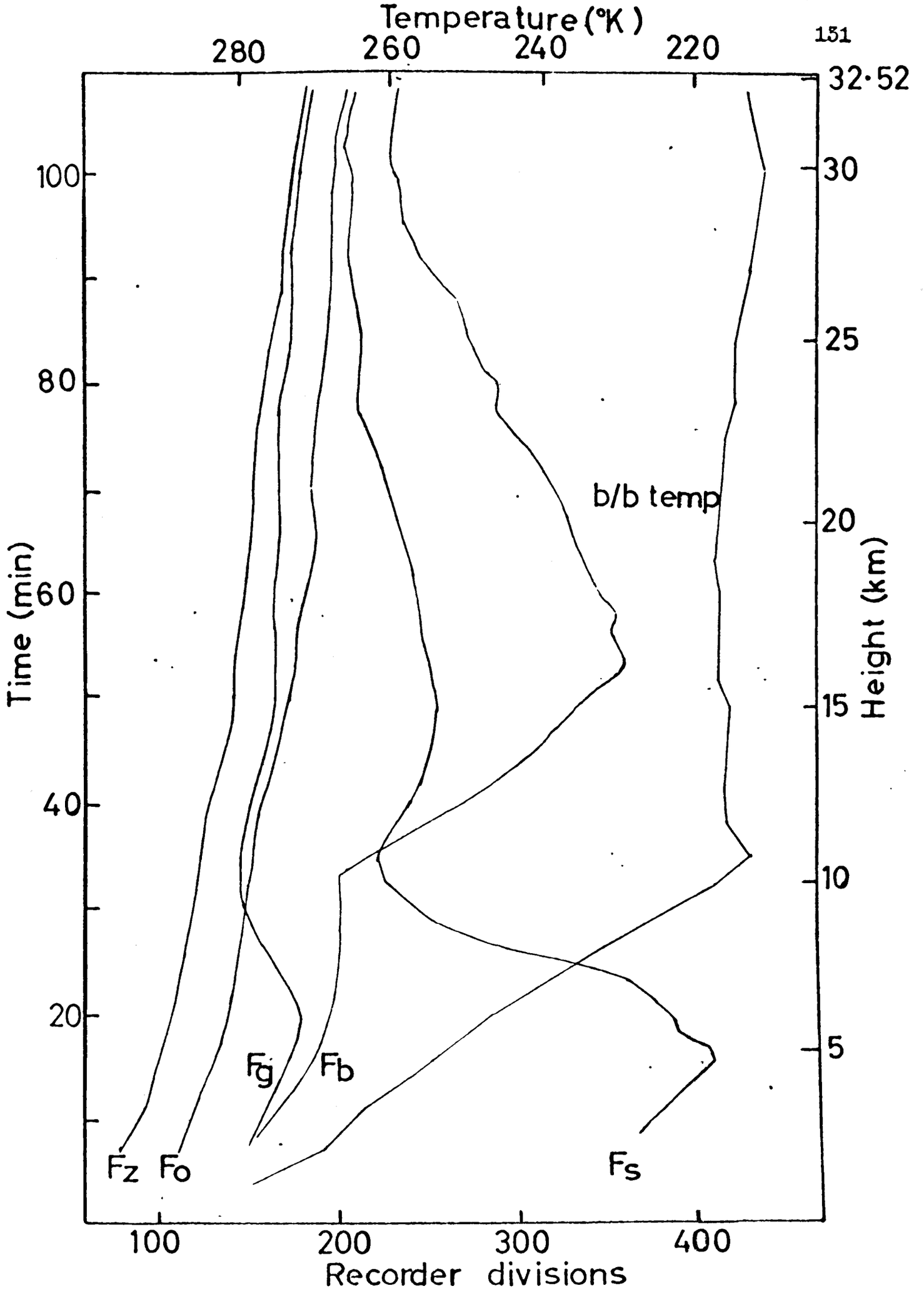


Fig. 6.5 Ascent 9 10-9-63

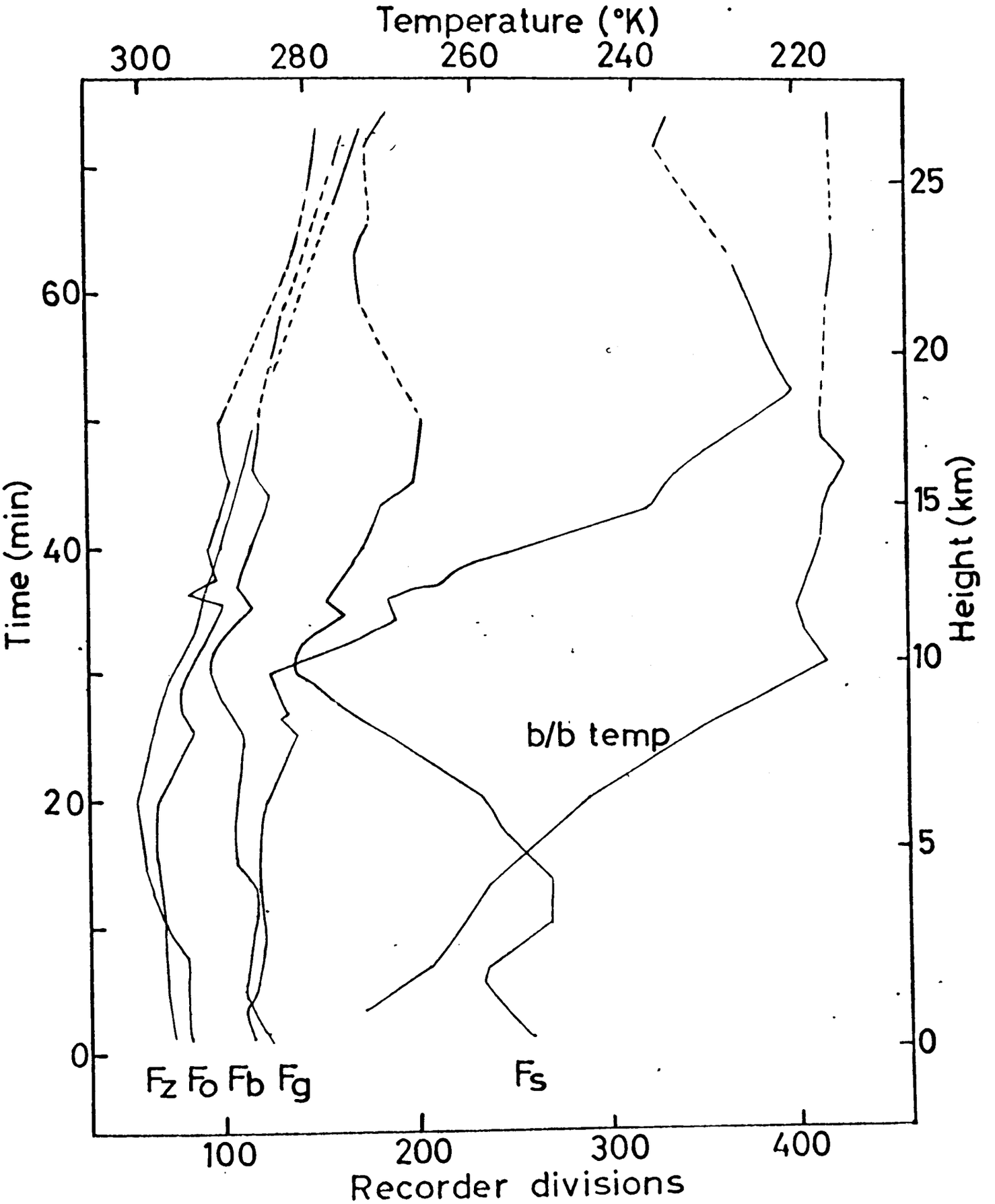


Fig. 6.6 Ascent 10 11-9-63

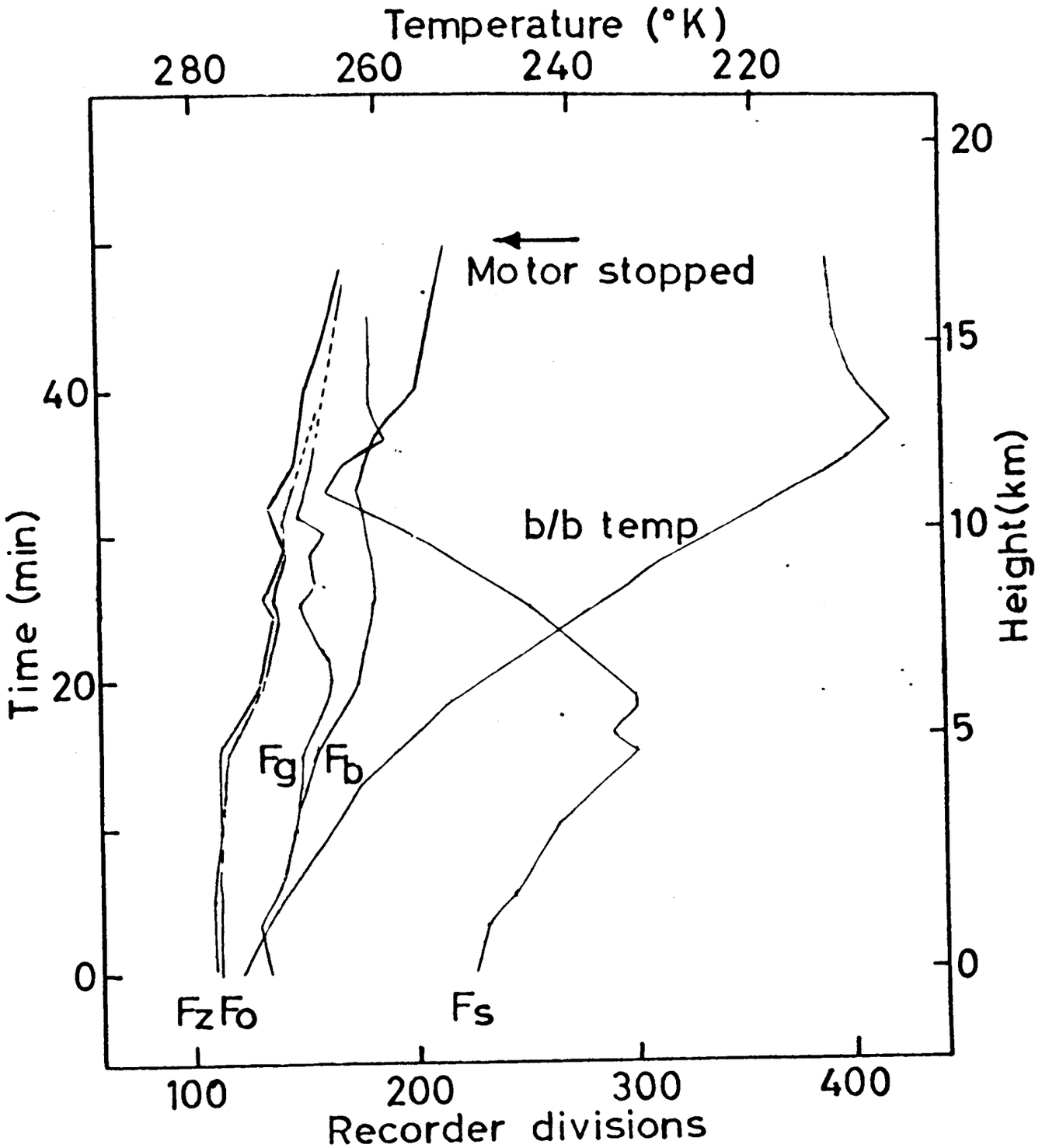


Fig. 6.7 Ascent 11 12-9-63

Chapter 7

Analysis of ascent data

7.1 Optical considerations

The radiometer-sonde measures total downward emission from the night sky within the pass band of the detector and filter. The spectral response of this combination is an important factor in the subsequent analysis of ascent data. Laboratory measurements of spectral response are discussed in Chapter 8.

The field of view of the detector is limited by internal stops to an included angle of 25^{o} and the axis of view normally set at 30^{o} to the vertical. The distance between the balloon and the sonde is made sufficiently large to ensure that no part of the balloon, at any time, comes into the field of view of the detector. The angle of offset used would allow for expansion of the balloon up to a diameter of about 150 feet, which is four times the maximum anticipated size at 30 km.

Because of the offset direction of view of the detector, the path lengths involved in the atmosphere are greater than the corresponding vertical distances by a factor sec Θ . This factor has little effect, except in the case of the last four ascents, when it represents an increase of about 40%.

The radiometer does not, in fact, receive parallel radiation. However, the range of angles involved (25°) is sufficiently small that little error is introduced if a parallel beam is assumed. In any case, as was stated in Section 5.1, the effect can also be represented, if it is significant, by a suitable multiplying factor.

7.2 Evaluation of water vapour mixing ratios

The downward vertical intensity of infra-red radiation of frequency ν at a height z in the atmosphere was shown in Chapter 5 to be given by

$$I_{\nu}(z) = \int_{z'=z}^{\infty} B_{\nu}(z') \frac{d}{dz'} \tau_{\nu}(z,z')\, dz'$$

where the notation is the same as was previously used.

We may now define the spectral sensitivity α_{ν} of the radiometer detector as its relative responsivity to radiation of frequency ν at any given height. The overall responsivity $R(z)$ is the net output at a height z, resulting from a given incident flux of radiation. $R(z)$ changes with height as a result of the variation in detector resistance as is discussed in Chapter 4. α_{ν} is assumed to be independent of height.

The signal which is produced by the detector at a height z is thus given by

$$S(z) = R(z)\int_0^\infty \alpha_\nu \int_{z'=z}^\infty B_\nu(z') \frac{d}{dz'} \tau_\nu(z,z')\, dz'.\, d\nu \quad - 7.1$$

The quantity $S(z)$ is the telemetered detector signal and represents the only information which is obtained regarding the infra-red flux at height z.

Interpretation of ascent data proved to be more difficult than was at first imagined. Of the quantities in equation 7.1, $R(z)$ can be determined from the black body calibration signal, α_ν is known and $B_\nu(z')$ can be calculated from air temperature data. There remains the transmission $\tau_\nu(z,z')$. As well as being a function of z, z' and ν the transmission is dependent on the pressure, temperature and water vapour concentration along the path length, together with spectroscopic data concerning the 6.3 μ band. Of these, the only unknown is the water vapour concentration so that, in theory, this can be determined.

However, without any information regarding the spectral distribution of the signal making up $S(z)$, it is not possible to derive any analytical solution of equation 7.1 and it is necessary to employ numerical methods.

The method of approach which has been adopted consists of finding a distribution of water vapour which would produce the same radiometer signals, calculated as a

function of height, as those observed. This must then be a unique solution.

For the purpose of analysis, the atmosphere was divided up into layers by a set of horizontal levels at 1 km intervals. At any height z the value of $S(z)$ can be calculated from equation 7.1, for a given water vapour distribution above z, and compared with the value actually measured by the sonde. If the amount of water in the layer immediately above z is the only unknown quantity, then clearly this may be determined by adjusting it iteratively until satisfactory agreement between calculated and observed values of $S(z)$ is obtained. The initial assumption is made that the signal measured at the top of the ascent is due to water vapour which is distributed with a constant mixing ratio above that level. The mixing ratio is chosen to provide agreement between observed and calculated values of $S(z_{max})$. Having determined the residual water vapour, the procedure outlined above is performed in 1 km steps down through the atmosphere, beginning with the level below z_{max} and the water vapour distribution is built up layer by layer.

For the purpose of numerical computation, the integrals in the expression for $S(z)$ were replaced by summations. Path length summations were carried out over the 1 km intervals as described above, the upper limit of the outer

summation being z_{max} , the height of the highest measurement. Calculations were made at intervals of 50 cm^{-1} and the frequency summation was carried out over the pass band of the detector.

At each level, the responsivity of the detector $R(z)$ was calculated from the measured black body reference signal, $S'(z)$ using the formula

$$S'(z) = R(z) \sum_{\nu} \alpha_{\nu} B'_{\nu}(z) \Delta\nu$$

where $B'_{\nu}(z)$ is the Planck function at a frequency ν and at a temperature corresponding to that of the black body at a height z.

In determining the transmissions of atmospheric path lengths, the statistical model, which was described in Chapter 5, was used in the form

$$\bar{\tau}_{\nu}(z,z') = \exp\left\{-u\left(G_{\nu} + \frac{u}{P} H_{\nu} \frac{T_0}{T}\right)^{-\frac{1}{2}}\right\} \qquad 7.2$$

where

$$G_{\nu} = \frac{\delta^2}{S^2} \qquad \text{and} \qquad H_{\nu} = \frac{P_0 \delta}{\pi \alpha_0 S}$$

G_{ν} and H_{ν} are parameters which contain the information relating to the average spectral properties of the absorption band at the frequency ν. Other symbols are as defined in Chapter 5. u was taken to be the arithmetic sum of the amounts of water in each interval of

the path, while p was determined from the Curtis-Godson approximation. A weighted mean value for the temperature was calculated in the same way as the pressure.

The dependence of line half width on temperature and pressure gives rise to these two parameters in the transmission formula. There is also a certain variation of line strength with temperature due to the effect of the latter on the population of the molecular energy levels. This results in an increase with temperature of line strengths in the wings of the band and a decrease of those near the band centre. The variation would be difficult to allow for, and as it does not produce any significant effect on transmission calculations over the whole band, it has been ignored in the present study.

Reduction of ascent data was carried out using the University Ferranti Mercury computer and a brief description of the programme is given in Appendix III.

7.3 Determination of the parameters G_ν and H_ν

The statistical model parameters G_ν and H_ν were determined for 50 cm^{-1} intervals of the 6.3 μ water vapour band by making use of the published absorption spectra of Burch, Gryvnak, Singleton, France and Williams (1962). Some of these spectra are shown in fig. 7.1. The spectra were divided up, as shown, and the mean transmission in

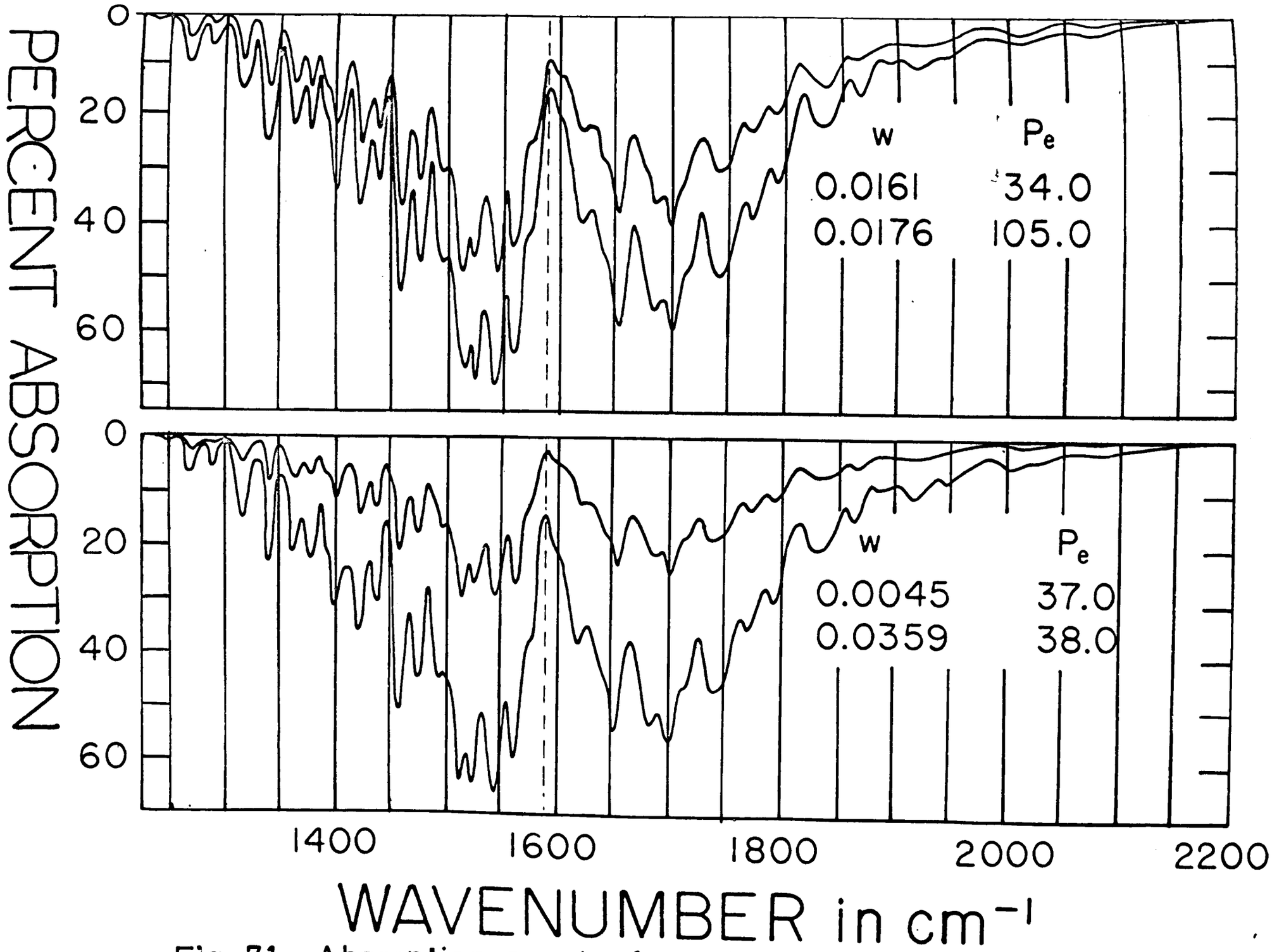


Fig. 7.1 Absorption spectra from the 6.3 μ water vapor band

each frequency interval determined by planimetering. This was performed for 15 spectra taken at different pressures and with different path lengths of water vapour. Some of the spectra had been taken using large absorber concentrations. Effective pressures are quoted by Burch et al which correspond to equivalent path lengths reduced to infinite dilution, assuming a self broadening factor of 4.

If the transmission data for each frequency interval can be represented by the statistical model, then a plot of $(\log \tau / u)^2$ against u/p will be a straight line. The gradient m and intercept c on the $(\log \tau / u)^2$ axis will be given by

$$m = \frac{p_0 \delta^2}{\pi \alpha_0 S} \sqrt{\frac{T_{lab}}{T_0}} \quad ; \quad c = \frac{\delta^2}{S^2}$$

where α_0, δ and S are appropriate mean values for the particular interval of the spectrum. G_ν and H_ν follow directly from m and c and the value of T_{lab}, the temperature at which the laboratory spectra were taken. A least squares method was used to fit the best straight line to each set of planimetered data. Values of H_ν, obtained from the gradients, are plotted in fig. 7.2 and are of the form expected. Intercepts, on the other hand, showed a large amount of scatter, especially near the band centre and

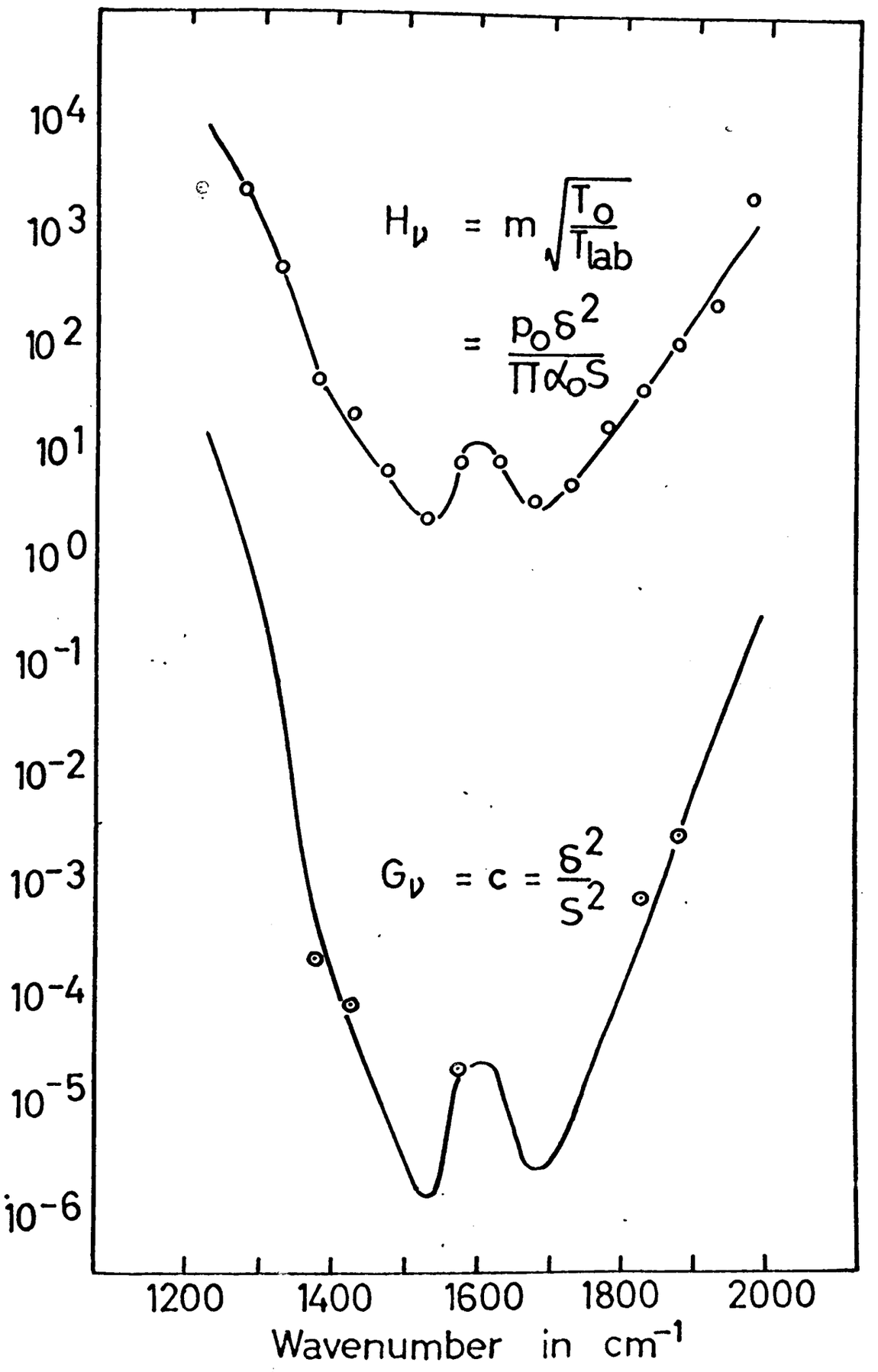


Fig. 7.2. The statistical model parameters G_ν and H_ν.

in the wings. This is explained by the fact that nearly all the planimetered data can be represented by the strong line approximation of the statistical model. This is obtained when the second term predominates in the exponent of the right hand side of equation 7.2 or, quantitatively, when

$$\frac{S u P_o}{\pi p \alpha_o} \sqrt{\frac{T}{T_o}} \gg 1$$

Using the value 0.065 cm^{-1} given for α_o by Benedict and Kaplan (1959) the above condition may be written as

$$S \gg 10^{-4} \frac{P}{u}$$

Values of P/u for the planimetered spectra used ranged from about 10^3 to 5×10^5 so that, in the majority of cases, the strong line approximation would apply in all but the wings of the band. Here, though, the accuracy of the planimetered data was too small to provide any reliable results. However, a few reasonable values of C were obtained for intermediate spectral regions on both sides of the band centre and are plotted in fig. 7.2. Using the value of α_o given by Benedict and Kaplan (1959) and the relation

$$\frac{m}{c} = \frac{P_o \delta}{\pi \alpha_o} \sqrt{\frac{T_{lab}}{T_o}}$$

a mean value of $\delta = 0.45\ cm^{-1}$ was calculated for the part of the band which gave usable intercepts. This value was assumed to be representative of the whole band, and the remaining intercepts were calculated from the corresponding values of gradient using the relation

$$c = \frac{m^2 \pi^2 \alpha_0 T_0}{P_0^2 \delta^2 T_{lab}}$$

A test, which was made to investigate the accuracy of the statistical model as defined above, is described in the next chapter.

7.4 Spurious signals

Immediate interpretation of ascent data was hampered by two anomalous phenomena, one or both of which occurred on all the flights. The first of these, namely the sudden change in detector signal accompanied by a shift in the zero signal, was mentioned in Chapter 4 and has been attributed to malfunctioning of the reference signal generator. The fault was cured on the last four ascents by an improved design of circuit.

A second irregular effect was the appearance of negative values of the reduced gain sky signal S_g. One example of this can be seen in fig. 6.5 which shows data obtained from Ascent 9. The level F_g, corresponding to

the received sky signal on reduced gain, is seen to cross the zero signal level F_o at minute 30.2 and to remain below this level throughout the remainder of the flight.

It was noticed that the zero signal level was positive with respect to the electrical signal level F_z and that F_g never dropped below F_z. These observations lead to the idea that a spurious signal originating in the detector or cathode follower circuits might be responsible for the negative signals. This may be explained as follows.

Fig. 7.3 (i) shows the positions of the various levels associated with signals on full gain. Z is assumed to be the true zero signal level and differs from F_o by an amount equal to P, the spurious signal introduced. Providing measurements are referred to F_o, the value of the full gain signal S is unaffected, since the level F_s will also be higher than the true level by an amount P.

When transmitting the signal on reduced gain, however, the spurious signal does not cancel out, as can be seen by reference to fig. 7.3 (ii). The spurious signal P is reduced by the gain factor g so that the effective zero level F_o' is now nearer to the true zero. The true reduced gain signal S/g is the difference between the levels F_g and F_o', but because measurements are still referred to F_o, the indicated value S_g is less than the true value by an amount $P(1-1/g)$

Hence

$$S_g = \frac{S}{g} - P(1 - 1/g)$$

Clearly this is negative if

$$P(1-1/g) > S/g$$

that is if

$$P > S/(g-1)$$

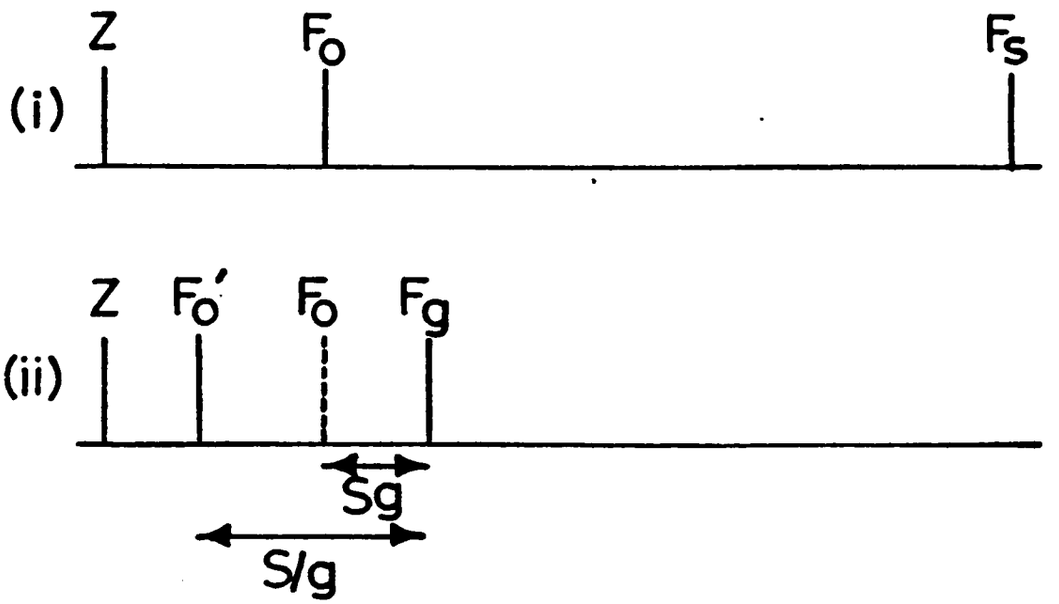


Fig. 7.3

The exact nature of the spurious signal is not clear. Possible sources are electrical pick-up from the chopper originating in the detector or cathode follower circuits, or some form of R.F. interference. In either case the effect appears to be dependent on the resistance of the detector as it becomes more pronounced towards the end of the ascent.

All that need be assumed in order to interpret data in the above fashion is that the spurious signal is introduced before the gain change occurs and that it remains constant at a given level. The value of P can then be determined; it is

$$P = \frac{S - gS_g}{g-1}$$

This information can be used to calculate the true value of the black body signal S'. If the indicated value referred to F_o is S_b, then it is easy to show that

$$S' = g(S_b - S_g) + S$$

Good evidence in favour of the above explanation of negative signals is provided by the fact that the ratio

$$\frac{F_s - F_z}{F_g - F_z}$$

is found to remain fairly constant throughout the ascent and close to the known value of the gain factor g. This suggests that the true signal zero is close to the electrical zero F_z. The ratio

$$\frac{F_s - F_o}{F_g - F_o}$$

which is equal to S/S_g would correspond to the gain factor if no spurious signal were present. In practice this ratio varied over wide limits during the ascent.

It is known (see Section 4.2.6) that the true signal zero does correspond closely with the electrical zero near ground level. As an extra check, therefore, the value of g used in the calculation of corrected black body signals was determined from the mean value of

$$\frac{F_s - F_z}{F_g - F_z}$$

for data near ground level.

All results which are presented in the following sections are based on data which have been interpreted as above.

Chapter 8

Interpretation of results based on data from Ascent 9

8.1 Introduction

The first ascent data on which analysis was attempted was Ascent 6, made on 9th October, 1962. The results possessed rather unexpected features and it was later realised that this was probably due to incorrect functioning of the apparatus. In consequence, interpretation of the results proved to be dubious.

For the purpose of this discussion, all remarks refer to Ascent 9 which was made on 10th September, 1963. Good data were obtained on this occasion up to a height of 31 km and, apart from the slight uncertainty attached to the interpretation of the negative signals, discussed in Chapter 7, the apparatus appeared to function satisfactorily.

The results of an early analysis of the data from this ascent are shown in fig. 8.1. The following features required further explanation.

1. Large fluctuations of mixing ratio occurred between successive levels. The fluctuation was so great between 24 km and 28 km that results were meaningless and are not plotted.

2. A very large value was obtained for the residual amount of water above the level of the highest measurement.

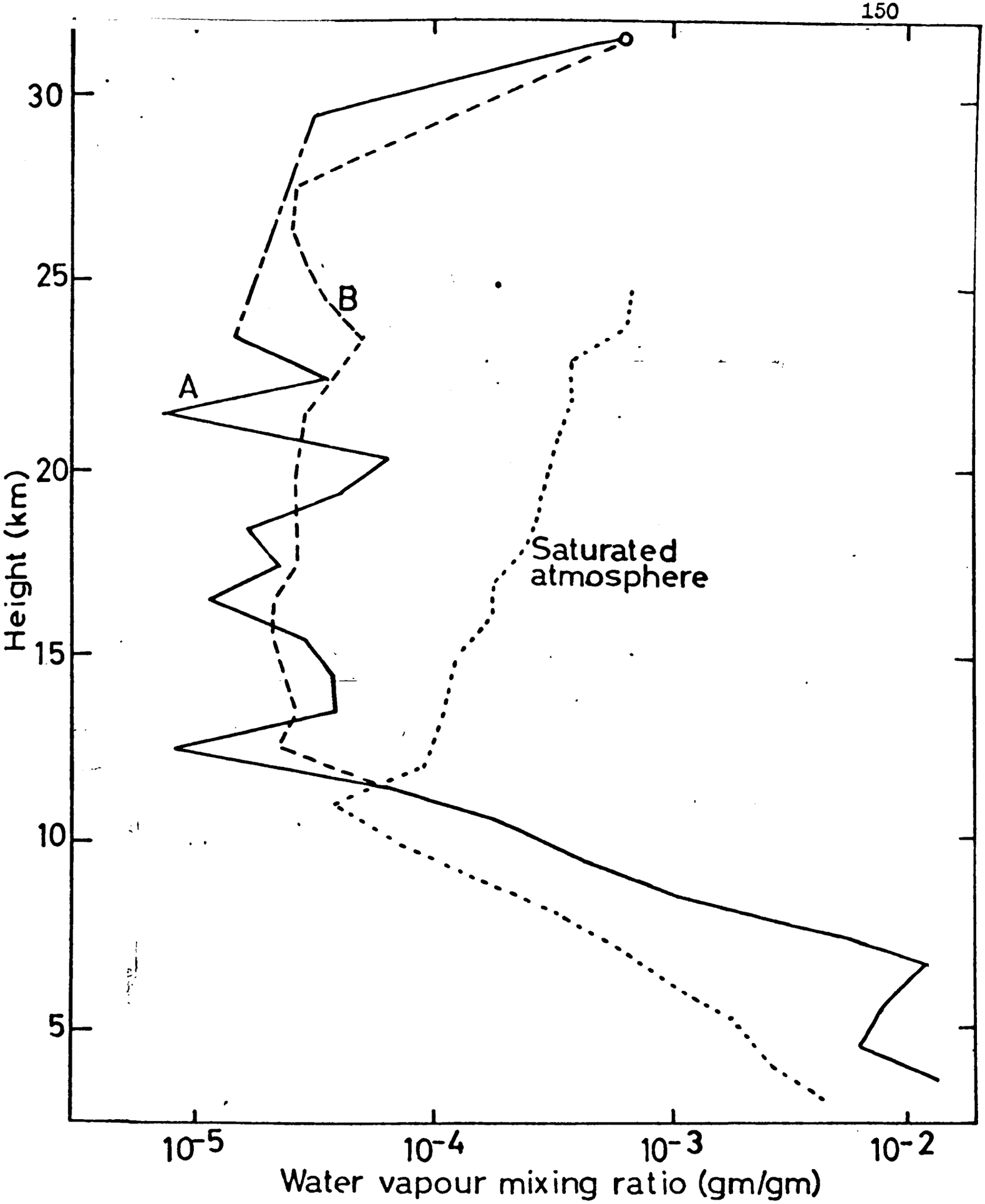


Fig. 8.1. A. Results of the first analysis of data from Ascent 9.

B. As above but using smoothed ascent data.

It corresponded to a mean mixing ratio of about 6×10^{-4} above 32 km.

3. The mixing ratio just above the tropopause was nearly an order of magnitude greater than that normally expected.

4. The mixing ratio in the troposphere represented humidities which were supersaturated by a factor of 2 or 3.

8.2 Data smoothing

The fluctuations in results from level to level are mostly due to errors in the radiometer-sonde data and cannot be said to represent real structure. The calculation of downward flux at each level involves the transmission gradient which, in turn, depends on the values of mixing ratio in higher levels previously calculated, again from the sonde data. Small random errors in the raw data can therefore be expected to have a considerable effect on values of transmission gradient and thus to affect the final results.

It seemed desirable to eliminate this, if possible, by smoothing the original data. The sensitivity of the radiometer was known to be a smooth function of pressure (see Section 4.2.4) which, in turn, is a smooth function of height. It was shown in Chapter 7 that the responsivity $R(z)$ at a height z could be represented by an expression of the form

$$R(z) = \frac{S'(z)}{\int_{\nu} \alpha_{\nu} B'_{\nu}(z)\, d\nu}$$

where the same notation has been used. Computed values of $R(z)$ are plotted in fig. 8.2 and a smooth curve has been drawn in. Smoothed responsivity data were then used to compute corrected values of the black body calibration signal $S'(z)$ and these were then used in the main calculation.

Hand smoothing of responsivity data was later replaced by an analytical process which could be performed by the computer as part of the main calculation. This consisted of fitting an eighth degree polynomial to the data by the method of least squares. The result was almost identical with the hand drawn curve and a great deal quicker to obtain.

A further improvement was obtained by smoothing the sky signal $S(z)$ (fig. 8.2). Although this is not necessarily a smooth function of height, it was clear that the major part of the fluctuations in sky signal data was due to experimental error. It was therefore felt that no information would be lost in the second smoothing. That this theory is borne out can be seen from fig. 8.1, which shows the result of smoothing both sets of data. Sky signals had to be smoothed by hand, as the profile involved was too complicated

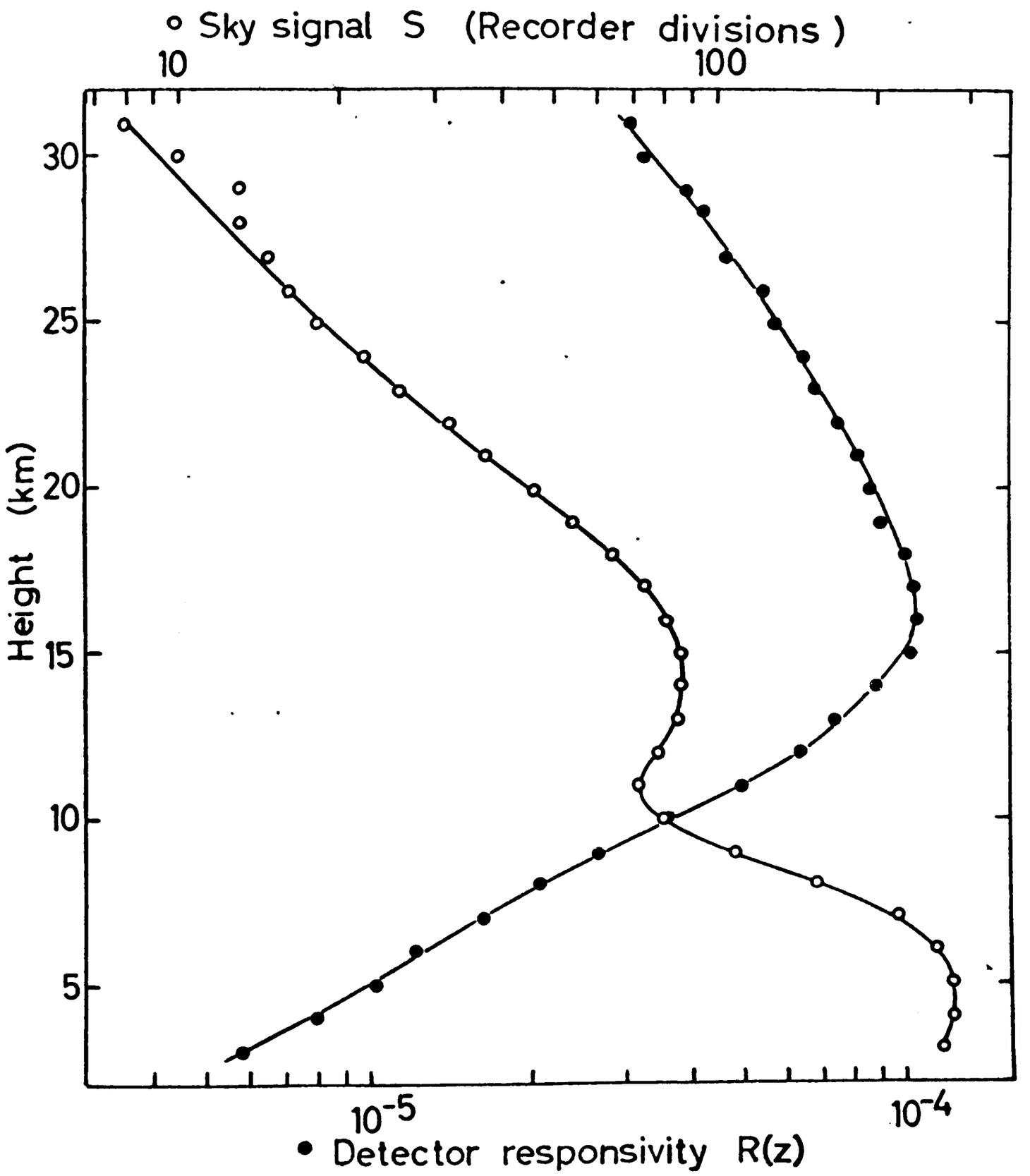


Fig. 8.2. Smoothing of detector responsivity and sky signal data.

for simple polynomial fitting. Data smoothing was adopted in all subsequent calculations.

8.3 Residual mixing ratio

The large result obtained at 31 km seemed to indicate that energy from a source other than atmospheric water vapour was being received by the detector. The existence of emission, originating in the high stratosphere, has been suggested by Hampson (private communication), but little is known of its exact nature. The possibility of any local source of radiation reaching the detector can be discounted as every precaution was taken to avoid this.

If it is assumed that the residual signal received by the sonde at 31 km is not due to water vapour, and that it originates above this level, then its effect can be removed in the subsequent analysis. Such radiation will not suffer absorption by water vapour in the lower atmosphere to nearly the same extent as that emitted by water vapour itself. In the latter case absorption takes place at just those frequencies where the emission occurs, whereas the mean absorption of the whole spectral region is the significant factor in the case of emission from a black body or from another uncorrelated line spectrum.

As the mean transmission of water vapour in the stratosphere is small, radiation from a high altitude foreign

source would be expected to extend well down into the troposphere and affect measurements made at all but the lowest levels. By calculating the magnitude of the signal which would occur at each height and subtracting it from the result actually obtained, contributions from the external source were removed. As can be seen in fig. 8.3 the effect on results above 20 km is large. Even at the tropopause the foreign signal is responsible for a substantial factor in the indicated mixing ratio.

8.4 Excessive mixing ratios .

It remained to explain why the values of mixing ratio obtained from the calculation were consistently too large. It is well known that the water vapour mixing ratio in the lower stratosphere is in the region of 3×10^{-6} gm/gm, whereas the value given by the calculation was several times greater than this. The degree of supersaturation indicated in the troposphere was clearly impossible. There was little cloud present on the particular night that the ascent had been made, but even if there had been, it is difficult to see how it could have had such a consistent effect on the results. It certainly could not be used to explain the large results in the stratosphere. The effect was more indicative of a systematic error in the analysis. The following were considered as possible causes of the trouble:

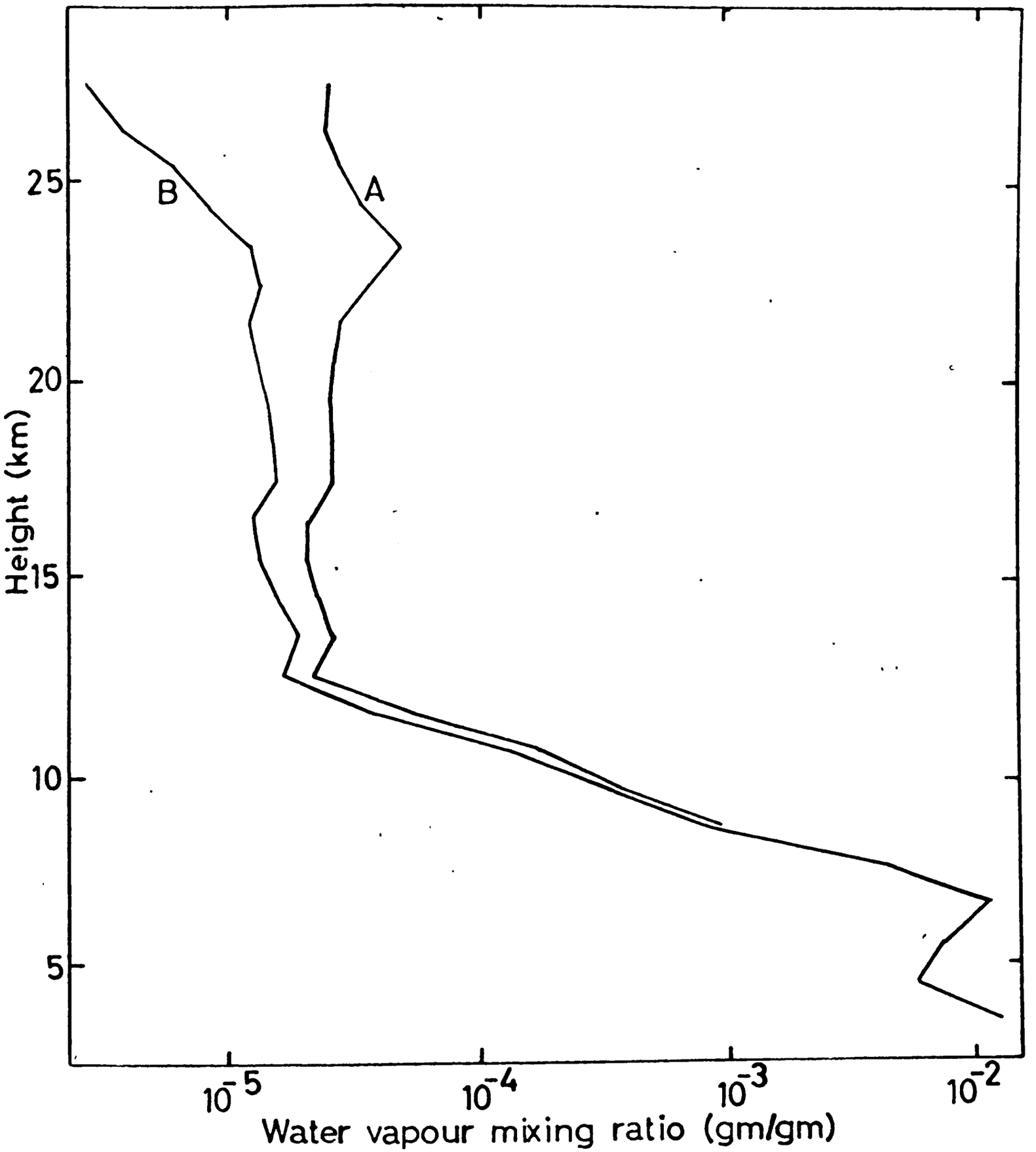


Fig. 8.3. The effect of the residual signal at 31 km.

A. Signal assumed to be due to water vapour emission

B. Signal assumed to be due to a foreign emission.

1. Fault in the computer programme
2. Statistical model inaccurate
3. Emissivity of calibration black body not unity
4. Detector spectral sensitivity data wrong
5. Signals due to atmospheric emissions other than water vapour.

These possibilities will now be discussed in turn.

8.4.1 A check on the computer programme

As any form of hand checking of the main calculation would have been very difficult, the following method was adopted. By means of an independent calculation sets of synthetic flight data were produced from several different atmospheric water vapour profiles. These were then put into the main calculation and the resulting mixing ratios compared with the original values. Agreement was perfect in every case.

8.4.2 The accuracy of the statistical model

Some calculations of total band absorption for the 6.3 μ band were made to test the accuracy of the statistical model used in the main calculation. The path lengths and pressures were chosen from those which had been used in the laboratory measurements by Burch, Gryvnak, Singleton, France and Williams (1962). The calculated absorptions were compared with the measured values given by Burch et al.

Fig. 8.4 shows the measure of agreement obtained. The statistical model appears to produce rather greater absorption for small path lengths and pressures and vice-versa, agreement being best for values of pressure x path length in the region of 1 mb ppt. cm. This value is of a similar magnitude to that associated with path lengths in the middle troposphere.

8.4.3 Detector spectral sensitivity data

The long-wave cut-off of the detector occurs at a frequency at which the Planck radiation function for atmospheric temperatures rises steeply. As a result, the value of the detector responsivity $R(z)$ determined in the main calculation will be very much influenced by the position of the long-wave edge. It has been assumed that the shape of the spectral sensitivity curve is independent of detector temperature and laboratory measurements have shown that the variation is small. What had not been realised, however, was that the size of the detector itself had a considerable effect on the position of the long-wave edge. Results of some early measurements made on a comparatively large specimen are shown in fig. 8.5. These data were used in the analyses which have been described so far. Measurements subsequently made using a detector and filter taken from one of the sondes are also shown in

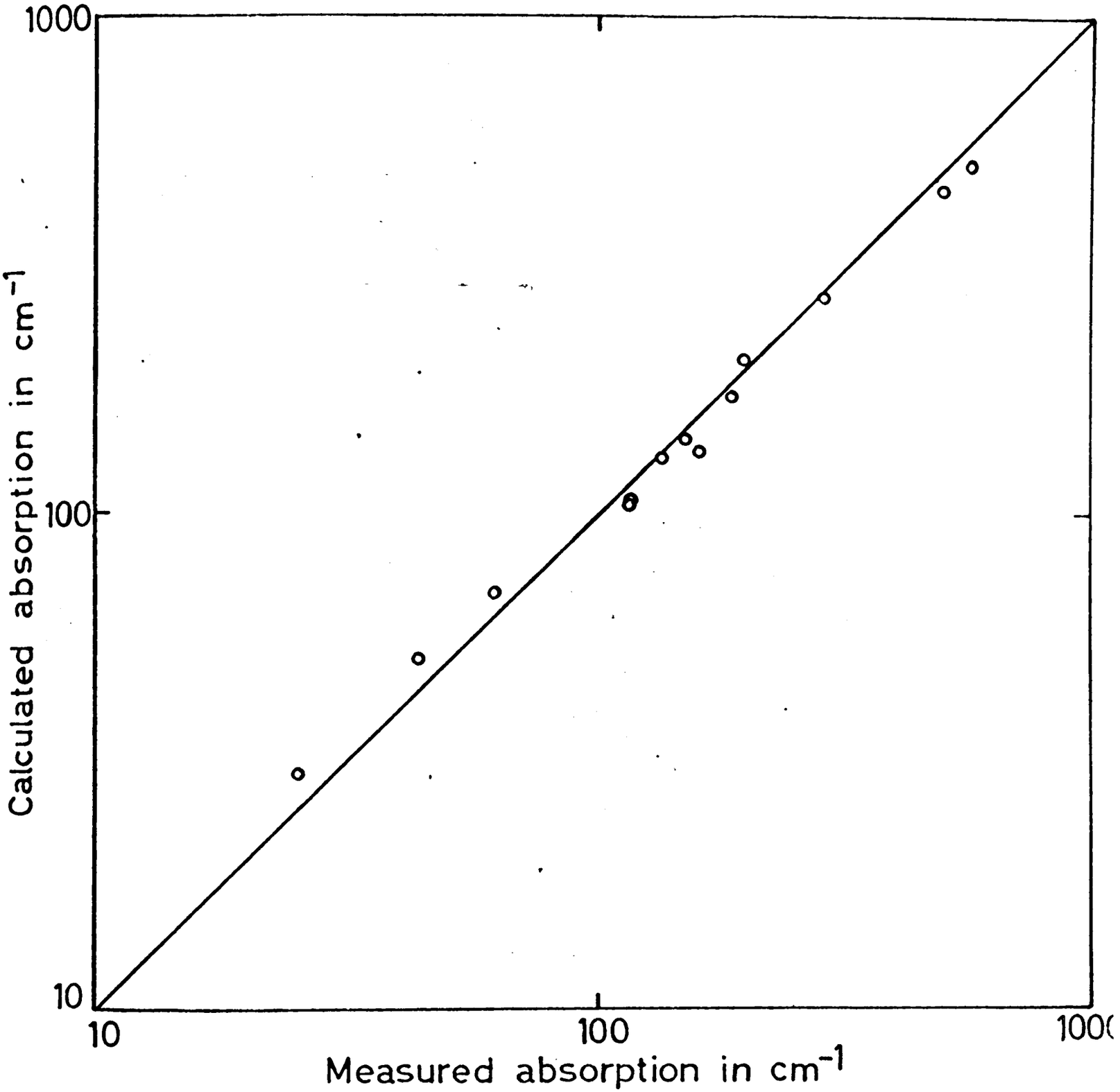


Fig. 8.4. Total absorption by the 6.3 μ water vapour band calculated on the basis of the statistical model, compared with the original measurements of total absorption by Burch et al (1962)

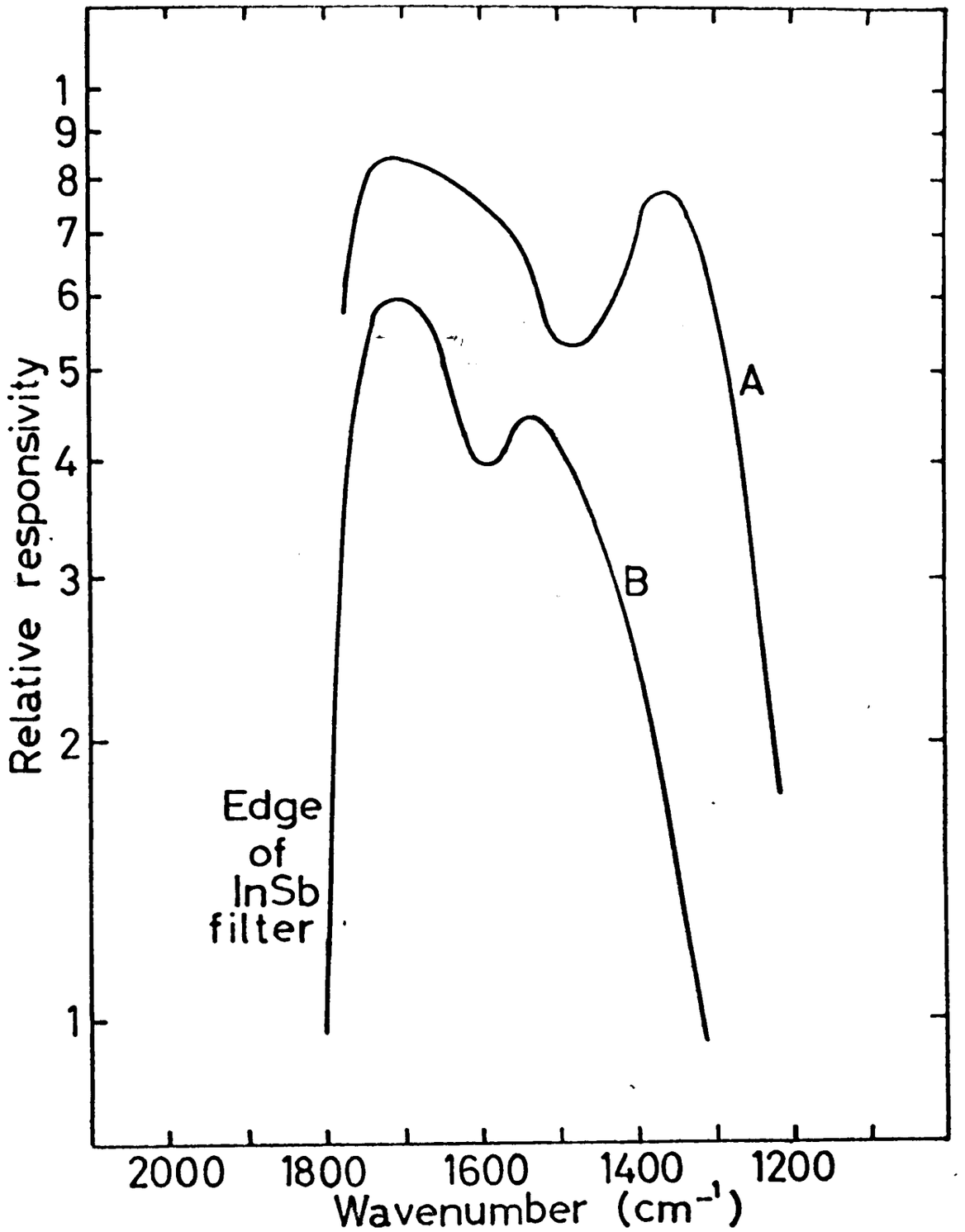


Fig. 8.5. Detector spectral sensitivity profiles.

A. Large specimen

B. Detector used in radiometer-sonde

fig. 8.5. It can be seen that the position of the edge differs by about half a micron from that of the previous results. The effect that this has on mixing ratios produced by the calculation can be seen from fig. 8.6.

8.4.4 The emissivity of the black body

As the spectral sensitivity of the detector did not extend beyond about 7 μ, it was felt that the absorbing properties of ordinary optical black paint would be sufficiently good to enable it to be used on the surface of the black body cone. As a check on this, a sonde was set up in a darkened room with the detector pointing at the ceiling. The black body, also at room temperature, was then placed over the detector aperture. The change in the signal measured by the detector was less than 5%. Had the black paint been at all reflecting, a reduction in signal would have occurred due to the close proximity of the cold detector enclosure.

Whether or not the black paint remained 'black' at all times during an ascent would be very difficult to assess, but there seemed to be no good reason for doubting that this would be the case. However, black body emissivities of 0.95 and 0.9 were included in the calculation to determine the effect. It was found to be only significant in the first few kilometers of the troposphere.

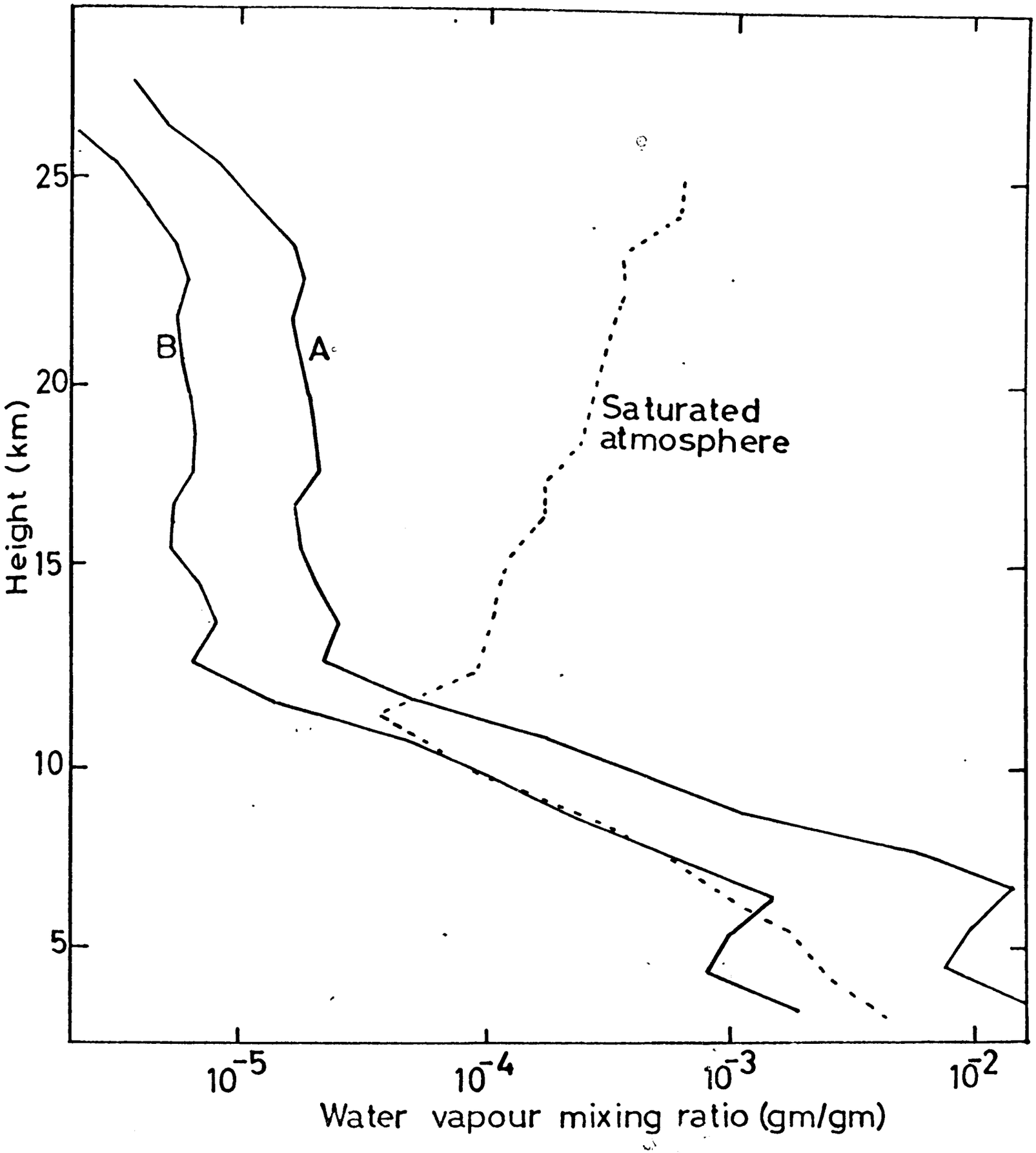


Fig. 8.6. The effect of the spectral profile of the detector on calculated mixing ratios.

A. Profile from large specimen

B. Radiometer-sonde detector profile.

8.4.5 Atmospheric emissions other than from water vapour

When all the above factors had been taken into account, results obtained for the troposphere still represented saturation. Emission from other atmospheric constituents was then considered. There appeared to be three possibilities. Methane has a band at 7.65 μ and nitrous oxide one at 7.78 μ. There is also pressure induced emission in molecular oxygen in a band centred at 6.45 μ. Little attention had originally been given to the first two of these as it had been assumed that they would contribute little, compared with the emission from water vapour, especially as they both occurred near the edge of the pass band of the detector where the sensitivity was relatively small. However, more detailed investigation revealed that they had a very significant effect, especially in the lower stratosphere and middle troposphere.

Data for methane were taken from the laboratory spectra of Migeotte, Neven and Swensson (1957). Mean absorptions in 50 cm^{-1} intervals were measured from the spectra and used to calculate constants for a square root absorption law of the form

$$\bar{A}_\nu = K_\nu(CH_4)\sqrt{p\,u(CH_4)}$$

where $\bar{A}_\nu$ is the mean absorption in a 50 cm^{-1} interval centred at ν of a path length containing $u(CH_4)$ gm of methane at a pressure P. It was considered that a square root law would be sufficiently accurate, as the lines of the methane band are widely separated and, in any case, the effect was only being introduced in the form of a correction. Results for nitrous oxide given by Goody and Wormell (1951) were treated similarly.

Provided the absorption is not very large, the combined effects of the two bands at any one frequency will be given by

$$\bar{A}_\nu = A_\nu(CH_4) + A_\nu(N_2O)$$

$$= K_\nu(CH_4)\sqrt{pu(CH_4)} + K_\nu(N_2O)\sqrt{pu(N_2O)}$$

The atmospheric path length of each absorber can be calculated in terms of its volume mixing ratio y (assumed constant) and molecular weight M by the relation

$$u = y\frac{M}{M_{air}} \times u_{air}$$

Hence we have for the two absorbers

$$\bar{A}_\nu = \left\{K_\nu(CH_4)\sqrt{y_{CH_4} M_{CH_4}} + K_\nu(N_2O)\sqrt{y_{N_2O} M_{N_2O}}\right\}\sqrt{\frac{u_{air}}{M_{air}}}$$

$$= C_\nu \cdot \frac{u_{air}}{M_{air}}$$

This treatment can be extended to include any number of minor atmospheric constituents. The value of C_ν is plotted in fig. 8.7. Mixing ratios were assumed to be 1.5×10^{-6} cm^3/cm^3 for methane and 3.5×10^{-7} cm^3/cm^3 for nitrous oxide.

Using the results obtained above, the signals which would result from emission from methane and nitrous oxide were calculated at each kilometer level in the atmosphere. These are listed in Table 2 together with the values of sky signal measured by the radiometer sonde. The former values represent about 20% of the total signal at the tropopause.

Pressure induced absorption in oxygen occurs as a result of the dipole moment induced in the oxygen molecule by collision with other molecules. The gas may then be regarded as having an absorption coefficient which is proportional to the partial pressure of oxygen as well as the total gas pressure. The transmission of a column of air, length l, is given by

$$\tau = \exp\left(-k\gamma^2 p^2 l\right)$$

where γ is the volume mixing ratio of oxygen and p the total pressure in atmospheres. The constant k, which is the absorption coefficiert per cm per atmos^2, is given

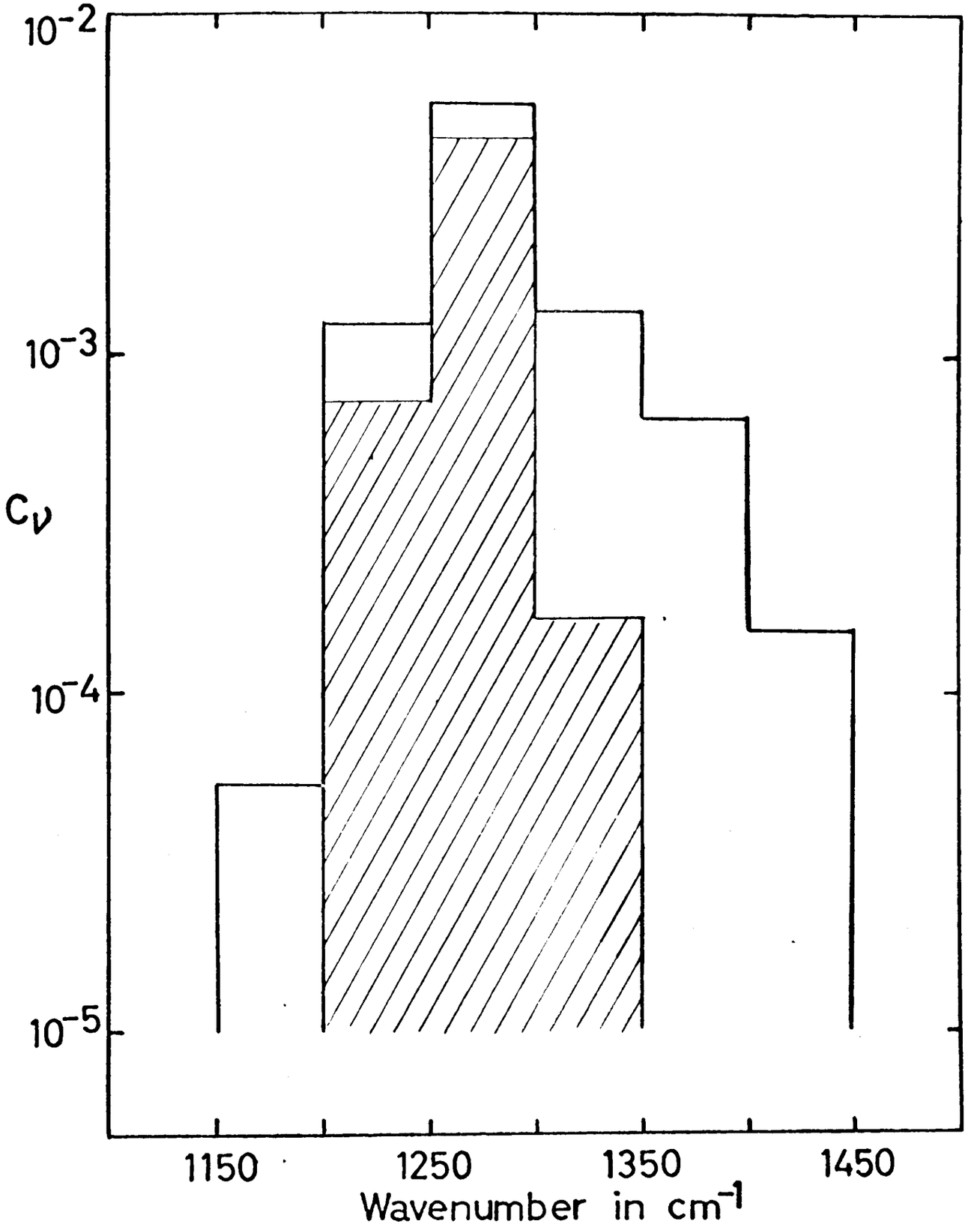


Fig. 8.7. The constant C_ν used in the square root absorption law for CH_4 and N_2O. The shaded area represents the contribution by N_2O.

Height km	Computed signal from CH_4 and N_2O	Observed sky signal (smoothed)
31	0.081	8.30
30	0.212	9.47
29	0.350	10.80
28	0.535	12.35
27	0.768	14.20
26	1.070	16.25
25	1.459	18.75
24	1.940	21.85
23	2.522	26.00
22	3.289	31.20
21	4.304	37.25
20	5.571	44.60
19	7.176	53.60
18	9.001	63.70
17	10.860	73.20
16	12.697	80.00
15	14.117	83.80
14	14.866	85.00
13	15.014	84.00
12	14.374	77.00
11	12.493	71.00
10	10.812	78.00
9	10.578	106.00
8	11.187	151.00
7	12.270	216.00
6	13.766	256.00
5	15.593	271.00
4	17.197	272.00
3	17.596	261.00

Table 2. Computed signal due to methane and nitrous oxide compared with that actually observed.

by Crawford, Welsh and Lock (1949) and is shown in fig. 8.8.

If the volume mixing ratio of oxygen is assumed to remain constant with height in the atmosphere, it can be shown that for an isothermal atmosphere, the transmission of a path between pressures p_1 and p_2 is given by

$$\tau = \exp\left[\frac{-k\gamma}{2p_0\rho_0 g}\left(p_1^2 - p_2^2\right)\right]$$

where ρ_0 is air density at standard pressure p_0. Assuming a value of 0.2 for γ and putting in values for the other constants, we obtain

$$\tau = \exp\left\{-7{\cdot}18\times10^{-2}\ k\left(p_1^2 - p_2^2\right)\right\}$$

This expression was used to obtain values for oxygen transmission in different path lengths. The water vapour transmissions obtained in the main calculation were then multiplied by the appropriate values. The effect was nowhere very large, being greatest in the lower atmosphere where it amounted to a few percent.

When the combined effect of methane, nitrous oxide and oxygen were incorporated into the calculation, mixing ratios in the troposphere were found to agree well with values calculated from radiosonde humidity measurements made during the same ascent. Mixing ratios in the lower

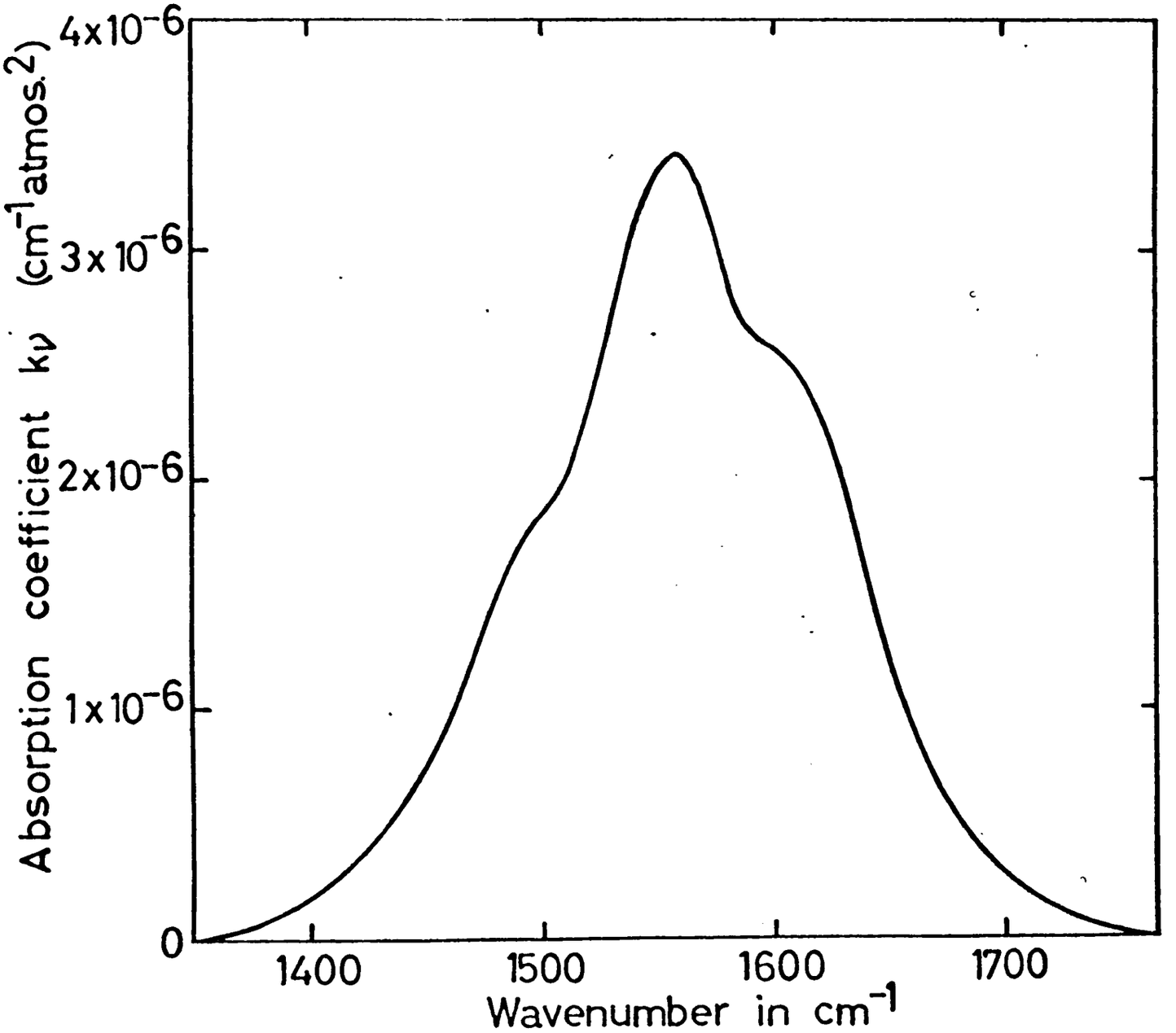


Fig. 8.8. Coefficient of pressure induced absorption in oxygen.
(After Crawford, Welsh and Lock (1949))

stratosphere were also of the correct magnitude. Fig. 8.9 may be regarded as the final result of the analysis of Ascent 9.

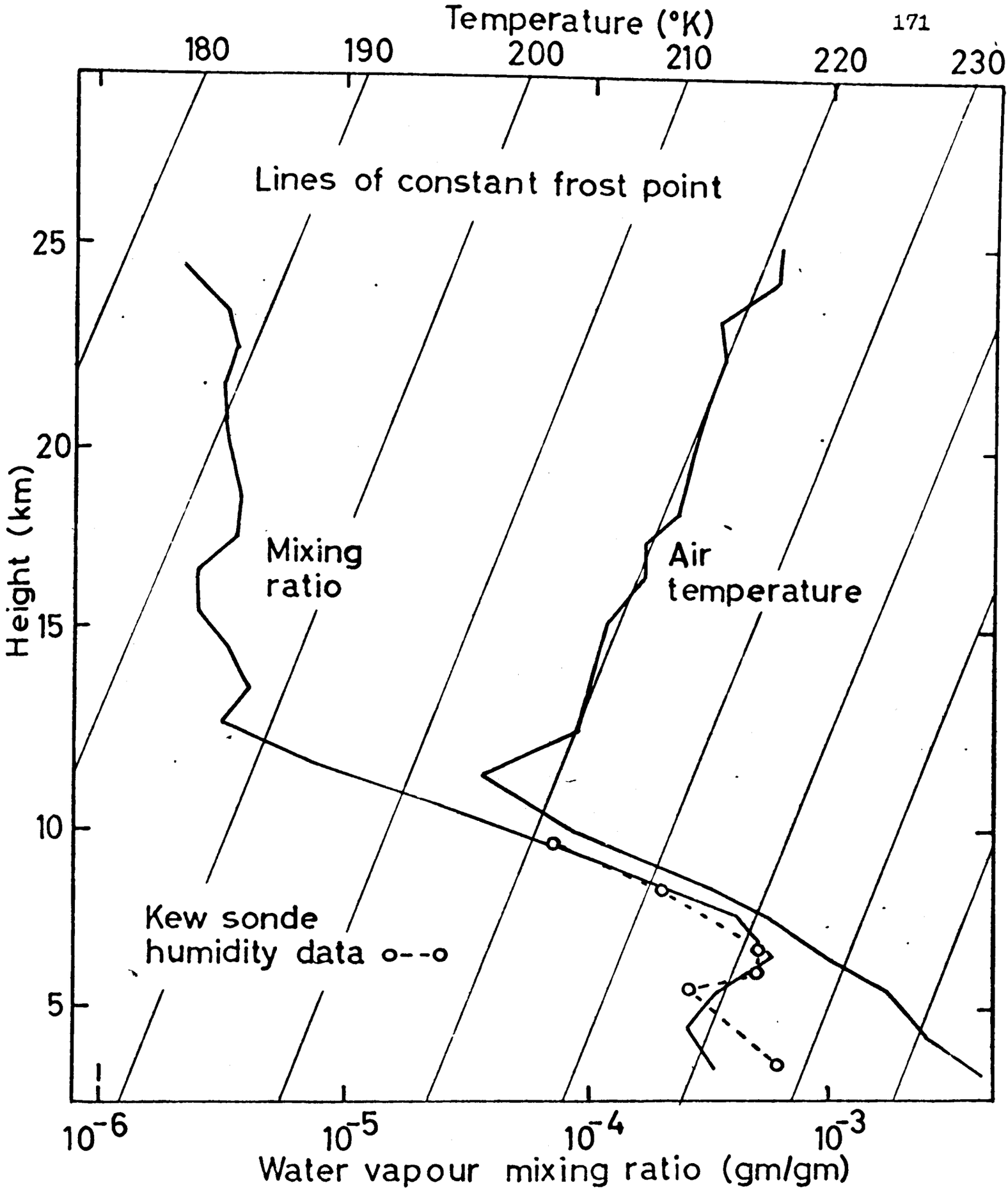


Fig. 8.9. Final water vapour mixing ratio profile from Ascent 9.

Chapter 9

The remaining ascents

Ascent 9, which has been discussed in detail in the last chapter, was the only one of the twelve to yield significant information in the stratosphere. Analysis has however been attempted of five of the remaining seven ascents which yielded some useful information.

Results from ascents 6 and 8, which were made before the improved phasing circuit was incorporated into the sonde, are open to doubt, as can be seen from the profiles (figs. 9.1 and 9.2). They are, however, included for the sake of completeness. Mixing ratios above the tropopause obtained from ascent 6 show a marked increase compared with the value at 12 km. The responsivity of the detector on this occasion showed the usual maximum near the tropopause but then, after decreasing for a few kilometers, began to rise again. It is difficult to imagine that this was a real effect and must have resulted from failure of the reference signal. Results above the tropopause must therefore be looked upon with suspicion.

The sudden drying below the tropopause indicated by ascent 8 may have been due to the presence of a cloud layer. This could also account for the very large mixing ratios obtained at 10 km. As can be seen from the ascent

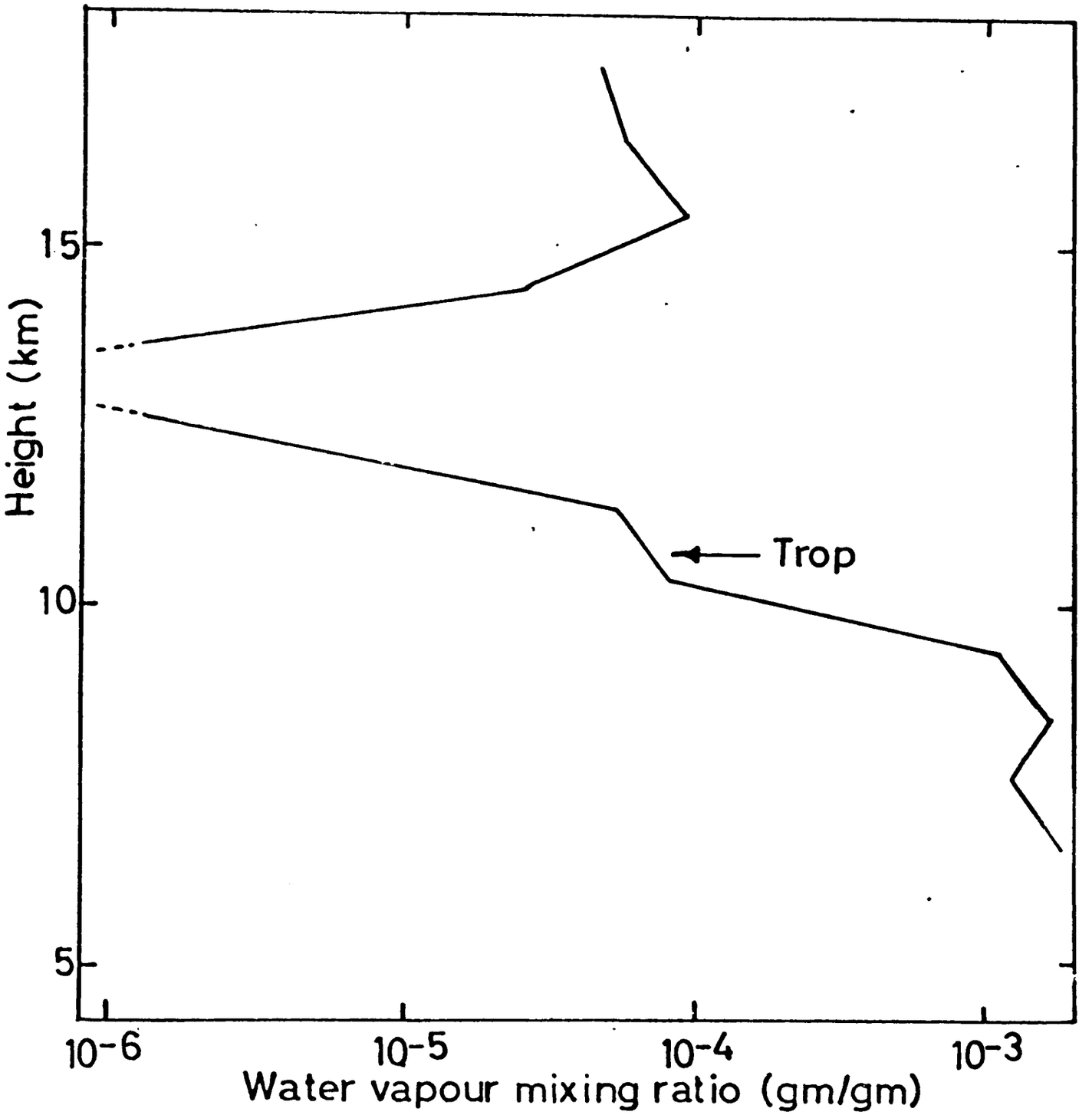


Fig. 9.1. Results from Ascent 6.

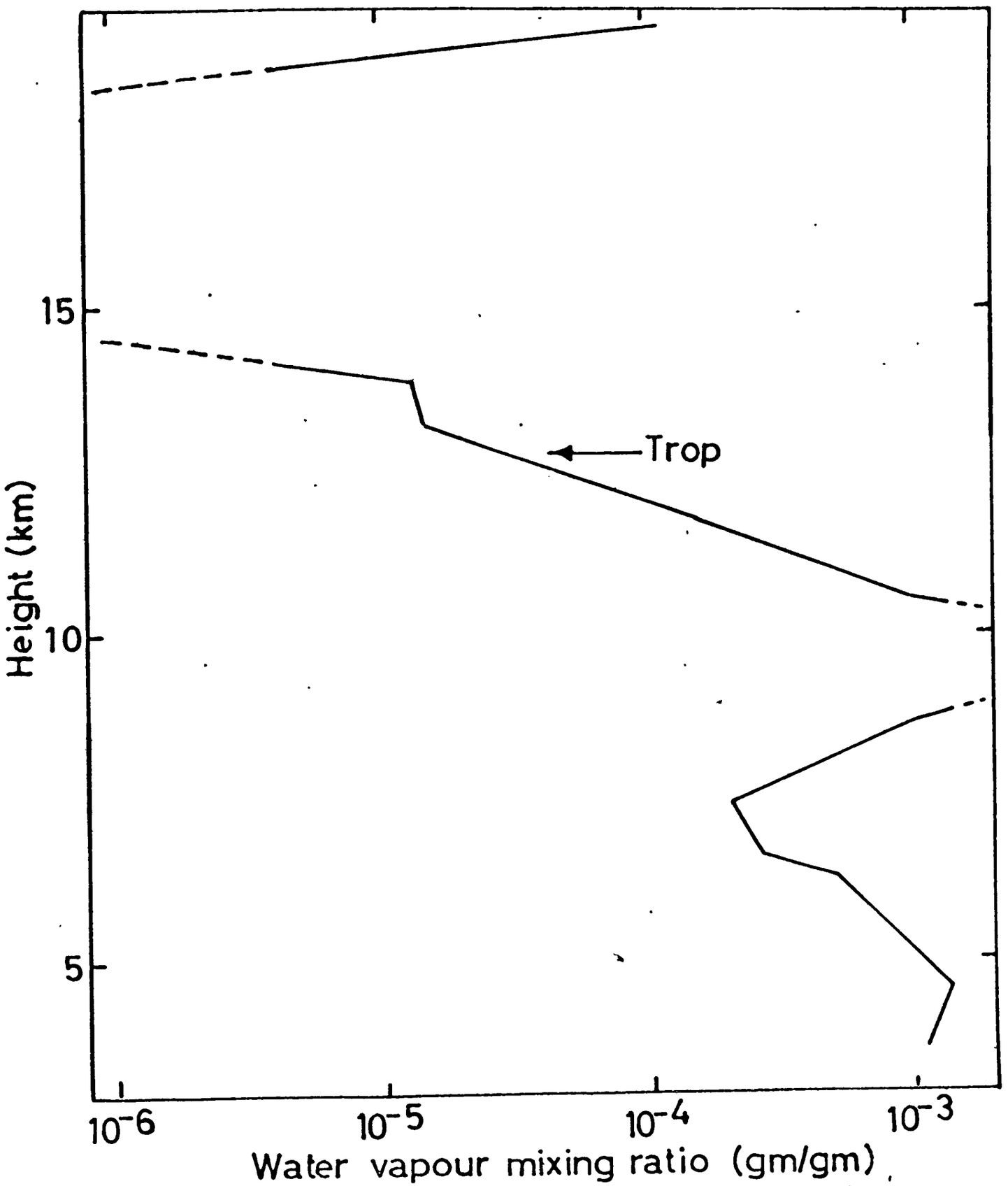


Fig. 9.2. Results from Ascent 8.

data (fig 6.4), the drop in sky emission is quite sudden. This does seem, however, to be a real effect, rather than a failure of the sonde, since the black body signal does not show a similar drop. A certain amount of cloud was known to be present on the night of ascent 8 and, if this extended to the tropopause, results in the lower stratosphere are probably unreliable. Data obtained above 15 km were clearly anomalous since atmospheric transmissions of greater than 100% would have been required to produce such signals.

Ascent 10, which was made on the night immediately following that of ascent 9, performed well. Unfortunately, noisy signals made interpretation of data difficult. No useful information could be obtained above 17 km although the sonde actually reached 28 km. It cannot be assumed that at 17 km all the sky signal obtained is due to foreign emission, as was the case with the signal at the highest level of ascent 9, and the data have been analysed on the assumption that emission is entirely due to water. Furthermore, since no allowance has been made for CH_4 and N_2O emission, results shown in fig. 9.3 will be too large by about a factor of 3. Nevertheless, the profile is of interest for it is found to agree well with that obtained from ascent 9 when analysis is performed under similar

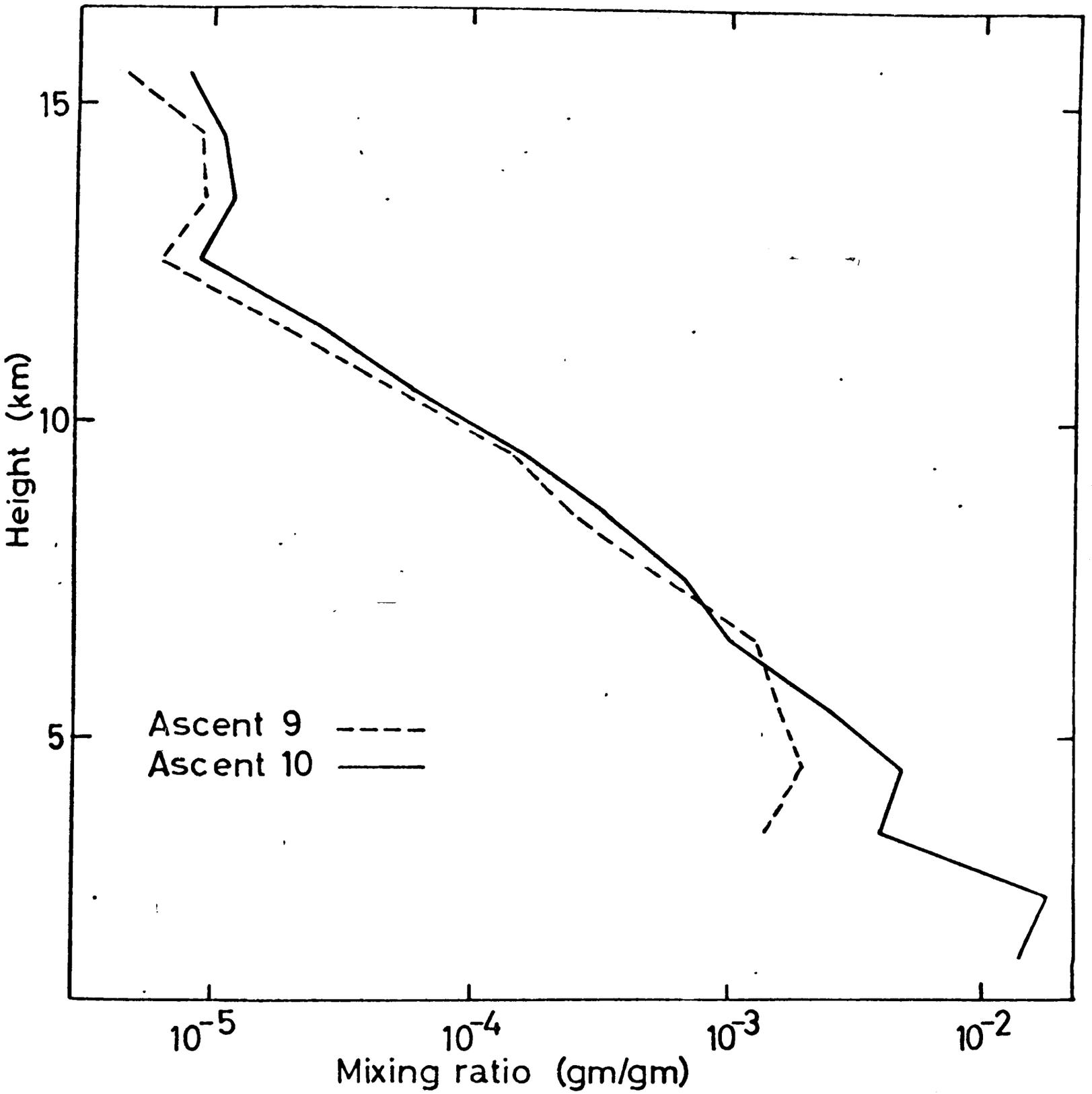


Fig. 9.3. Results from Ascent 10 compared with those from Ascent 9 calculated under the same conditions.

conditions. This is also plotted in fig. 9.3. A true comparison is justified since the weather situation on the two nights was very similar.

Neither of the remaining ascents on which analysis was attempted gave any useful information above the tropopause and no results are presented.

Chapter 10

Summary and further work

The results presented in Chapter 8 indicate a mixing ratio in the stratosphere which is substantially constant, in the region of 3×10^{-6}, up to a height of at least 26 km. It is difficult to estimate the absolute accuracy of values of mixing obtained from the analysis, as the chief uncertainty must be the assumptions on which the actual analysis is based. Tests have shown that errors in ascent data at any given point do not result in cumulative errors in mixing ratios lower in the atmosphere, or to instability in the calculation as was at first feared might have been the case. There is no doubt that random errors in ascent data are very much magnified in final mixing ratios but absolute values are probably quite reliable. This is borne out by the fact that the smoothing processes described in detail in Chapter 8 do not greatly affect mean values of calculated mixing ratios.

The accuracy of the telemetry is probably better than 1% of the complete range. The chief uncertainty in the ascent data arises from the interpretations of the negative signals. This, and the foreign emission received in the stratosphere, are the two main problems which require further investigation.

The first should be solved by suitable modifications to the sonde. Some efforts have been made to locate the source of the trouble, but investigation has been hampered because it has not been possible to simulate the effect in the laboratory.

A complete investigation of foreign emissions arising in the upper stratosphere will require measurements to be made over much narrower wavelength intervals. Calculations have suggested that, if the mixing ratio of the upper stratosphere has the same low value observed above the tropopause, the contribution by water vapour to emission received at 30 km will be more than an order of magnitude less than the total value at present measured. By restricting the band width of the detector to a region where no foreign emission exists, the total energy received will be very small. This could present problems of measurement with the detector in its present form.

In connection with the apparatus, there is considerable room for improvement in the method of telemetry. As has been described, the system employed at present was designed for use in conjunction with hand plotting of received signals. Since this method has now been superseded, there would seem to be no reason why the present system need be preserved. With automatic recording of data, much higher multiplexing rates could be employed. At present, one

minute is required for a complete cycle and only three measurements of any one quantity can be made per kilometer.

The work described in this thesis has not been without its setbacks. The apparatus which has been developed has given useful information but can hardly be described as fully proven and further refinements are required to increase its reliability. Results which have been obtained to date do, however, serve to illustrate the value of atmospheric emission measurements as an approach to the determination of stratospheric humidity.

Appendix I

Power supplies required by radiometer-sonde

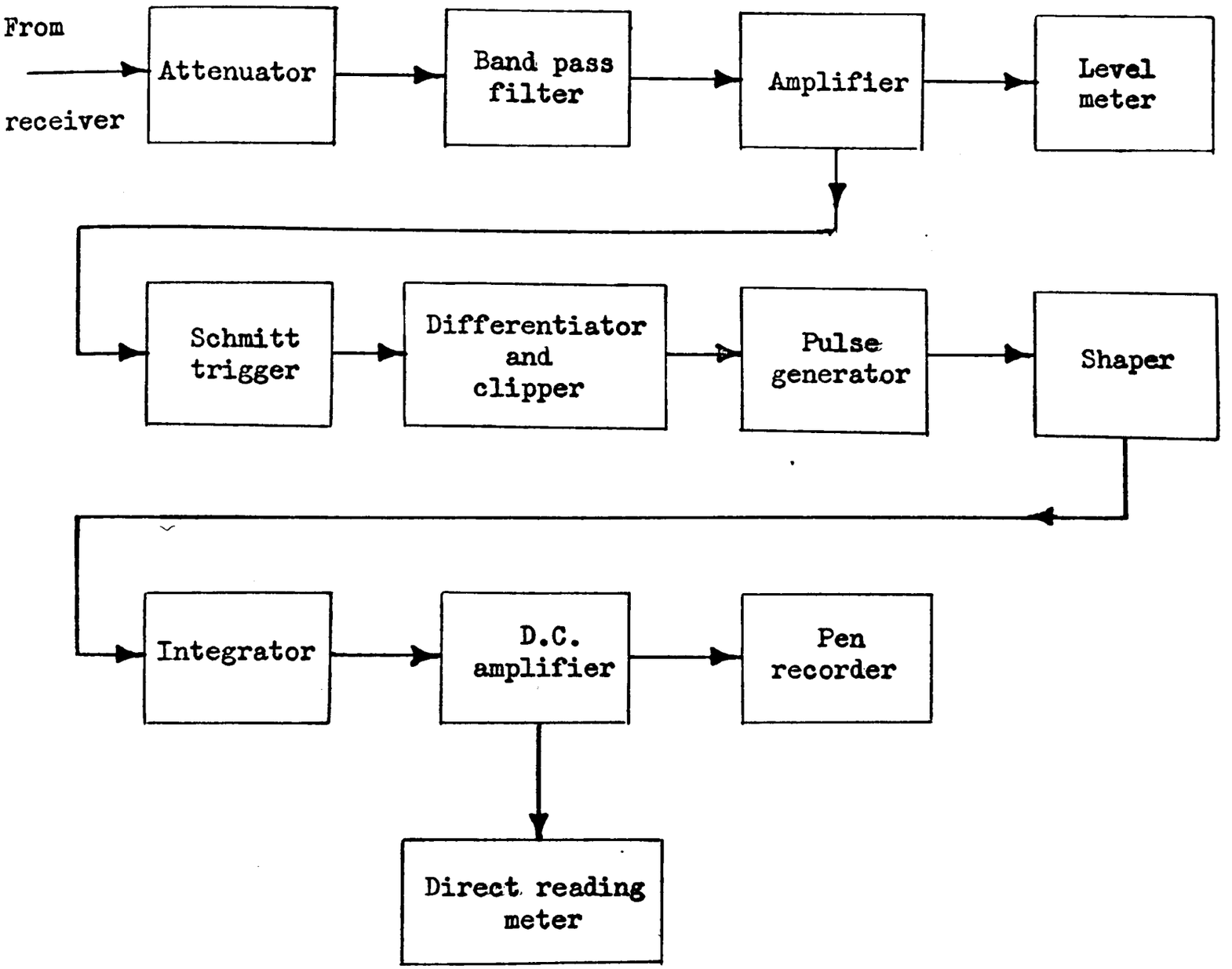
No	Function	Battery type		Voltage	Nominal capacity	Current supplied
B1	Filament of cathode follower	Ni-Cd accumulator	Deac type 450 DK	1.3	450 mAh	25 mA
B2	H.T. for detector and cathode follower	Layer-type dry battery	2 x Exide type DH 521 or equiv.	30	-	~ 500 µA
B3	Signal amplifier	Layer-type dry battery	Ever Ready type PP3 or equiv.	9	-	1.5 mA
B4	Chopper drive and reference generator	Layer-type dry battery	Ever Ready type PP3 or equiv.	9	-	5 mA
B5	Thermistor bridge	Mercury cell	Mallory type RM 625	1.34	250 mAh	up to 0.25 mA
B6	Bias for transductor and A.F. oscillator	Mercury cell	Mallory type RM 625	1.34	250 mAh	~ 1 mA
B7	Transmitter and A.F. oscillator	Layer-type dry battery	Ever Ready type PP3 or equiv.	9	-	5 mA
B8	Motor	PbO_2-Zn primary cell	Barnard Batteries special type	2.7	300 mAh	~ 100 mA

Appendix II

Radiosonde frequency recording equipment

A block diagram of the system, which was referred to in section 4.8, is given on page 183 and is self explanatory.

The Schmitt trigger circuit provides a rectangular wave form at signal frequency provided that the amplitude of the incoming signal is greater than about 10 mV R.M.S. From this wave form, narrow pulses are derived which trigger a monostable circuit. The latter provides constant width pulses of approximately 500 uS duration. The integrated output level is thus proportional to frequency. This is passed to a balanced D.C. amplifier which drives a pen recorder and a direct reading meter calibrated from 700 - 1000 c/s. By careful design of the delay circuit and D.C. amplifier, and with the provision of a stabilised power supply, the temperature coefficient can be reduced to a minimum. The linearity of the device was found to be good over the required range. A portion of a typical record is shown in fig. 4.23.



Block diagram of frequency recording equipment.

Appendix III

The Computer Programme

Basically, the calculation consisted of a routine to compute the value of the sky signal S_c at height z due to a given water vapour distribution above z. The amount of water vapour in the layer immediately above z was adjusted by iteration until S_c was within 0.1% of the measured values S_m. The procedure was performed at 1 km intervals down through the atmosphere, beginning at the level of the highest measurement.

At each level, the amount of water $u(z)$ in the layer under consideration was initially set equal to that in the layer above (i.e. the last quantity determined) and a value for S_c calculated. The amount of water was then doubled and S_c calculated again. If the agreement with the measured signal was found to decrease in the second case the water was halved. This process was repeated until the value of $S_c - S_m$ changed sign. Newton's method was then used to interpolate a more accurate value of $u(z)$ which was used for the next calculation of S_c. Each subsequent interpolation was performed with the nearest value of $S_c - S_m$ having the opposite sign to that last calculated. When agreement was found to be better than 0.1% the last calculated value was stored and the calculation proceeded to the next level.

Random errors in the ascent data occasionally produced impossible signals - signals which could only result from negative values of mixing ratio. If this was found to be the case, the water in the appropriate level was set to zero. This appeared to have a stabilising effect on the calculation and, although mixing ratios following immediately below the level were invalidated, little effect was observed beyond 3 or 4 km.

As has been described, values of S_c were calculated on the basis of the statistical model using the Curtis-Godson approximation to derive mean pressures and temperatures. Values of the parameters G_ν and H_ν were provided at 50 cm^{-1} intervals in the form of data as was information regarding the detector spectral sensitivity profile. The range of frequencies considered in the calculation was from 1125 cm^{-1} to 1975 cm^{-1}.

Values of the Planck function corresponding to black body emission in each 50 cm^{-1} interval at a number of 1 km levels in the atmosphere were required each time a value of S_c was calculated. In order to avoid repeating the same calculation each time, a matrix was built up at the beginning of the programme. This had to be transferred to the slow (drum) store owing to the limited capacity (1024) words of the working store in Mercury. At a given level, the appropriate section of the matrix was dealt with.

The initial calculation of the matrix required about 20 seconds. The time taken to compute a value of S_c depended on the level being considered but was about 2 seconds at the summit of the ascent and up to a minute near ground level. Usually three or four iterations were required to obtain each value of $u(z)$ so that a complete calculation would take up to 45 minutes.

References

Adel, A. (1941), Astrophys. J. 94, 451.

Avery, D. G. and Bowes, R. C. (1958), J. Sci. Instrum. 35, 212.

Bannon, J. K., Frith, R. and Shellard, H. C. (1952), Met. Off., Geophys. Mem., Lond., No. 88.

Barrett, E. W., Herndon, L. R. and Carter, H. J. (1949), J. Met. 6, 367.

Barrett, E. W., Herndon, L. R. and Carter, H. J. (1950), Tellus 2, 302.

Benedict, W. S. and Kaplan, L. D. (1959), J. Chem. Phys. 30, 388.

Benedict, W. S. and Plyler, E. K. (1951), Bur. Stand. J. Res., Wash. 46, No. 3, 246.

Brewer, A. W. (1949), Quart. J. R. Met. Soc. 75, 351.

Brewer, A. W. (1955), Air Ministry, Met. Res. Cttee., M.R.P., No. 946.

Brewer, A. W. (1958), Air Ministry, Met. Res. Cttee., M.R.P., No. 1084.

Brewer, A. W., Cwilong, B. M. and Dobson, G. M. B. (1948), Proc. Phys. Soc. 60 A, 52.

Brewer, A. W. and Milford, J. R. (1960), Proc. Roy. Soc. A 246, 470.

Bridgers, H. E., Scaff, J. H. and Shive, J. N. (1958), Transistor Technology, Volume I. New York: Van Nostrand.

Brown, F., Goldsmith, P., Green, H. F., Holt, A. and Parham, A. G. (1961), Tellus 13, 407.

Brown, D. A. H. and Roberts, V. (1953), J. Sci. Instrum. 30, 5.

Burch, D. E., Gryvnak, D., Singleton, E. B., France, W. L. and Williams, D. (1962), Ohio State University Research Report, Contract No. AF 19(604) - 2633.

Butterworth, S. (1914), Proc. Phys. Soc. 26, 264.

Butterworth, S. (1915), Proc. Phys. Soc. 27, 410.

Butterworth, S. (1920), Proc. Phys. Soc. 32, 345.

Cowling, T. G. (1950), Phil. Mag. 41, 109.

Crawford, M. F., Welsh, H. L. and Lock, J. L. (1949), Phys. Rev. 75, 1607.

Curtis, A. R. (1952), Quart. J. R. Met. Soc. 78, 638.

de Tourville, C. M. (1961), Nature, Lond., 190, 156.

Dobson, G. M. B. (1956), Proc. Roy. Soc. A 236, 187.

Dobson, G. M. B., Brewer, A. W. and Cwilong, B. M. (1946), Proc. Roy. Soc. A 185, 144.

Dunlap, W. C. Jr. (1953), Phys. Rev. 91, 1282.

Eccles, W. H. (1919), Proc. Phys. Soc. 31, 269.

Elsasser, W. M. (1942), Harv. Met. Stud. No. 6.

Feely, H. W. and Spar, J. (1960), Nature, Lond., 188, 1062.

Fowle, F. E. (1912), Astrophys. J. 35, 149.

Fowle, F. E. (1913), Astrophys. J. 37, 359.

Gates, D. M. (1956), J. Met. 13, 369.

Gates, D. M., Calfee, R. F. and Hanson, D. W. (1963), Appl. Opt. 2, 1117.

Gates, D. M., Murcray, D. G., Shaw, C. C. and Herbold, R. J. (1958), J. Opt. Soc. Amer. 48, 1010.

Godson, W. L. (1954), Proc. Toronto Meteorological Conference, 1953, p. 35.

Godson, W. L. (1955), J. Met. 12, 272.

Goldsmith, P. (1954a), Air Ministry, Met. Res. Cttee., M.R.P., No. 859.

Goldsmith, P. (1954b), Met. Mag. 83, 329.

Goldsmith, P. and Brown, F. (1961), Nature, Lond., 191, 1033.

Goody, R. M. (1952), Quart, J. R. Met. Soc. 78, 165.

Goody, R. M. (1958), The Physics of the Stratosphere. Cambridge University Press, p. 170.

Goody, R. M. (1961a), Atmospheric Radiation, Chapter 1, (to be published).

Goody, R. M. (1961b), Quart. J. R. Met. Soc. 87, 428.

Goody, R. M. and Wormell, T. W. (1951), Proc. Roy. Soc. A 209, 178.

Griggs, M. (1961), D. Phil. thesis, University of Oxford.

Gutnick, M. (1961), J. Geophys. Res. 66, 2867.

Hitschfeld, W. and Houghton, J. T. (1961), Quart. J. R. Met. Soc. 87, 562.

Helliwell, N. C. and Mackenzie, J. K. (1957), Air Ministry, Met. Res. Cttee. M.R.P., No. 1024.

Helliwell, N. C., Mackenzie, J. K. and Kerley, M. J. (1957), Quart, J. R. Met. Soc. 83, 257.

Houghton, J. T. (1963), Quart, J. R. Met. Soc. 89, 332.

Houghton, J. T., Hughes, N. D. P., Moss, T. S. and Seeley, J. S. (1961), Phil. Trans. Roy. Soc. A, 254, 47.

Houghton, J. T., Moss, T. S. and Chamberlain, J. P. (1958), J. Sci. Instrum. 35, 329.

Houghton, J. T., Moss, T. S., Seeley, J. S. and Hawkins, T. D. E. (1957), Nature, Lond., 180, 1187.

Houghton, J. T. and Seeley, J. S. (1960), Quart. J. R. Met. Soc. 86, 358.

Johns Hopkins University (1949), Progress Report, Contract N5ori-166.

Johnson, L. and Levinstein, H. (1960), Phys. Rev. 117, 1191.

Jones, O. C., Maddever, R. S. and Sanders, J. H. (1959), J. Sci. Instrum. 36, 24.

Jones, F. E. and Roberts, V. (1956), Proc. Roy. Soc. A 236, 171.

Kaiser, W. and Fan, H. Y. (1954), Phys. Rev. 93, 977.

Kaplan, L. D. (1952a), J. Met. 9, 1.

Kaplan, L. D. (1952b), J. Met. 9, 139.

Kaplan, L. D. (1954), Proc. Toronto Meteorological Conference, 1953, p.43.

Kobayashi, J. and Toyama, Y. (1962), Geophys. Mag. 31, 167.

Landenburg, R. and Reiche, F. (1911), Ann. der Phys. 42, 181.

Mastenbrook, H. J. (1962), U.S. Naval Research Laboratory Report 5817.

Mastenbrook, H. J. (1963), Rep. Proc. Int. Ass. Met. and Atmos. Phys. 1963.

Mastenbrook, H. J. and Dinger, J. E. (1961), J. Geophys. Res. 66, 1437.

Migeotte, M., Neven, L. and Swensson, J. (1957/8), Institut d'Astrophysique de l'Université de Liège, Special volumes parts I and II.

Murcray, D., Brooks, J., Murcray, F. and Shaw, C. (1958), J. Geophys. Res. 63, 289.

Murcray, D. G., Murcray, F. H. and Williams, W. J. (1962), J. Geophys. Res. 67, 759.

Murcray, D. G., Murcray, F. H., Williams, W. J. and Leslie, F. E. (1960), J. Geophys. Res. 65, 3641.

Murgatroyd, R. J., Goldsmith, P. and Hollins, W. E. A. (1955), Quart. J. R. Met. Soc. 81, 533.

Newman, R. (1954), Phys. Rev. 94, 278.

Nickless, C. A. (1962), B.Sc. thesis, University of Oxford.

Richards, J. C. S. (1955), J. Sci. Instrum. 32, 340.

Robinson, G. D. (1947), Quart. J. R. Met. Soc. 73, 127.

Robinson, G. D. (1950), Quart. J. R. Met. Soc. 76, 37.

Shellard, H. E. (1950), Met. Mag. 79, 355.

Sheppard, P. A. (1963), Rep. Progr. Phys. 26, 213.

Tucker, G. B. (1957), Air Ministry, Met. Res. Cttee, M.R.P., No. 1052.

Yamamoto, G. (1952), Sci. Rep. Tôhoku Univ., Geophys. 4, 9.

Yarnell, J. and Goody, R. M. (1952), J. Sci. Instrum. 29, 352.